

# Exact and Superconvergent Solutions of the Multi-Point Flux Approximation O-method: Analysis and Numerical Tests

Master's Thesis in Applied and Computational Mathematics

Daniel S. Olderkjær



University of Bergen  
Faculty of Mathematics and Natural Sciences  
Department of Mathematics

02.06.2014



# *Acknowledgements*

A special thanks to my supervisors Jan M. Nordbotten and Eirik Keilegavlen. Thank you for your enlightening guidance and invaluable advice, which has been a huge source of education the last two years. I would also like to thank Lars Jordanger, David Seus and Professor Christian Rohde for their input and discussions on my thesis.

I am also grateful for the funding provided by BKK for my travels during this period, and Professor Rainer Helmig and all the other people at the Department of Hydromechanics and Modelling of Hydrosystems at the University of Stuttgart for welcoming me to Germany.

Thanks to my friends at the department, and especially those I have studied with the last five years, in addition to my family, and my girlfriend Ragnhild for her inspiration and support.

Lastly, I would like to acknowledge my high school teacher in mathematics Jon Lund as an invaluable inspiration for my choice to study mathematics, may he rest in peace.



## *Abstract*

In this thesis we prove the multi-point flux approximation O-method (MPFA) to yield exact potential and flux for the trigonometric potential functions  $u(x, y) = \sin(x) \sin(y)$  and  $u(x, y) = \cos(x) \cos(y)$ . This is done on uniform square grids in a homogeneous medium with principal directions of the permeability aligned with the grid directions when having periodic boundary conditions. Earlier theoretical and numerical convergence articles suggests that these potential functions should only yield second order convergence. Hence, our motivation for the analysis was to gain new insight into the convergence of the method, as well as to develop theoretical proofs for what seems as decent examples for testing implementation. An extension of the result to uniform rectangular grids in an isotropic medium is also briefly discussed, before we develop a numerical overview of the exactness phenomenon for different types of boundary conditions. Lastly, an investigation of application of these results to obtain exact potential and flux using the MPFA method for general potential functions approximated by Fourier series was conducted.

# Contents

<b>Acknowledgements</b>	<b>i</b>
<b>Abstract</b>	<b>ii</b>
<b>1 Introduction</b>	<b>1</b>
<b>2 Governing Equations for Single-Phase Flow in Porous Medium</b>	<b>5</b>
2.1 Physical Properties . . . . .	5
2.1.1 Porous Medium . . . . .	5
2.1.2 Fluid Properties . . . . .	6
2.2 Darcy's Law . . . . .	7
2.3 Mass Conservation . . . . .	9
2.4 Some Simplifications of the Model . . . . .	11
2.5 Representative Equations . . . . .	11
<b>3 Control Volume Methods</b>	<b>13</b>
3.1 General Theory of the Two-Point Flux Approximation Method (TPFA) and the Multi-Point Flux Approximation $O(\eta)$ -Method (MPFA) . . . . .	13
3.2 The TPFA Method . . . . .	15
3.3 The MPFA method . . . . .	18
3.4 Convergence Theory of the MPFA Method . . . . .	24
3.5 Theoretical Framework for the MPFA Method on a Uniform Parallelo- gram Grid in a Homogeneous Medium . . . . .	25
<b>4 Theoretical Results</b>	<b>29</b>
4.1 Foundation and Assumptions . . . . .	29
4.2 Approach to the Error Analysis for the Potential . . . . .	32
4.3 Approach to the Error Analysis for the Flux . . . . .	35
4.4 Error Analysis for Inner Cell and Edge Stencils on a Uniform Square Grid for General Permeabilities . . . . .	37
4.4.1 Error Bound of the Potential . . . . .	38
4.4.2 Error Bound of the Fluxes . . . . .	47
4.4.3 Analysis of the Error Bounds . . . . .	49
4.5 Error Analysis for Inner Cell Stencils on a Uniform Rectangular Grid in an Isotropic Medium . . . . .	54
4.6 Summary of the Theoretical Results . . . . .	59

<b>5</b>	<b>Numerical Results</b>	<b>61</b>
5.1	Numerical Results with Periodic Boundary Conditions . . . . .	61
5.2	A Short Comment on Boundary Conditions . . . . .	66
5.3	Numerical Overview of the Exactness Phenomenon . . . . .	66
5.4	Investigation of Application of the Exactness Phenomenon to Fourier Series	68
<b>6</b>	<b>Conclusion</b>	<b>71</b>
<b>A</b>	<b>General Truncation Error Formulas for Inner Cell and Edge Stencils on Uniform Square Grids</b>	<b>73</b>
A.1	General Formula for the Potential . . . . .	73
A.2	General Formulas for the Flux . . . . .	78
<b>B</b>	<b>Detailed Calculation of the Truncation Errors in Section 4.4.2</b>	<b>83</b>
<b>C</b>	<b>Two Dimensional Taylor Expansion and Properties</b>	<b>91</b>
C.1	Two Dimensional Taylor Expansion and Pascal's Triangle . . . . .	91
C.2	The Binomial Theorem and Applications . . . . .	93
	<b>Bibliography</b>	<b>95</b>

# Chapter 1

## Introduction

Mathematical modeling is one of today's most important tools for gaining insight into complex processes in nature. The problem of describing how fluid flows in porous medium is no exception, and has long been a field of study within applied and computational mathematics. Motivated by the need for simulation of oil and gas flow in reservoirs, the field has bloomed during the time when fossil fuels have been among the most important energy sources on earth. Today, those same equations are used to model everything from storage of  $CO_2$  [1] and transport of heat in geothermal energy, see for example [2], to drug release through collagen matrices in the skin [3].

Complex geometries and varying fluid conductivity often arise from for example non-parallel layers of different porous mediums and fractures when modeling flow in porous medium. Robust and flexible numerical methods are needed to successfully handle these conditions. To recognize the most optimal numerical methods, we introduce a set of conditions we would like the methods to satisfy. Among others, these conditions include the physical principle of mass conservation, as well as the method's ability to be flexible for different geometries and to yield explicit expressions for the fluid flux inside the medium at a lowest possible CPU time. The classical methods such as finite difference (FD), finite element method (FEM) and mixed finite element method (MFEM) are not optimal in regard to these criteria [4].

The control volume methods (CVMs) two-point flux approximation (TPFA) and multi-point flux approximation (MPFA) are two methods satisfying these conditions. The MPFA method, developed simultaneously and independently by I. Aavatsmark et al. [5] and M. G. Edwards and C. F. Rogers [6], is the more flexible method of the two, and was created to handle the deficiencies of the TPFA method for certain geometries [4].

The original version of the MPFA method is known as the MPFA  $O(\eta)$ -method. Through the years several different version of the original MPFA method has been developed, see for example [7–9]. In this thesis we will only consider the MPFA  $O(\eta)$ -method, from now on referred to as the MPFA method.

The convergence theory of the MPFA method has been an area of extensive research up until today. By construction, the method is exact for linear potential fields. Else, second order convergence for the potential and first order convergence for the fluxes on quadrilateral grids in two dimensions has been proved theoretically. Second order convergence is seen for the fluxes numerically, but this result has not been proved. Analytical convergence proofs can be found in [10–16], and numerical convergence tests are presented in [17–20].

Through numerical tests we discovered that for certain grids and physical situations on two dimensional square domains, the MPFA method yield superconvergent, and even exact, potential and flux for the following trigonometric potential functions

$$u(x, y) = \sin(x) \sin(y), \quad u(x, y) = \cos(x) \cos(y). \quad (1.1)$$

In this thesis we have established conditions for when the method yield exact potential and flux for an elliptic equation having periodic boundary conditions. This is done on a uniform square grid in a homogeneous medium using the potential functions (1.1). An extension of the exactness phenomenon to uniform rectangular grids is also briefly discussed, showing that the phenomenon occurs for a limited number of ratios between the side lengths of the rectangular cells. The proofs and the discussion are based on the theoretical framework of the MPFA method developed by Nordbotten et al. in [21], and are verified by numerical tests. We have also developed an overview of numerical results differing from known convergence theory for the MPFA method when using different types of boundary conditions. This overview, along with the results for the periodic boundary conditions case, indicates that the exactness phenomenon is a result of a cancellation effect occurring when the trigonometric potential functions (1.1) are applied to the MPFA method on a uniform square grid for a certain physical situation.

Our motivation for examining this phenomenon is to gain new insight into the MPFA method, which, hopefully, will prove to be useful in the ongoing academic work of analyzing the method. In addition, by proving the numerical results analytically we hope to have established a useful example for testing implementation of the method. The example would of course prove more useful if the proof could be extended to problems with Neumann and Dirichlet boundary conditions. This extension would be a natural "next step" in the research process.

Building on our results, both theoretical and numerical, we briefly investigate the possibility of obtaining exact potential and flux for the MPFA method from general potential functions by approximating these functions using Fourier series. The investigation proved the idea to hold for a very limited number of potential functions, and was therefore not pursued further. The results did however yield new insight into the overview of numerical results for the functions (1.1). This was achieved by observing that the cancellation effect occurred not only when applying a uniform square grid, but when the trigonometric potential functions (1.1) had an equal number of oscillations in both spatial directions within the domain.

The outline of this thesis is set up in the following way. In **Chapter 2** we will develop a mathematical model describing single-phase flow in porous medium. **Chapter 3** gives an introduction to the TPFA and MPFA methods using the flow model developed in Chapter 2. Here we will also discuss in greater detail the convergence theory of the MPFA method and a theoretical framework, found in [21], of the method for uniform parallelogram grids in homogeneous mediums. This framework will prove crucial in obtaining the theoretical results in this thesis. The theoretical results are then presented in **Chapter 4**, with additional details found in Appendix B. These results are built on the general formulas developed in Appendix A and the theory from Appendix C. In **Chapter 5** numerical tests are conducted, and the results are compared with the theoretical results from Chapter 4. This chapter then develops a numerical overview of the exactness phenomenon for different boundary conditions. We also look closer at the possibility of obtaining exact results for the MPFA method having approximated general potential functions using Fourier series in the last section of Chapter 5. The conclusion is given in **Chapter 6**.



## Chapter 2

# Governing Equations for Single-Phase Flow in Porous Medium

This chapter is devoted to giving an overview of the equations describing single-phase flow in porous medium. We will first discuss the physical properties of the fluid and the porous medium, before deriving the governing equations for single-phase flow in porous medium and constructing a mathematical model. At the end of the chapter we will discuss how to simplify our model by making assumptions about both the fluid and the porous medium, eventually establishing a representative model which will be used in the numerical methods discussed later in the thesis. The theory described in this chapter is mainly based on the lecture notes by I. Aavatsmark [4] from the course *Conservation Methods for Elliptic Equations* (MAT362) and the PhD thesis of S. S. Mundal [22]. Additional details are also found in the book by J. M. Nordbotten and M. A. Celia [1], and obtained through personal communication with A. F. Radu [23] while he was lecturing the department's course *Flow in Porous Medium* (MAT254).

## 2.1 Physical Properties

### 2.1.1 Porous Medium

A porous medium is a medium consisting of inner void spaces which allows fluid to be transported through the medium. These inner void spaces are referred to as pores, and often make up a complex structure of both interconnected and isolated pores. In practice it is almost impossible to resolve the exact structure of these internal pores. Therefore,

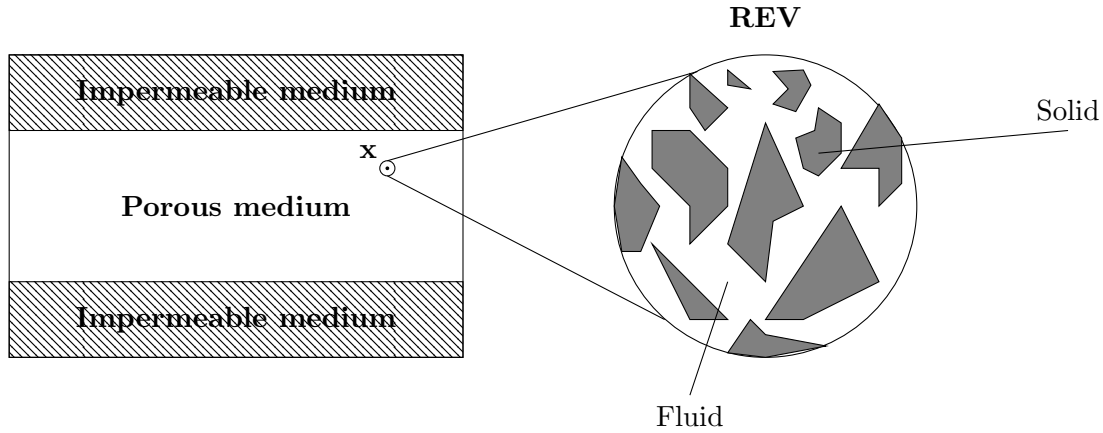


FIGURE 2.1: The REV of point  $x$  in space of a porous medium situated between two layers of impermeable medium.

in applications, we use the *continuum approach*, which yields a volume-averaged flow model. The non-void parts of the porous medium are referred to as the *solid parts*.

The continuum approach is based on defining a length scale called the *representative elementary volume* (REV). The length scale of the REV must be large enough to capture a meaningful average of the void spaces and the solid parts inside the REV. Then to one mathematical point in space, within the porous medium, we associate the properties of the REV surrounding this point, see Figure 2.1. The continuum approach is widely recognized due to the approach preserving heterogeneities in the medium even though we do not obtain an exact resolution of the pores.

To be able to describe single-phase flow in porous medium we need to define the *porosity*,  $\phi$ . The porosity is a property of the medium, and it describes the percentage of void volume in a REV

$$\phi = \frac{\text{Volume of voids in REV}}{\text{Volume of REV}}. \quad (2.1)$$

### 2.1.2 Fluid Properties

There are two important properties of a fluid used in the modeling of single-phase flow in porous media. The first one is the *viscosity*,  $\mu$ , of a fluid. The viscosity is a measure of the internal friction in the fluid, and the larger it gets the slower a fluid flows.

The second important property is the *density*,  $\rho$ , of a fluid. The density is defined as the ratio between mass and volume of the fluid

$$\rho = \frac{\text{Mass of fluid}}{\text{Volume of fluid}}. \quad (2.2)$$

For a given temperature,  $T$ , the density of a fluid is normally dependent on the pressure,  $p$ , applied to the fluid. Therefore, in practice, a fluid is usually *compressible*.

## 2.2 Darcy's Law

When considering flow in porous medium, the equation giving the *volumetric flux*  $\mathbf{q}$ , volumetric flow rate per area, of the fluid is called *Darcy's law*. This law is a development of the original law constructed by the results of the empirical experiments conducted by Henry Darcy, which was published in 1856 (detailed explanation of experiments in [1], p.17-19). The law is given by

$$\mathbf{q} = -\mathbf{K} \frac{\rho g}{\mu} \nabla u, \quad (2.3)$$

where  $g$  represents the gravitational acceleration and  $u$  a quantity called the *hydraulic head*. Tensor  $\mathbf{K}$  is called the *permeability tensor*. Both  $\mathbf{K}$  and  $u$  will be explained in detail below.

The hydraulic head,  $u$ , is found by examining the state of a fluid in a porous medium, which can be described by its energy. Recall from elementary physics that

$$\text{Energy} = \text{Kinetic Energy} + \text{Potential Energy}. \quad (2.4)$$

Assuming that the flow of the fluid is sufficiently slow, we may neglect the kinetic energy. This situation is referred to as *laminar flow*. If we in addition disregard the influence on the flow by all other factors than the pressure and gravitational forces acting on the fluid, the potential energy at a given spatial point in the porous medium may be written as

$$\text{Potential Energy} = \text{Pressure Potential} + \text{Gravitational Potential}. \quad (2.5)$$

The potential energy of the fluid in a porous medium is often called the *hydraulic potential* or simply the *potential*. Writing Equation (2.5) using the formulas for the different potentials yields the following equation

$$mgu = pV + mgz. \quad (2.6)$$

Here  $p$  is the pressure on the fluid at the spatial point being considered,  $m$  the mass of the fluid and  $z$  the elevation from a reference level called the *datum*, which has zero elevation.  $V$  gives the volume of the fluid. By manipulating Equation (2.6) we obtain a formula describing the hydraulic head

$$u = \frac{pV}{mg} + z = \frac{p}{\rho g} + z. \quad (2.7)$$

The second equality arises from the fact that  $m = \rho V$ . In a porous medium fluid flows from higher to lower hydraulic head, which is why we add the minus sign in Darcy's law (2.3). The gradient of the hydraulic head represents a fluid's ability to flow at a given spatial point in the porous medium.

The permeability tensor,  $\mathbf{K}$ , is a measure of the fluid conductivity of the porous medium in the different spatial directions, and arises from the development of Darcy's law. A porous medium with a large permeability has a higher ability to transmit fluid through its pore spaces than a porous medium with a small permeability. If a porous medium has a permeability sufficiently close to zero it does not transmit fluid through its pores, and the medium is called *impermeable*. Below we discuss some of the properties related to the permeability. These properties will be central in both understanding the numerical method and the analysis done in later chapters.

To further understand the permeability we need to understand the concepts of *isotropic* and *anisotropic* material and *homogeneous* and *heterogeneous* material. If the solid parts of the porous medium consists of an *anisotropic* material, the permeability changes value depending on the spatial direction being considered in the porous medium. Conversely, if the permeability has no directional differences, the material is called *isotropic*. When the permeability changes as a function of spatial location, the material is referred to as *heterogeneous*. Conversely, when a material is spatially uniform, it is called *homogeneous*<sup>1</sup>.

The reason for writing the permeability as a tensor is to handle the case when the porous medium is anisotropic. This is because for an anisotropic medium, the expression  $\mathbf{K}\mathbf{e}$ , where  $\mathbf{e}$  is a unit vector, will depend on the direction of  $\mathbf{e}$ . The permeability will always satisfy  $\mathbf{e}^T\mathbf{K}\mathbf{e} > 0$ , and Onsager's principle dictates that the permeability has to be symmetric. Hence,  $\mathbf{K}$  is always a symmetric positive definite tensor.

If the porous medium is heterogeneous, the permeability becomes a function of spatial location. Therefore, we usually write the permeability as  $\mathbf{K}(\mathbf{x})$ . Note that both a heterogeneous and a homogeneous porous medium may be both isotropic and anisotropic. In this thesis we will only consider homogeneous mediums.

The nature of the permeability imposes some additional properties on  $\mathbf{K}$  for different situations. If our frame of reference is orthogonal,  $\mathbf{K}$  becomes a symmetric and positive definite *matrix*. There are also some *principal directions* associated with  $\mathbf{K}$ . These directions are the specific directions for which the fluid conductivity of the porous medium assumes its maximum and minimum along. The principal directions of  $\mathbf{K}$  are

---

<sup>1</sup>These definitions holds for any property or parameter associated with a system or material, not only for the permeability.

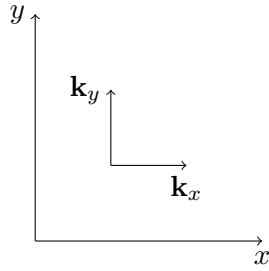


FIGURE 2.2: Principal directions of  $\mathbf{K}$ ,  $\mathbf{k}_x$  and  $\mathbf{k}_y$ , when the matrix is diagonal.

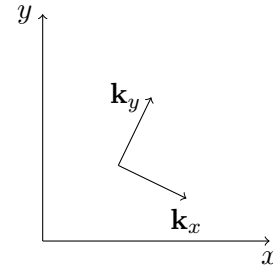


FIGURE 2.3: Example of principal directions of  $\mathbf{K}$ ,  $\mathbf{k}_x$  and  $\mathbf{k}_y$ , when the matrix is *not* diagonal.

always orthogonal to each other. If they are aligned with the directions of the orthogonal frame of reference,  $\mathbf{K}$  becomes a diagonal matrix with off-diagonal elements equal to zero. For a non-diagonal  $\mathbf{K}$ , the deviation between the directions of the frame of reference and the principal directions  $\mathbf{K}$  is given by the size of the off-diagonal elements. Examples of both cases are shown in Figures 2.2 and 2.3.

The term  $\mathbf{K} \frac{\rho g}{\mu}$  in Darcy's law is called the *hydraulic conductivity*. Since the gravitational acceleration, and the density and viscosity of a fluid are all scalars, the directions of the *hydraulic conductivity* coincides with the principal directions of the permeability,  $\mathbf{K}$ . Therefore we regard the hydraulic conductivity as analogous to the permeability.

## 2.3 Mass Conservation

Modeling of flow in porous media is built on the physical principle of mass conservation for the fluid. For any arbitrary domain,  $\Omega$ , in space, the accumulation of mass of the fluid in the domain minus the fluxes over the boundary of the domain has to equal the mass pumped in or drained out of the domain through a source or a sink. This can be visualized as

$$\{\text{accumulation}\} - \{\text{outflux}\} = \{\text{source/sink}\}. \quad (2.8)$$

To describe this principle using previously introduced properties of the fluid and the porous medium we first need to make two observations. The mass of a fluid in a REV of the porous medium is described by  $\phi\rho$ ,

$$\phi\rho = \frac{\text{Volume of fluid}}{\text{Volume of REV}} \frac{\text{Mass of fluid}}{\text{Volume of fluid}} = \frac{\text{Mass of fluid}}{\text{Volume of REV}}. \quad (2.9)$$

In this case we have assumed that the fluid fills the entire void space in the REV. The change of mass of the fluid inside the medium over time can thus be written as

$$\frac{d}{dt} \int_{\Omega} \phi \rho \, d\tau. \quad (2.10)$$

Using Leibniz integral rule this expression becomes

$$\int_{\Omega} \frac{\partial}{\partial t} (\phi \rho) \, d\tau. \quad (2.11)$$

The second observation is that the *mass flow density* of the fluid through the boundary,  $\partial\Omega$ , of  $\Omega$  equals the integral over the boundary of the normal flux multiplied with the density of the fluid

$$\int_{\partial\Omega} \rho \mathbf{q} \cdot \mathbf{n} \, d\sigma. \quad (2.12)$$

Here  $\mathbf{q}$  is the volumetric flux from Darcy's law (2.3), and  $\mathbf{n}$  is the outer unit normal of the boundary  $\partial\Omega$ .

By introducing the *mass source density*,  $f$ , we can now describe the principle of mass conservation (2.8) by the following equation

$$\int_{\Omega} \frac{\partial}{\partial t} (\phi \rho) \, d\tau + \int_{\partial\Omega} \rho \mathbf{q} \cdot \mathbf{n} \, d\sigma = \int_{\Omega} f \, d\tau. \quad (2.13)$$

Applying the divergence theorem of calculus on the boundary integral, assuming  $\mathbf{q}$  is sufficiently smooth, and acknowledging that Equation (2.13) holds for an arbitrary volume  $\Omega$  we get the differential form of the mass conservation equation

$$\frac{\partial}{\partial t} (\phi \rho) + \nabla \cdot (\rho \mathbf{q}) = f. \quad (2.14)$$

Finally, inserting Darcy's law (2.3) for  $\mathbf{q}$  in Equation (2.14) yields

$$\frac{\partial}{\partial t} (\phi \rho) - \nabla \cdot \left( \mathbf{K} \frac{\rho^2 g}{\mu} \nabla u \right) = f. \quad (2.15)$$

Equation (2.15) is a partial differential equation (PDE) consisting of the second derivative with respect to space and the first derivative with respect to time. Thus, we recognize it as a *parabolic* PDE.

## 2.4 Some Simplifications of the Model

Summing up the equations for single-phase flow in porous medium introduced in Sections 2.2 and 2.3 yields the following model

$$\begin{cases} \mathbf{q} = -\mathbf{K} \frac{\rho g}{\mu} \nabla u, \\ \frac{\partial}{\partial t}(\phi \rho) + \nabla \cdot (\rho \mathbf{q}) = f. \end{cases} \quad (2.16)$$

Assuming we are in  $d$ -dimensional space, Darcy's law (2.3) yields  $d$  equations, and from the mass conservation equation (2.14) we obtain one equation. This results in a total of  $d + 1$  equations. The total number of unknowns in Equation (2.16) is  $d + 3$ , these are  $u$ ,  $\rho$ ,  $\phi$  and  $\mathbf{q}$  (yielding  $d$ -unknowns). This means that the model in Equation (2.16) is underdetermined, and we need further conditions on the unknowns to close the model and obtain a unique solution.

There are different approaches for closing the model in Equation (2.16) for single-phase flow. In this thesis we will do so by assuming that both the fluid and the porous medium are incompressible. This is done by letting the porosity,  $\phi$ , of the porous medium and the density,  $\rho$ , of the fluid be constants. Then Equation (2.16) reduces to

$$-\nabla \cdot \left( \mathbf{K} \frac{\rho^2 g}{\mu} \nabla u \right) = f. \quad (2.17)$$

These assumptions yields a model with  $d + 1$  unknowns in  $d + 1$  equation, and hence our new model, Equation (2.17), has a unique solution.

Looking at the structure of the simplified model, Equation (2.17), we see that the assumptions made to the porosity and density yielded an elliptic PDE instead of the parabolic PDE obtained in Equation (2.15).

## 2.5 Representative Equations

Since we are only interested in analyzing a numerical method, we further simplify the closed single-phase flow model, Equation (2.17). This is done by introducing the new potential

$$u' = \rho g u, \quad (2.18)$$

and new right-hand side source term

$$f' = \frac{f}{\rho}. \quad (2.19)$$

From now on we will only refer to potential  $u'$  and source  $f'$  as  $u$  and  $f$  respectively. By also setting  $\mu = 1$  and taking into account boundary conditions, the model becomes

$$\begin{cases} -\nabla \cdot (\mathbf{K}\nabla u) = f, & \text{in } \Omega, \\ u = u_0 \text{ or } \mathbf{n}^T \mathbf{K}\nabla u = q_0, & \text{on } \partial\Omega. \end{cases} \quad (2.20)$$

Here  $u_0$  and  $q_0$  are Dirichlet and Neumann conditions respectively, and  $\Omega$  is a domain in space consisting of a porous medium. This representative model is the model we will use when discussing numerical methods later in this thesis.

Note that the representative model (2.20) may also be written in integral form as

$$\int_{\partial\Omega} \mathbf{q} \cdot \mathbf{n} \, d\sigma = \int_{\Omega} f \, d\tau, \quad \forall \Omega. \quad (2.21)$$

As seen in Section 2.3, the integral formulation (2.21) is the original formulation of the model for single-phase flow in porous medium. The differential form (2.20) of the representative model follows from Equation (2.21) when  $\mathbf{q}$  is sufficiently smooth for the divergence theorem of calculus to be applicable.

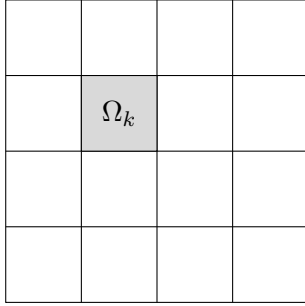
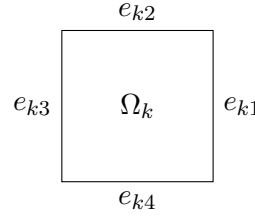
## Chapter 3

# Control Volume Methods

Control volume methods (CVMs) are a class of numerical methods used to apply spatial discretization to PDEs. CVMs are popular methods due to the fact that they satisfy the physical principle of mass conservation, in addition to being fairly easy to formulate for complex grids. The two CVMs TPFA and MPFA are the preferred CVMs when simulating flow in porous medium. This is due to the two methods yielding explicit expressions for the fluxes and harmonic averaging of the permeability, see [4], in addition to the CVM class properties. In this chapter we will first introduce the general background theory for these two CVMs, before deriving the methods explicitly. At the end of the chapter, we will look closer at the convergence theory of the MPFA method and develop a theoretical framework for the method on a uniform square grid in a homogeneous medium. All theory in Sections 3.1 to 3.3 is based on the lecture notes and article by I. Aavatsmark [4, 24] and the PhD thesis of S. S. Mundal [22]. The theoretical framework in Section 3.5 is found in the article by Nordbotten et al. [21].

### **3.1 General Theory of the Two-Point Flux Approximation Method (TPFA) and the Multi-Point Flux Approximation $O(\eta)$ -Method (MPFA)**

Starting with our representative equation (2.20), the two CVMs TPFA and MPFA are based on the integral formulation (2.21) of the problem. Recall, the integral formulation is a representation of the principle of mass conservation when both the fluid and the porous medium are incompressible. By discretizing the square domain  $\Omega$  into cells  $\Omega_k$ , see Figure 3.1, and assuming that the principle of mass conservation (2.21) holds for

FIGURE 3.1: Discretization of a domain  $\Omega$  into cells  $\Omega_k$ .FIGURE 3.2: Numbering of the edges of cell  $\Omega_k$ .

each of these cells, we obtain the following equation

$$\int_{\partial\Omega_k} \mathbf{q} \cdot \mathbf{n}_i \, d\sigma = \int_{\Omega_k} f \, d\tau, \quad \forall \Omega_k. \quad (3.1)$$

Here  $\partial\Omega_k$  denotes the boundary of cell  $\Omega_k$ , and  $\mathbf{n}_k$  the outwards unit normal vector of  $\partial\Omega_k$ . As in Chapter 2,  $f$  and  $\mathbf{q}$  refers to the mass source density and the volumetric flux.

The boundary  $\partial\Omega_k$  of cell  $\Omega_k$  may be decomposed into the edges  $e_{ki}$ ,  $i = 1, 2, \dots, N_{e_k}$ , see Figure 3.2, where  $N_{e_k}$  is the total number of edges present in  $\partial\Omega_k$ . Then, by letting  $q_{ki}$  denote the flux through edge  $e_{ki}$ , we can write the flux through the boundary  $\partial\Omega_k$  of cell  $\Omega_k$  as a sum of the fluxes across the edges,  $e_{ki}$ ,  $i = 1, 2, \dots, N_{e_k}$ ,

$$\sum_{i=1}^{N_{e_k}} q_{ki} = - \sum_{i=1}^{N_{e_k}} \int_{e_{ki}} \mathbf{K} \nabla u(\mathbf{x}) \cdot \mathbf{n}_{ki} \, d\sigma_{ki}. \quad (3.2)$$

Here  $\mathbf{n}_{ki}$  is the outwards unit normal of edge  $e_{ki}$  and  $d\sigma_{ki}$  the infinitesimal length of the same edge. In Equation (3.2) the volumetric flux  $\mathbf{q}$  is expressed in accordance with Darcy's law (2.3) from Section 2.2.

Equation (3.2) yields a continuous expression for the fluxes through the edges  $e_{ki}$ ,  $i = 1, 2, \dots, N_{e_k}$ , from cell  $\Omega_k$ . This expression forms the basis of the discrete framework used to calculate the fluxes in the TPFA and MPFA method. By requiring that the fluxes are continuous across the boundary of each cell  $\Omega_k$  in  $\Omega$ , the flux  $q_j$  through edge  $e_j$  has to be the same on both sides of the edge. Using this continuity property, the flux through an edge may be represented as a weighted sum of cell center potentials

$$q_j = \sum_{k \in V_j} t_{j,k} u_k. \quad (3.3)$$

Here  $V_j$  is the collection of all cells making contributions to the flux through edge  $e_j$ , and  $u_k$  is the potential in the cell centers of the cells in  $V_j$ . The coefficients  $t_{j,k}$  are called the

*edge transmissibilities* through edge  $e_j$  from cell  $k$ , and are the discrete representation of the integral over edge  $e_j$  of the permeability in cell  $k$  dotted with the normal vector. Therefore, the edge transmissibilities  $t_{j,k}$  are only dependent on the geometry of the grid and the permeability. In addition, these coefficients have to satisfy the fact that if the potential in each cell is the same there are no potential differences creating a flow. This means that if all the cell center potentials are the same, there should be no flux between the cells. Hence, the edge transmissibilities should satisfy

$$\sum_{k \in V_j} t_{j,k} = 0. \quad (3.4)$$

In Equation (3.3) we have implicitly assumed that the potential is continuous at a specific point on each edge of the cells  $\Omega_k$ . These points are called *continuity points*, and are used when calculating the discrete representation of the gradient of the potential in a cell. The gradient is approximated by the difference in potential between the continuity point and the cell center. Since the potential is continuous at the continuity points, these values may be removed from Equation (3.3) by various methods.

To calculate the cell center potentials using the TPFA or MPFA method we first need to sum the fluxes across all the edges of each cell  $\Omega_k$  to get the total divergence of fluid from the cell. Setting these sums equal to a chosen discrete representation of the source term in each cell, we obtain a global system of equations which can be solved for the potentials in the cell centers. The discrete representation of the source may for example be the integral of the source term over the cell, or the source term evaluated in the cell center.

## 3.2 The TPFA Method

The TPFA method is the simplest of our two CVMs, and is therefore widely used. However, the method only yields consistent flux approximations if the discretized grid is what we call  *$\mathbf{K}$ -orthogonal*.

The  $\mathbf{K}$ -orthogonality of a grid is connected with the expression giving the flux through the edges of a cell, Equation (3.2). From this equation we see that the flux expression for one edge reads

$$q_j = - \int_{e_j} \mathbf{K} \nabla u(\mathbf{x}) \cdot \mathbf{n}_j \, d\sigma_j. \quad (3.5)$$

By assuming that  $\mathbf{K}$  is constant in each cell and that the edge  $e_j$  is a straight line, the vector  $\mathbf{K}\mathbf{n}_j$  is constant on each edge  $e_j$ ,  $j = 1, 2, \dots, N_{e_k}$ , of a cell. Recall from Section 2.1 that the permeability  $\mathbf{K}$  is a positive definite matrix (assuming we have an orthogonal

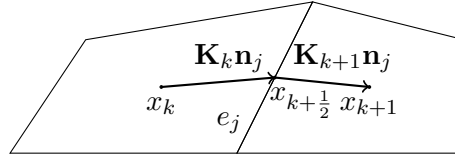


FIGURE 3.3: The direction of vectors  $\mathbf{K}_k \mathbf{n}_j$  and  $\mathbf{K}_{k+1} \mathbf{n}_j$  in a  $\mathbf{K}$ -orthogonal grid.

frame of reference). Thus we obtain  $\mathbf{n}_j^T \mathbf{K}_j \mathbf{n}_j > 0$ , which means that  $\mathbf{K}_j \mathbf{n}_j$  points into the same cell as  $\mathbf{n}_j$ .

Having seen these properties on  $\mathbf{K}_j \mathbf{n}_j$ , we define a  $\mathbf{K}$ -orthogonal grid to be a grid where the lines connecting the cell centers of two adjacent cells to the midpoint on the interface between them runs along the directions of  $\mathbf{K}_j \mathbf{n}_j$  in each cell, see Figure 3.3. This meaning, if  $x_k$  and  $x_{k+1}$  are the cell centers of two adjacent cells and  $x_{k+\frac{1}{2}}$  the midpoint on the interface between the cells, the line connecting  $x_k$  and  $x_{k+\frac{1}{2}}$  runs along  $\mathbf{K}_k \mathbf{n}_j$  and the line connecting  $x_{k+1}$  and  $x_{k+\frac{1}{2}}$  runs along  $\mathbf{K}_{k+1} \mathbf{n}_j$ . Subscripts  $k$  and  $k+1$  on the permeability denotes the cells for which it belongs to. Note that the vectors  $\mathbf{K}_j \mathbf{n}_j$  can be both longer or shorter than the lines connecting the cell centers and the midpoint of the edge, only the direction is considered. For further properties of  $\mathbf{K}$ -orthogonal grids see [4] p. 144-146.

Assuming our grid is  $\mathbf{K}$ -orthogonal, we may now develop the TPFA method. Let  $x_k$  and  $x_{k+1}$  be the cell centers of cells  $k$  and  $k+1$ , and  $x_{k+\frac{1}{2}}$  the midpoint on edge  $e_j$ , acting as interface between the cells, as seen in Figure 3.3. Equation (3.5) tells us that the flux across edge  $e_j$  may be expressed as the directional derivative of the potential in the direction of  $\mathbf{K}_j \mathbf{n}_j$  integrated over  $e_j$ . If the gradient of the potential,  $\nabla u$ , is constant on each side of the interface  $e_j$ , the directional derivative of the potential in the direction of  $\mathbf{K}_j \mathbf{n}_j$  can be approximated by the potential difference between the cell center and the midpoint of edge  $e_j$  in each cell divided by the length between the two points. Hence, we get the following approximation of the flux across  $e_j$  from cell  $k$  and  $k+1$  respectively

$$q_j \approx \Gamma_j \|\mathbf{K}_k \mathbf{n}_j\|_2 \frac{u_k - \bar{u}_{k+\frac{1}{2}}}{\|x_k - x_{k+\frac{1}{2}}\|_2}, \quad (3.6)$$

$$q_j \approx \Gamma_j \|\mathbf{K}_{k+1} \mathbf{n}_j\|_2 \frac{\bar{u}_{k+\frac{1}{2}} - u_{k+1}}{\|x_{k+1} - x_{k+\frac{1}{2}}\|_2}. \quad (3.7)$$

Here  $\Gamma_j$  is the length of edge  $e_j$ , which is multiplied into the expression to approximate the integral over  $e_j$ . The potential values  $u_k$  and  $u_{k+1}$  corresponds to the cell center potentials in cells  $k$  and  $k+1$  respectively, and  $\bar{u}_{k+\frac{1}{2}}$  the potential value at  $x_{k+\frac{1}{2}}$ . Subscript 2 on the norms in Equations (3.6) and (3.7) refers to the  $p$ -norm with  $p=2$ . Note that Equations (3.6) and (3.7) yield exact fluxes whenever the gradient of the

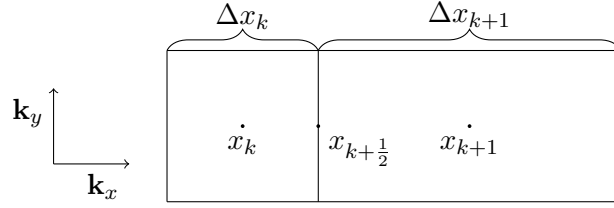


FIGURE 3.4: Orthogonal grid with principal directions of the permeability tensor,  $\mathbf{k}_x$  and  $\mathbf{k}_y$ , parallel to the grid directions.

potential,  $\nabla u$ , is constant on each side of the edge. This is the case whenever the potential,  $u$ , is a constant or a linear function.

Recall that we assume the fluxes to be continuous across all the edges in the domain when using the TPFA and MPFA methods. If we also set the potential continuity points to be the midpoints on the edges, we can add the two Equations (3.6) and (3.7) to get rid of the potential on the edge midpoint,  $\bar{u}_{k+\frac{1}{2}}$ . Rearranging the obtained equation into a difference between the cell center potentials yields the following result

$$u_k - u_{k+1} = \frac{q_j}{\Gamma_j} \left( \frac{\|x_k - x_{k+\frac{1}{2}}\|_2}{\|\mathbf{K}_k \mathbf{n}_j\|_2} + \frac{\|x_{k+1} - x_{k+\frac{1}{2}}\|_2}{\|\mathbf{K}_{k+1} \mathbf{n}_j\|_2} \right) = q_j (t_{j,k}^{-1} + t_{j,k+1}^{-1}). \quad (3.8)$$

Here  $t_{j,k}$  refers to the edge transmissibilities from the general expression for the fluxes in the TPFA and MPFA methods, Equation (3.3).

If the grid used in the TPFA method is orthogonal and the principal directions of the permeability matrix is parallel to the grid directions, see Figure 3.4, the TPFA formula (3.8) reduces to

$$q_j = - \frac{u_{k+1} - u_k}{\frac{1}{2} \left( \frac{\Delta x_k}{k_{x,k}} + \frac{\Delta x_{k+1}}{k_{x,k+1}} \right)}. \quad (3.9)$$

In this equation  $k_{x,k}$  refers to the  $x$ -directional element of the permeability tensor in cell  $k$ . Recall from Section 2.1 that only the diagonal elements of  $\mathbf{K}$  are non-zero when the principal directions of  $\mathbf{K}$  are aligned with the directions of an orthogonal grid. The values  $\Delta x_k$  and  $\Delta x_{k+1}$  corresponds to the length of cells  $k$  and  $k+1$ .

This special case of the TPFA method, Equation (3.9), corresponds to a one dimensional finite difference scheme in the  $x$ -direction. Similarly, we can construct a one dimensional finite difference scheme in the  $y$ -direction. Hence, using the TPFA method on an orthogonal grid with the principal directions of  $\mathbf{K}$  aligned with the grid directions is equivalent to using a one dimensional finite difference scheme in each grid direction.

### 3.3 The MPFA method

The MPFA method, developed simultaneously and independently by I. Aavatsmark et al. [5] and M. G. Edwards and C. F. Rodgers [6], is the CVM we are mainly interested in in this thesis. For a  $\mathbf{K}$ -orthogonal grid the MPFA method reduces to the TPFA method described in Section 3.2. However, unlike TPFA, the MPFA method does not yield inconsistent flux expressions when considering a grid which is *not*  $\mathbf{K}$ -orthogonal. The method is therefore convergent for a broader range of problems. In this section we will develop the MPFA method on a uniform square grid in two dimensions. The expansion to different grids and higher dimensions follows from the theory below.

To develop the MPFA method we first need to discretize the domain of the representative equation (2.20) for single-phase flow in porous medium. An example of this is shown in Figure 3.1 in Section 3.1. Then by drawing stapled lines between the cell centers and continuity points defined on each half-edge in the grid we draw what is called a *dual grid*. Figure 3.5 shows the dual grid of a uniform two dimensional discretization of a square domain with the continuity points being the edge midpoints. The cells confined by the dual grid are referred to as *interaction volumes*.

Figure 3.6 gives a closer look at one of the interaction volumes defined in Figure 3.5. Here  $x_1, \dots, x_4$  and  $\bar{x}_1, \dots, \bar{x}_4$  are respectively the cell centers and the continuity points on the half-edges in the original discretization grid. Inside the interaction volume there are four half-edges. The MPFA method is based on approximating the fluxes over these four half-edges for all the interaction volumes in the domain. Having found these, the fluxes are added together edgewise to obtain the fluxes across the entire edges in the original discretization grid.

To find the fluxes over the half-edges within an interaction volume we first express the potential,  $u$ , as a linear function in each of the four subcells inside the interaction volume. In two dimensions a general linear function is determined by three coefficients. Thus, we get a total of twelve degrees of freedom for the four linear functions within an interaction volume. Four of these are determined by the potential values at the cell centers of the subcells. The remaining eight are obtained by assuming that the flux is continuous over each of the four half-edges, and that the potential is continuous at the continuity points on the half-edges.

In Figure 3.5 we have assumed that the continuity points of the MPFA method are situated at the midpoint of the edges in the discretization grid. This is not always the case. The  $\eta$  in multi-point flux approximation  $O(\eta)$ -method refers to the placement of these continuity points. By considering a half-edge in an interaction volume,  $\eta$  gives the percentage of distance, relative to the length of the half-edge, away from the midpoint

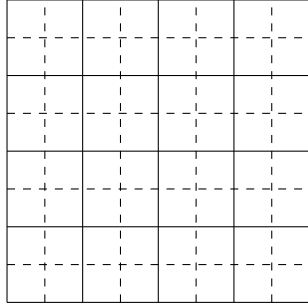


FIGURE 3.5: The dual grid on a uniform two dimensional discretization of a square domain.

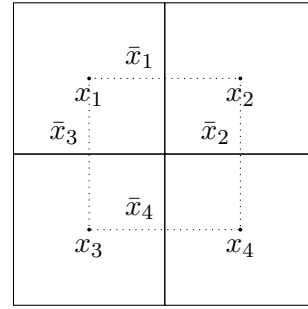


FIGURE 3.6: The interaction volume between four square cells.

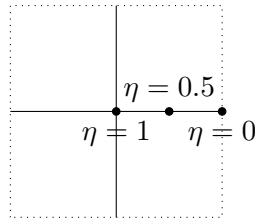


FIGURE 3.7: Placement of the continuity point on a half-edge for different values of  $\eta$ .

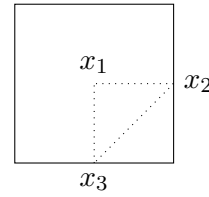


FIGURE 3.8: Triangle in a subcell made up by the cell centers and the continuity points.

of the edge the continuity point is to be situated. Figure 3.7 shows how the position of the continuity point shifts for different values of  $\eta$ . Hence, the MPFA method is not just *one* method, but a family of CVMs differing from one another by the placement of the continuity points.

Notice that in each subcell in an interaction volume, the cell center and the edge continuity points make up a triangle. Let us name the coordinates of these points by  $\mathbf{x}_j$ ,  $j = 1, 2, 3$ , in accordance to Figure 3.8. By using barycentric coordinates we may then represent  $u$  as the following linear function in each subcell

$$u(\mathbf{x}) = \sum_{i=1}^3 u_i \phi_i(\mathbf{x}). \quad (3.10)$$

The functions  $\phi_i(\mathbf{x})$  are the linear barycentric basis functions, satisfying  $\phi_i(\mathbf{x}_j) = 0$  for  $i, j \in [1, 3]$ ,  $i \neq j$ , and  $\phi_i(\mathbf{x}_j) = 1$  for  $i = j$ . Recall from Darcy's law (2.3) that the flux is calculated by the gradient of the potential. Hence, we need to calculate the gradient of the linear representation of the potential, Equation (3.10).

Each of the three basis functions  $\phi_i(\mathbf{x})$ ,  $i = 1, 2, 3$ , can be written as general linear functions in two dimensions

$$\phi_1(\mathbf{x}) = a_1 + b_1x + c_1y, \quad (3.11)$$

$$\phi_2(\mathbf{x}) = a_2 + b_2x + c_2y, \quad (3.12)$$

$$\phi_3(\mathbf{x}) = a_3 + b_3x + c_3y, \quad (3.13)$$

where  $\mathbf{x} = (x, y)^T$ . Let the vertices of the triangle be denoted by  $\mathbf{x}_j = (x_j, y_j)^T$ ,  $j = 1, 2, 3$ . Then, by using the fact that  $\phi_i(\mathbf{x}_j) = 0$  for  $i, j \in [1, 3]$ ,  $i \neq j$  and  $\phi_i(\mathbf{x}_j) = 1$  for  $i = j$ , we can determine the coefficients  $a_i$ ,  $b_i$  and  $c_i$ ,  $i = 1, 2, 3$ , in Equations (3.11) to (3.13) by solving the following linear system

$$\begin{pmatrix} 1 & x_1 & y_1 \\ 1 & x_2 & y_2 \\ 1 & x_3 & y_3 \end{pmatrix} \begin{pmatrix} a_1 & a_2 & a_3 \\ b_1 & b_2 & b_3 \\ c_1 & c_2 & c_3 \end{pmatrix} = \begin{pmatrix} 1 & 0 & 0 \\ 0 & 1 & 0 \\ 0 & 0 & 1 \end{pmatrix}. \quad (3.14)$$

Having found the coefficients of the basis functions, the gradient of the potential can be calculated by

$$\nabla u(\mathbf{x}) = \sum_{i=1}^3 u_i \nabla \phi_i(\mathbf{x}), \quad (3.15)$$

where the gradients of the basis functions are given by

$$\nabla \phi_i(\mathbf{x}) = (b_i, c_i)^T, \quad i = 1, 2, 3. \quad (3.16)$$

Equation (3.2) states that the flux through an edge can be calculated by the integral over the edge of the volumetric flux from Darcy's Law (2.3) dotted with the outwards unit normal vector of the edge. In accordance to Figure 3.6, the fluxes across the half-edges in the interaction volume from subcell 1 may thus be approximated by

$$\begin{aligned} \begin{pmatrix} q_1^{(1)} \\ q_3^{(1)} \end{pmatrix} &= - \begin{pmatrix} \Gamma_1 \mathbf{n}_1^T \\ \Gamma_3 \mathbf{n}_3^T \end{pmatrix} \mathbf{K}_1 \nabla u(\mathbf{x}) \\ &= - \begin{pmatrix} \Gamma_1 \mathbf{n}_1^T \mathbf{K}_1 (u_1 \nabla \phi_1^{(1)}(\mathbf{x}) + \bar{u}_1 \nabla \phi_2^{(1)}(\mathbf{x}) + \bar{u}_3 \nabla \phi_3^{(1)}(\mathbf{x})) \\ \Gamma_3 \mathbf{n}_3^T \mathbf{K}_1 (u_1 \nabla \phi_1^{(1)}(\mathbf{x}) + \bar{u}_1 \nabla \phi_2^{(1)}(\mathbf{x}) + \bar{u}_3 \nabla \phi_3^{(1)}(\mathbf{x})) \end{pmatrix}. \end{aligned} \quad (3.17)$$

Here  $\Gamma_j$  and  $\mathbf{n}_j$  is the length and the outwards unit normal of half-edge  $j$  respectively, and  $q_j^{(k)}$  the flux through half-edge  $j$  from cell  $k$ . The superscript on  $\phi_i^{(1)}(\mathbf{x})$ ,  $i = 1, 2, 3$ , represent the cell the basis function belongs to.

The MPFA method is based on the assumptions of continuity of fluxes across the half-edges in an interaction volume and continuity of the potential at continuity points on the

half-edges. This means that the following equalities holds for the fluxes in the interaction volume in Figure 3.6

$$q_1 = q_1^{(1)} = q_1^{(2)}, \quad (3.18)$$

$$q_2 = q_2^{(2)} = q_2^{(4)}, \quad (3.19)$$

$$q_3 = q_3^{(1)} = q_3^{(3)}, \quad (3.20)$$

$$q_4 = q_4^{(3)} = q_4^{(4)}. \quad (3.21)$$

Inserting similar formulas as the one obtained in Equation (3.17) for the fluxes in Equations (3.18) to (3.21) yields

$$\begin{aligned} q_1 &= \Gamma_1 \mathbf{n}_1^T \mathbf{K}_1 (u_1 \nabla \phi_1^{(1)}(\mathbf{x}) + \bar{u}_1 \nabla \phi_2^{(1)}(\mathbf{x}) + \bar{u}_3 \nabla \phi_3^{(1)}(\mathbf{x})) \\ &= \Gamma_1 \mathbf{n}_1^T \mathbf{K}_2 (u_2 \nabla \phi_1^{(2)}(\mathbf{x}) + \bar{u}_1 \nabla \phi_2^{(2)}(\mathbf{x}) + \bar{u}_2 \nabla \phi_3^{(2)}(\mathbf{x})), \end{aligned} \quad (3.22)$$

$$\begin{aligned} q_2 &= \Gamma_2 \mathbf{n}_2^T \mathbf{K}_2 (u_2 \nabla \phi_1^{(2)}(\mathbf{x}) + \bar{u}_1 \nabla \phi_2^{(2)}(\mathbf{x}) + \bar{u}_2 \nabla \phi_3^{(2)}(\mathbf{x})) \\ &= \Gamma_2 \mathbf{n}_2^T \mathbf{K}_4 (u_4 \nabla \phi_1^{(4)}(\mathbf{x}) + \bar{u}_4 \nabla \phi_2^{(4)}(\mathbf{x}) + \bar{u}_2 \nabla \phi_3^{(4)}(\mathbf{x})), \end{aligned} \quad (3.23)$$

$$\begin{aligned} q_3 &= \Gamma_3 \mathbf{n}_3^T \mathbf{K}_1 (u_1 \nabla \phi_1^{(1)}(\mathbf{x}) + \bar{u}_1 \nabla \phi_2^{(1)}(\mathbf{x}) + \bar{u}_3 \nabla \phi_3^{(1)}(\mathbf{x})) \\ &= \Gamma_3 \mathbf{n}_3^T \mathbf{K}_3 (u_3 \nabla \phi_1^{(3)}(\mathbf{x}) + \bar{u}_4 \nabla \phi_2^{(3)}(\mathbf{x}) + \bar{u}_3 \nabla \phi_3^{(3)}(\mathbf{x})), \end{aligned} \quad (3.24)$$

$$\begin{aligned} q_4 &= \Gamma_4 \mathbf{n}_4^T \mathbf{K}_3 (u_3 \nabla \phi_1^{(3)}(\mathbf{x}) + \bar{u}_4 \nabla \phi_2^{(3)}(\mathbf{x}) + \bar{u}_3 \nabla \phi_3^{(3)}(\mathbf{x})) \\ &= \Gamma_4 \mathbf{n}_4^T \mathbf{K}_4 (u_4 \nabla \phi_1^{(4)}(\mathbf{x}) + \bar{u}_4 \nabla \phi_2^{(4)}(\mathbf{x}) + \bar{u}_2 \nabla \phi_3^{(4)}(\mathbf{x})). \end{aligned} \quad (3.25)$$

Similarly as for the TPF method we wish to express the fluxes over the half-edges in the interaction volume using only the cell center potentials. If the discretization grid is  $\mathbf{K}$ -orthogonal we may eliminate the potentials  $\bar{u}_i$  at the continuity points in the same way as for the TPF method. However, if the discretization grid is *not*  $\mathbf{K}$ -orthogonal, we need to eliminate the potentials at the continuity points in another way. This is done by assembling the fluxes and the potentials in Equations (3.22) to (3.25) in the vectors  $\mathbf{q}_{iv} = (q_1, q_2, q_3, q_4)^T$ ,  $\mathbf{u}_{iv} = (u_1, u_2, u_3, u_4)^T$  and  $\mathbf{v}_{iv} = (\bar{u}_1, \bar{u}_2, \bar{u}_3, \bar{u}_4)^T$ . Subscripts  $iv$  are introduced to emphasize the fact that these values are restricted to interaction volumes. Then the first and second equality in Equations (3.22) to (3.25) may be written as

$$\mathbf{q}_{iv} = \mathbf{C}_{iv} \mathbf{v}_{iv} + \mathbf{D}_{iv} \mathbf{u}_{iv}, \quad (3.26)$$

and

$$\mathbf{A}_{iv} \mathbf{v}_{iv} = \mathbf{B}_{iv} \mathbf{u}_{iv}, \quad (3.27)$$

respectively, where  $\mathbf{A}_{iv}$ ,  $\mathbf{B}_{iv}$ ,  $\mathbf{C}_{iv}$  and  $\mathbf{D}_{iv}$  are the coefficient matrices of the potentials. Solving Equation (3.27) for the vector  $\mathbf{v}_{iv}$  yields

$$\mathbf{v}_{iv} = \mathbf{A}_{iv}^{-1} \mathbf{B}_{iv} \mathbf{u}_{iv}. \quad (3.28)$$

Inserting Equation (3.28) into Equation (3.26) eliminates the potentials at the continuity points, and we get the following expression for the fluxes in the interaction volume in terms of the cell center potentials

$$\mathbf{q}_{iv} = \mathbf{C}_{iv} \mathbf{A}_{iv}^{-1} \mathbf{B}_{iv} \mathbf{u}_{iv} + \mathbf{D}_{iv} \mathbf{u}_{iv}. \quad (3.29)$$

This equation is usually written as

$$\mathbf{q}_{iv} = \mathbf{T}_{iv} \mathbf{u}_{iv}, \quad (3.30)$$

where

$$\mathbf{T}_{iv} = \mathbf{C}_{iv} \mathbf{A}_{iv}^{-1} \mathbf{B}_{iv} + \mathbf{D}_{iv} \quad (3.31)$$

is called the *local transmissibility matrix*.

Solving system (3.30) for each interaction volume in our dual grid yields the fluxes over each half-edge in the discretization grid. Adding the fluxes over the half-edges corresponding to the same edge gives us the flux across the entire edge. This can be written as the linear system

$$\mathbf{q} = \mathbf{T} \mathbf{u}. \quad (3.32)$$

Here  $\mathbf{q}$  and  $\mathbf{u}$  are the vectors containing the fluxes across all the edges in the grid and the cell center potentials of all the cells in the grid respectively. Matrix  $\mathbf{T}$ , called the *global transmissibility matrix*, holds the coefficients obtained by making the correct adjustments to the linear system in each interaction volume, Equation (3.30), to obtain the global system, Equation (3.32). This system is the MPFA method equivalent to Equation (3.3) in Section 3.1 giving the general form of the flux expressions in the TPFA and MPFA method.

The principle of mass conservation (2.8) asserts that the source input/output of mass in a region has to equal the accumulation minus the outflux of mass of the region. In our representative equation (2.20), and the cellwise equivalent integral formulation (3.1), for which we have based our development of the TPFA and MPFA method on, the accumulation term disappears due to the assumptions of the fluid and the medium being incompressible. Hence, the source of mass in the region only equals the outflux of

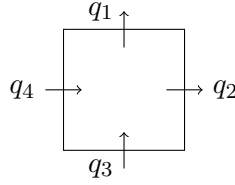


FIGURE 3.9: Fluxes through the edges of a cell

mass from the region. Therefore, the cellwise mass conservation (3.1) can be written as

$$q_1 + q_2 - q_3 - q_4 = f_k, \quad (3.33)$$

where  $q_i$ ,  $i = 1, 2, 3, 4$ , refers to the fluxes over the edges of cell  $k$ , see Figure 3.9. The  $f_k$  in Equation (3.33) is a discrete representation of the integral of the source over cell  $k$ .

By using Equation (3.32) to manipulate Equation (3.33) from being a sum of fluxes to being a sum of potentials, we obtain the following weighted sum of cell center potentials to describe mass conservation in cell  $k$

$$\sum_{l \in \mathcal{K}_k} m_l u_l = f_k. \quad (3.34)$$

Here the values  $m_l$  are weights defined by the elements in matrix  $\mathbf{T}$  in Equation (3.32), and  $\mathcal{K}_k$  is the set containing the indexes of the cells included in the potential stencil for cell  $k$ . The number of cells included in  $\mathcal{K}_k$  is dependent on the permeability and the continuity point indicator  $\eta$ . For example, for a permeability with principal directions aligned with the directions of the grid and  $\eta = 0$ , we get a five-point stencil for internal cells. This stencil consists of the cell center potential in cell  $k$  and the cells over, under, left and right of cell  $k$ . Then the MPFA method reduces to the TPFA method. However, if the principal directions are *not* aligned with the directions of the grid, a nine-point stencil is obtained. This is the case where the MPFA method shows its superiority over the TPFA method.

By assembling a linear system with the  $k$ 'th line in the system corresponding to Equation (3.34), we obtain the global system of the MPFA method describing mass conservation in each cell of the grid. Hence, the system describes mass conservation in the entire domain. This is a linear system with the cell center potentials as unknowns, and we write it as

$$\mathbf{A}\mathbf{u} = \mathbf{b}, \quad (3.35)$$

where  $\mathbf{b}$  is the vector containing the discrete representation of the source term in each cell. The system matrix  $\mathbf{A}$  contains the coefficients  $m_l$  from Equation (3.34).

### 3.4 Convergence Theory of the MPFA Method

Due to the suitability of the MPFA method for modeling flow in porous medium, convergence theory of the method has been an area of extensive research the last decade. In 2006, convergence of the MPFA  $O(0)$ -method, derived in reference space, on asymptotic  $h^2$ -parallelogram grids in two dimensions was proved [10]. Later that same year the proof was extended to general quadrilateral grids in two dimensions [11], this time for the method derived in physical space, like in Section 3.3. A convergence proof on quadrilateral grid for a method fairly similar to the MPFA  $O(0)$ -method was also published in 2006 [12]. All of these proofs relied on establishing a connection between the MPFA method and the mixed finite element method (MFEM) using a specific numerical quadrature.

In later years more general convergence proofs have been published. Following the discovery of a convergence proof of the mimetic finite difference method (MFDM) without using a connection to the MFEM in 2005 [25]. Convergence of the MPFA method on several new grid geometries and with different anisotropies in two and three dimensions was proved by looking at the method in a MFDM framework [13–15]. In 2008, a rather general proof of convergence of the MPFA method using a discrete hybrid variational formulation was presented [16]. This proof was further generalized in 2010 [26].

Numerical convergence tests of the MPFA method have been provided in [17–20]. Below we will give a brief overview of the results obtained in the theoretical and numerical convergence articles on the MPFA method needed to interpret the results obtained in this thesis.

Both the TPFA and MPFA method yield fluxes and potential exact to working precision for constant and linear potentials. This situation is equivalent to the gradient of the potential being constant. Due to the approximations of the fluxes being derived by assuming that the gradient of the potential is constant on both sides of an edge for the TPFA method, this property follows automatically from the development of the method. For the MPFA method, pages 1086-1087 in the article by G. T. Eigestad and R. A. Klausen [17] gives a simple proof of the property.

For general potential functions on quadrilateral grids in two dimensions second order convergence for the potential and first order convergence for the flux have been proved analytically in the literature. For asymptotic  $h^2$ -parallelogram grids in two dimensions second order convergence of the fluxes is observed numerically, but this result has not been proved. The results were based on using discrete  $\mathcal{L}^2$ -norms, found in for example [27]. These norms will be explained in detail in Sections 4.2 and 4.3.

### 3.5 Theoretical Framework for the MPFA Method on a Uniform Parallelogram Grid in a Homogeneous Medium

To apply an error analysis as general as possible for the MPFA method we wish to employ the theoretical framework for a special class of CVMs developed by J. M. Nordbotten et al. in [21]. This framework imposes general formulas on the weights  $t_{j,k}$  and  $m_l$  in Equations (3.3) and (3.34), which proves to be invaluable in the next chapter.

The class in question is comprised of all CVMs satisfying the following three properties; the method is locally conservative, it has local flux representation and it is exact for constant and linear potentials. In addition to these properties on the CVM, the discretization grid has to be a uniform parallelogram grid in a homogeneous medium for the theoretical framework to be valid. The MPFA method is part of this class of CVMs. Below we will give a brief introduction to the framework introduced in the article on a uniform square grid in a homogeneous medium.

From Equation (3.3) we know that fluxes  $q_1$  and  $q_2$ , shown in Figure 3.10, may be expressed as

$$q_1 = \sum_{k=1}^6 t_{1,k} u_k, \quad (3.36)$$

$$q_2 = \sum_{k=2,3,5,6,8,9} t_{2,k} u_k. \quad (3.37)$$

Here  $k$  refers to the cell numbering in Figure 3.10. The set of cells making contributions to each of the fluxes in Equations (3.36) and (3.37) make up a subset of the grid cells called the *flux molecule* of the considered flux, see Figures 3.12 and 3.13.

Recall Equation (3.17) from Section 3.3 giving the expression for the fluxes through the half-edges of a subcell in an interaction volume. In I. Aavatsmark's introduction to the MPFA method [24] the equivalent of this equation is given as

$$\begin{pmatrix} q_1^{(k)} \\ q_2^{(k)} \end{pmatrix} = -\mathbf{G}_k \begin{pmatrix} \bar{u}_1 - u_k \\ \bar{u}_2 - u_k \end{pmatrix}. \quad (3.38)$$

Here fluxes  $q_1^{(k)}$  and  $q_2^{(k)}$  are the fluxes going through the half-edges associated with cell  $k$  in an interaction volume, and  $\bar{u}_1$  and  $\bar{u}_2$  the potential values at the continuity points on the half-edges. When considering a uniform square grid, the formula for  $\mathbf{G}_k$  becomes

$$\mathbf{G}_k = \begin{pmatrix} a & c \\ c & b \end{pmatrix} = \frac{1}{V_k} \begin{pmatrix} \mathbf{a}_2^{(k)} & \mathbf{a}_1^{(k)} \end{pmatrix}^T \mathbf{K}_k \begin{pmatrix} \mathbf{a}_2^{(k)} & \mathbf{a}_1^{(k)} \end{pmatrix}. \quad (3.39)$$

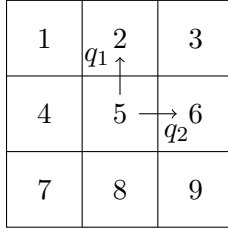


FIGURE 3.10: Two dimensional uniform square grid with specified cell numbering and fluxes.

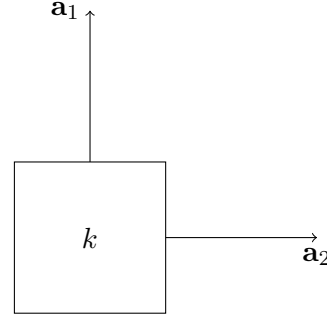


FIGURE 3.11: Normal vectors  $\mathbf{a}_1$  and  $\mathbf{a}_2$  of cell  $k$  having length equal to the edge lengths.

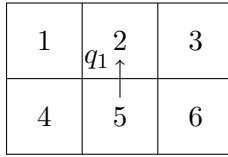


FIGURE 3.12: Flux molecule of  $q_1$ .

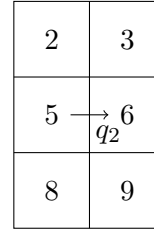


FIGURE 3.13: Flux molecule of  $q_2$ .

In this equation  $V_k$  and  $\mathbf{K}_k$  is the area and permeability of cell  $k$  respectively, and  $\mathbf{a}_1^{(k)}$  and  $\mathbf{a}_2^{(k)}$  are the normal vectors of the edges of cell  $k$  having length equal to the length of the edge it is normal to, see Figure 3.11. It is easy to see that Equation (3.39) is equivalent to a congruent transformation, which takes on the form

$$\mathbf{G}_k = \frac{1}{|\det(\mathbf{J}_k)|} \mathbf{J}_k^T \mathbf{K}_k \mathbf{J}_k. \quad (3.40)$$

From this it follows that  $\mathbf{G}_k$  is symmetric and positive definite if and only if  $\mathbf{K}_k$  is. Therefore on a uniform square grid in a homogeneous medium, the following symmetry conditions are imposed on the edge transmissibilities  $t_{j,k}$ ,  $j = 1, 2$ ,

$$\begin{aligned} t_{1,5} &= -t_{1,2}, & t_{1,6} &= -t_{1,1}, & t_{1,3} &= -t_{1,4}, \\ t_{2,5} &= -t_{2,6}, & t_{2,3} &= -t_{2,8}, & t_{2,2} &= -t_{2,9}. \end{aligned} \quad (3.41)$$

Using these symmetries, Equations (3.36) and (3.37) can be written as

$$q_1 = t_{1,5}(u_5 - u_2) + t_{1,6}(u_6 - u_1) + t_{1,3}(u_3 - u_4), \quad (3.42)$$

$$q_2 = t_{2,5}(u_5 - u_6) + t_{2,3}(u_3 - u_8) + t_{2,2}(u_2 - u_9). \quad (3.43)$$

By using Equation (3.38) instead of Equation (3.17) to calculate the fluxes over the half-edges in an interaction volume and by applying special linear potentials to manipulate the flux expressions, Nordbotten et al. was able to find a general representation for

the edge transmissibilities in Equations (3.42) and (3.43). Described by the quantities  $a$ ,  $b$  and  $c$  from Equation (3.39) and the indicator for the continuity points,  $\eta$ , the representations became

$$\begin{aligned} t_{1,5} &= b - \beta, & t_{2,5} &= a - \alpha, \\ t_{1,6} &= -\frac{c}{4} + \frac{\beta}{2}, & t_{2,3} &= -\frac{c}{4} - \frac{\alpha}{2}, \\ t_{1,3} &= -\frac{c}{4} - \frac{\beta}{2}, & t_{2,2} &= -\frac{c}{4} + \frac{\alpha}{2}. \end{aligned} \quad (3.44)$$

The coefficients  $\alpha$  and  $\beta$  are introduced to simplify notation, and are defined as

$$\alpha = \frac{ab\eta + c^2}{2b(1 + \eta)}, \quad (3.45)$$

$$\beta = \frac{ab\eta + c^2}{2a(1 + \eta)}. \quad (3.46)$$

Having calculated the fluxes across all the edges of a cell using Equations (3.42) and (3.43), we can use these expressions to get a general representation for the conservation of mass in a cell. From Equation (3.34) we know that a single line in the global system of equations describes the conservation of mass in one cell. By considering cell 5 in Figure 3.10, this line can be written as

$$\sum_{l=1}^9 m_l u_l = q_1 + q_2 - q_3 - q_4, \quad (3.47)$$

see Equations (3.33) and (3.34). Here  $q_3$  and  $q_4$  represent the fluxes between cell 8 and 5, and 4 and 5 respectively in Figure 3.10. When introducing

$$\gamma = \alpha + \beta = \frac{ab\eta + c^2}{d(1 + \eta)}, \quad d = \frac{2ab}{a + b}, \quad (3.48)$$

the weights  $m_l$ ,  $l = 1, \dots, 9$ , in Equation (3.47) can be represented by

$$\begin{aligned} m_1 = m_9 &= -t_{2,5} + t_{1,6} - t_{1,3} &= \frac{c}{2} - \frac{\gamma}{2}, \\ m_3 = m_7 &= t_{2,3} + t_{1,3} &= -\frac{c}{2} - \frac{\gamma}{2}, \\ m_4 = m_6 &= -t_{2,3} + t_{2,2} - t_{1,5} &= -a + \gamma, \\ m_2 = m_8 &= -t_{2,2} - t_{1,6} &= -b + \gamma, \\ m_5 &= -\sum_{l \in [1, 9] \setminus 5} m_l = 2(t_{2,5} + t_{1,5}) &= 2a + 2b - 2\gamma. \end{aligned} \quad (3.49)$$

Equations (3.42), (3.43) and (3.47) along with the coefficients given in Equations (3.44) and (3.49) imply that all CVMs being locally conservative, exact for constant and linear

potentials and having a local representation for the fluxes on a uniform square grid in a homogeneous medium are fully determined by four degrees of freedom. These four being  $a$ ,  $b$  and  $c$  from Equation (3.39) and the continuity point indicator  $\eta$ . Notice that the variables  $a$ ,  $b$  and  $c$  are only dependent on the permeability and the grid geometry. Therefore, if a grid and permeability is chosen, the only degree of freedom for determining a CVM satisfying the previously stated conditions is  $\eta$ .

## Chapter 4

# Theoretical Results

This chapter is devoted to using the theoretical framework developed in Section 3.5 in an error analysis of the MPFA method. In the first section we restate the the most important results obtained in the previous chapters, and specify a number of assumptions to ease the analysis. Sections 4.2 and 4.3 are used to explain how to approach the error analysis for both the potential and the fluxes. The central theoretical work is performed in Section 4.4. This section gives a general error analysis of the MPFA method for the trigonometric potential functions  $u(x, y) = \sin(x) \sin(y)$  and  $u(x, y) = \cos(x) \cos(y)$  for general permeabilities and different values of  $\eta$ . This analysis clearly showed that the MPFA should yield exact potential and fluxes on uniform square grids for diagonal permeabilities when  $\eta = 0$ . Building on these results, Section 4.5 is devoted to examining if similar results can be obtained for uniform rectangular grids in isotropic mediums when  $\eta = 0$ . The results obtained in Sections 4.4 and 4.5 are summarized in Section 4.6.

The error analysis done in this chapter only looks at the numerical stencils of the MPFA method associated with inner cells and edges which are *not* close to the boundary. These stencils are referred to as *full internal stencils*, an expression that will be defined in the beginning of Section 4.4. All the results summarized in Section 4.6 are linked to cells and edges yielding full internal stencils for the potentials and fluxes respectively. For a short comment on a priori conditions imposed on the boundary conditions in order for the MPFA method to retain the possibility of obtaining exact potential and flux for boundary stencils see Section 5.2.

### 4.1 Foundation and Assumptions

The representative equation (2.20) is the starting point for the theoretical analysis. Recall from Section 2.5, this equation is used to describe single-phase flow when both

the fluid and the porous medium are incompressible. For a given domain  $\Omega$ , the equation reads

$$\begin{cases} -\nabla \cdot (\mathbf{K}\nabla u) = f, & \text{in } \Omega, \\ u = u_0 \quad \text{or} \quad \mathbf{n}^T \mathbf{K}\nabla u = q_0, & \text{on } \partial\Omega. \end{cases} \quad (4.1)$$

The second line represents the boundary conditions, which can be either Dirichlet or Neumann conditions.

By using the MPFA method we discretize the elliptic Equation (4.1) to the linear system

$$\mathbf{A}\mathbf{u} = \mathbf{b}, \quad (4.2)$$

as shown in Section 3.3. The  $k$ 'th line in Equation (4.2) can be written as

$$\sum_{l \in \mathcal{K}_k} m_l u_l = f_k, \quad (4.3)$$

where the weights  $m_l$  are elements of matrix  $\mathbf{A}$ , and  $u_l$  and  $f_k$  elements in  $\mathbf{u}$  and  $\mathbf{b}$  respectively. Equation (4.3) represents mass conservation for one cell, and may therefore also take the form

$$\sum_{j=1}^{N_e} q_j = f_k. \quad (4.4)$$

Here  $q_j$ ,  $j = 1, \dots, N_e$ , are the fluxes from cell  $k$ , with  $N_e$  being the number of straight edges the cell comprises of. In this thesis we will always have  $N_e = 4$ . The fluxes in Equation (4.4) can be determined by

$$q_j = \sum_{k \in V_j} t_{j,k} u_k, \quad (4.5)$$

with  $t_{j,k}$  being the edge transmissibilities from cell  $k$  over edge  $j$ .

To simplify the error analysis of the MPFA method we will consider a uniform square grid with cell numbering from top left to bottom right. An example of a grid like this is showed in Figure 4.1, with  $x_i$  and  $y_i$ ,  $i = 1, 2, 3, 4$ , being arbitrary positions on the x- and y-axis respectively. The lengths  $\Delta x$  and  $\Delta y$  are set to be the half-length of the cell edges. This is done in order to ease the analysis when we start applying Taylor expansions. Notice that the grid having square cells yields  $\Delta x = \Delta y$ . We only consider the case with the grid directions being parallel to the axes of the coordinate system, this is to eliminate the possibility of a tilted grid. The edge normals are chosen to be

$$\mathbf{n}_1 = \begin{pmatrix} 0 \\ -1 \end{pmatrix}, \quad \mathbf{n}_2 = \begin{pmatrix} 1 \\ 0 \end{pmatrix}. \quad (4.6)$$

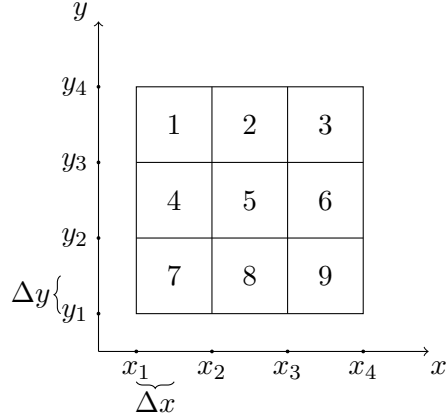


FIGURE 4.1: Two dimensional uniform square grid with cell numbering from top left to bottom right.

Assume the permeability

$$\mathbf{K} = \begin{pmatrix} k_1 & k_2 \\ k_2 & k_4 \end{pmatrix} \quad (4.7)$$

to be constant and equal for each cell in the grid. Calculating the  $\mathbf{G}_k$  matrix from Equation (3.39) then yields

$$\begin{aligned} \mathbf{G}_k &= \begin{pmatrix} a & c \\ c & b \end{pmatrix} = \frac{1}{V_k} \begin{pmatrix} \mathbf{a}_2^{(k)} & \mathbf{a}_1^{(k)} \end{pmatrix}^T \mathbf{K}_k \begin{pmatrix} \mathbf{a}_2^{(k)} & \mathbf{a}_1^{(k)} \end{pmatrix} \\ &= \frac{1}{\Delta x \Delta y} \begin{pmatrix} \Delta y & 0 \\ 0 & \Delta x \end{pmatrix} \begin{pmatrix} k_1 & k_2 \\ k_2 & k_4 \end{pmatrix} \begin{pmatrix} \Delta y & 0 \\ 0 & \Delta x \end{pmatrix} \\ &= \frac{1}{\Delta x \Delta y} \begin{pmatrix} k_1 (\Delta y)^2 & k_2 \Delta x \Delta y \\ k_2 \Delta x \Delta y & k_4 (\Delta x)^2 \end{pmatrix}. \end{aligned} \quad (4.8)$$

This formula holds for any cell  $k$ ,  $k = 1, 2, \dots, N_c$ , where  $N_c$  is the total number of cells in the grid. When  $\Delta x = \Delta y$ , Equation (4.8) becomes

$$\mathbf{G}_k = \begin{pmatrix} a & c \\ c & b \end{pmatrix} = \begin{pmatrix} k_1 & k_2 \\ k_2 & k_4 \end{pmatrix}. \quad (4.9)$$

Hence, each element in the permeability matrix corresponds directly to the element in the same position in  $\mathbf{G}_k$  when considering a uniform square grid.

Notice, by choosing the following permeability in our uniform square grid

$$\mathbf{K} = \begin{pmatrix} 0.5 & 0 \\ 0 & 2 \end{pmatrix}, \quad (4.10)$$

we obtain  $a = 0.5$  and  $b = 2$ . The same values of  $a$  and  $b$  are obtained in Equation (4.8)

when considering the situation where we have an isotropic permeability and a uniform *rectangular* grid with cells having side lengths  $\Delta x' = 2\Delta x$  and  $\Delta y' = \Delta y$ ,  $\Delta x$  and  $\Delta y$  being the original side lengths of the cells in the uniform square grid. The same thing is true for a permeability with  $k_2 \neq 0$ , only this would yield an isotropic permeability and a uniform *parallelogram* grid. Hence, having a uniform square grid with different anisotropies is equivalent to having an isotropic permeability on other uniform quadrilateral grid structures in the MPFA framework. We will look closer at the implications from this equivalence on the error analysis in Section 4.5.

## 4.2 Approach to the Error Analysis for the Potential

Consider the MPFA discretization (4.2) of our representative equation (4.1). By denoting the vectors containing exact and numerical cell center potentials by  $\mathbf{u}_e$  and  $\mathbf{u}_n$  respectively, we denote the potential error in the cell centers of the MPFA method in the discrete  $\mathcal{L}^2$ -norm by

$$\|\mathbf{u}_e - \mathbf{u}_n\|_{\mathcal{L}^2}. \quad (4.11)$$

This norm is found in Section 4 in [27] and is defined as follows

$$\|\mathbf{u}_e - \mathbf{u}_n\|_{\mathcal{L}^2} = \left( \frac{\sum_{k=1}^{N_c} A_k (u_{e,k} - u_{n,k})^2}{\sum_{k=1}^{N_c} A_k} \right)^{\frac{1}{2}}, \quad (4.12)$$

where  $k$  gives the indexes of the cells in the grid and  $A_k$  the area of cell  $k$ . The values  $u_{e,k}$  and  $u_{n,k}$  are the elements of vectors  $\mathbf{u}_e$  and  $\mathbf{u}_n$  related to cell  $k$ . To analyze the potential error in the cell centers, Equation (4.11), a similar analysis as the one explained in Sections 2.5 to 2.10 and 3.3 in [28] is applied.

Recall that the MPFA method is cellwise mass conservative. Thus, we know that

$$\mathbf{A}\mathbf{u}_n = \mathbf{b}_e. \quad (4.13)$$

Here it is assumed that the right-hand side vector  $\mathbf{b}$  is calculated exactly, hence the subscript  $e$ . Applying the vector containing the exact cell center potentials,  $\mathbf{u}_e$ , to matrix  $\mathbf{A}$  should therefore yield a perturbation vector  $\mathbf{v}$  on the right-hand side,

$$\mathbf{A}\mathbf{u}_e = \mathbf{b}_e + \mathbf{v}. \quad (4.14)$$

Vector  $\mathbf{v}$  contains the local truncation errors from the cellwise mass conservation, Equation (4.3), when applying the exact cell center potentials.

To find an expressions for the error in Equation (4.11) we can subtract Equations (4.13) and (4.14), resulting in

$$\begin{aligned}\mathbf{A}\mathbf{u}_e - \mathbf{A}\mathbf{u}_n &= \mathbf{b}_e - \mathbf{b}_n + \mathbf{v} \\ \mathbf{u}_e - \mathbf{u}_n &= \mathbf{A}^{-1}\mathbf{v}.\end{aligned}\tag{4.15}$$

Thus, we get the following upper bound on the potential error in the cell centers in the discrete  $\mathcal{L}^2$ -norm from Equation (4.12)

$$\|\mathbf{u}_e - \mathbf{u}_n\|_{\mathcal{L}^2} \leq \|\mathbf{A}^{-1}\|_{\mathcal{L}^2} \|\mathbf{v}\|_{\mathcal{L}^2}.\tag{4.16}$$

The inequality  $\|\mathbf{A}^{-1}\mathbf{v}\|_{\mathcal{L}^2} \leq \|\mathbf{A}^{-1}\|_{\mathcal{L}^2} \|\mathbf{v}\|_{\mathcal{L}^2}$  arises by defining  $\|\cdot\|_{\mathcal{L}^2}$  as the *subordinate matrix norm*

$$\|\mathbf{A}\|_{\mathcal{L}^2} = \sup_{\|\mathbf{x}\|_{\mathcal{L}^2} \neq 0} \frac{\|\mathbf{A}\mathbf{x}\|_{\mathcal{L}^2}}{\|\mathbf{x}\|_{\mathcal{L}^2}},\tag{4.17}$$

see Section 2.3 in [29], for vectors  $\mathbf{x}$  having equal dimension as  $\mathbf{v}$ . Since all matrix norms on matrices of equal dimensions are equivalent, see Section 2.3 in [29], we can write, as on page 23 in [30],

$$c' \|\mathbf{A}\|_{\mathcal{L}^2} \leq \|\mathbf{A}\|_2 \leq C' \|\mathbf{A}\|_{\mathcal{L}^2},\tag{4.18}$$

for constants  $c', C' > 0$ . It is easy to see that  $c'$  is of  $O(1)$ , and in fact  $c' = 1$ ,

$$\begin{aligned}\|\mathbf{A}\|_{\mathcal{L}^2} &= \sup_{\|\mathbf{x}\|_{\mathcal{L}^2} \neq 0} \frac{\|\mathbf{A}\mathbf{x}\|_{\mathcal{L}^2}}{\|\mathbf{x}\|_{\mathcal{L}^2}} = \sup_{\|\mathbf{x}\|_{\mathcal{L}^2} \neq 0} \left( \frac{\sum_{k=1}^{N_c} A_k y_k^2}{\sum_{k=1}^{N_c} A_k} \right)^{\frac{1}{2}} \left( \frac{\sum_{k=1}^{N_c} A_k x_k^2}{\sum_{k=1}^{N_c} A_k} \right)^{-\frac{1}{2}} \\ &\leq \sup_{\|\mathbf{x}\|_{\mathcal{L}^2} \neq 0} \left( \frac{M \sum_{k=1}^{N_c} y_k^2}{MN_c} \right)^{\frac{1}{2}} \left( \frac{M \sum_{k=1}^{N_c} x_k^2}{MN_c} \right)^{-\frac{1}{2}} \\ &= \sup_{\|\mathbf{x}\|_2 \neq 0} \frac{\|\mathbf{A}\mathbf{x}\|_2}{\|\mathbf{x}\|_2} \\ &= \|\mathbf{A}\|_2,\end{aligned}\tag{4.19}$$

where  $y_k$ ,  $k = 1, \dots, N_c$ , are the elements of  $\mathbf{A}\mathbf{x}$  and  $A_k \leq M$ . Using Equation (4.19), Equation (4.16) becomes

$$\|\mathbf{u}_e - \mathbf{u}_n\|_{\mathcal{L}^2} \leq \|\mathbf{A}^{-1}\|_2 \|\mathbf{v}\|_{\mathcal{L}^2} \leq O((\Delta x)^{\nu_A + \nu_v}),\tag{4.20}$$

where  $\nu_A$  and  $\nu_v$  are related to the bounds

$$\|\mathbf{A}^{-1}\|_2 \sim O((\Delta x)^{\nu_A}), \quad \|\mathbf{v}\|_{\mathcal{L}^2} \leq O((\Delta x)^{\nu_v}).\tag{4.21}$$

To find a value for  $\nu_A$  we first need to look at  $\|\mathbf{A}\|_2$ . From Section 3.4 we know that the MPFA method convergences on uniform parallelogram grids. This means that for this case matrix  $\mathbf{A}$  is invertible, and from the invertible matrix theorem (see for example

pages 145 and 328 in [31]) the matrix has only nonzero eigenvalues. This is also the case for the continuous elliptic operator for which  $\mathbf{A}$  is a discretization of, except for the case with Neumann boundary conditions [32]. The smallest eigenvalue of the continuous elliptic operator then equals zero, and  $\mathbf{A}$  becomes a singular matrix. However, this is handled in the discrete case by applying a least-squares procedure. The second smallest eigenvalue of the continuous operator does not approach zero when having Neumann boundary conditions [32]. Therefore no eigenvalues of  $\mathbf{A}$  approaches zero as  $\Delta x \rightarrow 0$  after applying the least squares procedure. Hence, the smallest possible eigenvalue of  $\mathbf{A}$ ,  $\lambda_{min}$ , is of  $O(1)$  magnitude.

Notice that matrix  $\mathbf{A}$  is the discretization of the second order derivative in space from the representative equation (4.1). Hence, the elements of the matrix should be similar to finite difference expressions, like

$$\frac{\partial^2 u}{\partial x^2} = \frac{u(x_{i+1}) - 2u(x_i) - u(x_{i-1}))}{(\Delta x)^2}, \quad (4.22)$$

and should therefore be of  $O((\Delta x)^{-2})$ . In our framework from Section 3.5 the factor  $(\Delta x)^{-2}$  has been omitted in the formulas for the elements in  $\mathbf{A}$ , so in order to obtain the correct eigenvalues of  $\mathbf{A}$  for our situation we need to multiply the eigenvalues with the factor  $(\Delta x)^2$ . This results in  $\lambda_{min}$  becoming of  $O((\Delta x)^2)$  magnitude.

The global MPFA matrix,  $\mathbf{A}$ , is symmetric for uniform parallelogram grids in homogeneous medium, see [24]. Since Section 2.10 in [28] states that if  $\mathbf{A}$  is symmetric then

$$\|\mathbf{A}^{-1}\|_2 = \max_{1 \leq i \leq n} \left| \frac{1}{\lambda_i} \right| = \frac{1}{\lambda_{min}} \sim O((\Delta x)^{-2}), \quad (4.23)$$

where  $\lambda_i$ ,  $i = 1, \dots, n$ , are the eigenvalues of  $\mathbf{A}$ , we obtain

$$\nu_A = -2. \quad (4.24)$$

Having found a bound on  $\|\mathbf{A}^{-1}\|_2$ , we only need to find an upper bound on  $\mathbf{v}$  to determine the error in Equation (4.20). Equation (4.3) gives a representation of each line in the global system. By choosing the discrete representation of the source term in each cell to be the integral of the source over the cell, this equation becomes

$$\sum_{l \in \mathcal{K}_k} m_l u_l^{(n)} = \int_{\Omega_k} f(x, y) d\tau. \quad (4.25)$$

Here  $u^{(n)}$  are the elements of vector  $\mathbf{u}_n$ . Exchanging the numerical values of the potential in Equation (4.25) with the exact values gives an expression for the local truncation

errors  $v_k$ ,  $k = 1, \dots, N_c$  for the potentials in accordance to Equation (4.14)

$$v_k = \sum_{l \in \mathcal{K}_k} m_l u_l^{(e)} - \int_{\Omega_k} f(x, y) d\tau, \quad k = 1, \dots, N_c. \quad (4.26)$$

In this equation  $u^{(e)}$  denote the elements of vector  $\mathbf{u}_e$ . Errors,  $v_k$ , makes up the elements of vector  $\mathbf{v}$  in Equation (4.14), and may therefore be used to obtain an expression for  $\nu_v$  in Equation (4.21).

### 4.3 Approach to the Error Analysis for the Flux

As for the potential we want to apply an error analysis similar to the one explained in Sections 2.5-2.10 and 3.3 in [28]. We start of by looking at the difference between the two expressions

$$\mathbf{q}_n = \mathbf{T}\mathbf{u}_n, \quad (4.27)$$

and

$$\mathbf{q}_e + \mathbf{w} = \mathbf{T}\mathbf{u}_e. \quad (4.28)$$

Subscripts  $n$  and  $e$  still denote the vectors containing numerical and exact values respectively. Subtracting Equation (4.27) from Equation (4.28) yield

$$\begin{aligned} \mathbf{q}_n - \mathbf{q}_e &= \mathbf{T}\mathbf{u}_n - \mathbf{T}\mathbf{u}_e + \mathbf{w} \\ &= \mathbf{T}(\mathbf{u}_n - \mathbf{u}_e) + \mathbf{w} \end{aligned} \quad (4.29)$$

A discrete  $\mathcal{L}^2$ -norm is once again applied to measure the difference between exact and numerical flux. This norm is given in Section 4 in [27] and is defined as

$$\|\mathbf{q}_n - \mathbf{q}_e\|_{\mathcal{L}^2} = \left( \frac{\sum_{j=1}^{N_e} G_j \left( \frac{q_{n,j} - q_{e,j}}{|e_j|} \right)^2}{\sum_{j=1}^{N_e} G_j} \right)^{\frac{1}{2}}, \quad (4.30)$$

where  $j$  refers to the index of the edges,  $|e_j|$  the length of edge  $j$  and

$$G_j = \frac{A_{k_{j1}} + A_{k_{j2}}}{4}. \quad (4.31)$$

Here  $A_{k_{j1}}$  and  $A_{k_{j2}}$  represents the area of the cells situated on each side of edge  $j$ . The values  $q_{n,j}$  and  $q_{e,j}$  are the elements of vectors  $\mathbf{q}_n$  and  $\mathbf{q}_e$  related to edge  $j$ . By applying this norm to Equation (4.29), the following error bound for the fluxes is obtained

$$\begin{aligned} \|\mathbf{q}_n - \mathbf{q}_e\|_{\mathcal{L}^2} &= \|\mathbf{T}(\mathbf{u}_n - \mathbf{u}_e) + \mathbf{w}\|_{\mathcal{L}^2} \\ &\leq \|\mathbf{T}\|_{\mathcal{L}^2} \|\mathbf{u}_n - \mathbf{u}_e\|_{\mathcal{L}^2} + \|\mathbf{w}\|_{\mathcal{L}^2}. \end{aligned} \quad (4.32)$$

Here we have used the triangle inequality and the definition of the subordinate matrix norm  $\|\cdot\|_{\mathcal{L}^2}$ , Equation (4.17). As in Equation (4.19), it is easy to show that

$$\|\mathbf{T}\|_{\mathcal{L}^2} \leq \|\mathbf{T}\|_2, \quad (4.33)$$

and from Section 2.3.2 in [29] we know that

$$\|\mathbf{T}\|_2 \leq \sqrt{N_e} \|\mathbf{T}\|_{\infty}. \quad (4.34)$$

Equation (4.20) gives a bound on the difference between the exact and numerical cell center potentials. Using this bound in Equation (4.32) along with Equation (4.34), we obtain

$$\begin{aligned} \|\mathbf{q}_n - \mathbf{q}_e\|_{\mathcal{L}^2} &\leq \sqrt{N_e} \|\mathbf{T}\|_{\infty} \|\mathbf{u}_n - \mathbf{u}_e\|_{\mathcal{L}^2} + \|\mathbf{w}\|_{\mathcal{L}^2} \\ &\leq \sqrt{N_e} \|\mathbf{T}\|_{\infty} \|\mathbf{A}^{-1}\|_2 \|\mathbf{v}\|_{\mathcal{L}^2} + \|\mathbf{w}\|_{\mathcal{L}^2} \\ &\leq O((\Delta x)^{\nu_T + \nu_A + \nu_v}) + O((\Delta x)^{\nu_w}) \\ &\leq O((\Delta x)^{\nu_q}), \quad \nu_q = \min\{\nu_T + \nu_A + \nu_v, \nu_w\}. \end{aligned} \quad (4.35)$$

The  $\nu_A$  and  $\nu_v$  are the same values as for the potential in Equation (4.21), and  $\nu_T$  and  $\nu_w$  refers to the bounds

$$\sqrt{N_e} \|\mathbf{T}\|_{\infty} \sim O((\Delta x)^{\nu_T}), \quad \|\mathbf{w}\|_{\mathcal{L}^2} \leq O((\Delta x)^{\nu_w}). \quad (4.36)$$

The orders  $\nu_A$  and  $\nu_v$  have already been discussed in the previous section, therefore we only need to look closer at  $\nu_T$  and  $\nu_w$ .

The discrete MPFA flux expression

$$\mathbf{q} = \mathbf{T}\mathbf{u}, \quad (4.37)$$

is a discretization of Darcy's law

$$\mathbf{q} = -\mathbf{K} \frac{\rho g}{\mu} \nabla u. \quad (4.38)$$

The gradient of the potential,  $\nabla u$ , represents a first order derivative in space, and  $\mathbf{T}$  should therefore, similarly as for  $\mathbf{A}$ , have elements of  $O((\Delta x)^{-1})$ . Since we are considering matrix  $\mathbf{T}$  in the matrix maximum norm, it is easy to see that if each element is of the same order of  $\Delta x$  we obtain

$$\|\mathbf{T}\|_{\infty} \sim O((\Delta x)^{-1}). \quad (4.39)$$

Once again we have omitted the factor  $(\Delta x)^{-1}$  from the formulas of the elements in

$\mathbf{T}$  from Section 3.5, and in order to obtain the correct elements of  $\mathbf{T}$  for our situation we need to multiply them with the factor  $\Delta x$ . Hence, we obtain  $\|\mathbf{T}\|_\infty \sim O(1)$ , which yields

$$\nu_T = -1. \quad (4.40)$$

Here we have used the fact that  $\sqrt{N_e} \sim O((\Delta x)^{-1})$ . To find a bound on the error in Equation (4.35) we then only need to find the order  $\nu_w$ .

Let  $q_{te,j}$  and  $q_{e,j}$ ,  $j = 1, 2, \dots, N_e$ , be the elements of vectors  $\mathbf{T}\mathbf{u}_e$  and  $\mathbf{q}_e$  respectively. Similarly as for the potential, we state an expression for the elements  $w_j$  of vector  $\mathbf{w}$  giving the local truncation error of the fluxes over each edge in the grid

$$w_j = q_{te,j} - q_{e,j}, \quad j = 1, 2, \dots, N_e. \quad (4.41)$$

By analyzing these expressions, it is possible to obtain a bound on vector  $\mathbf{w}$  in the discrete  $\mathcal{L}^2$ -norm from Equation (4.30).

## 4.4 Error Analysis for Inner Cell and Edge Stencils on a Uniform Square Grid for General Permeabilities

In this section we look at how the error in potentials and fluxes for the MPFA method behaves for cells and edges yielding *full internal stencils* for the potentials and the fluxes respectively. This meaning cells and edges which does *not* yield potential or flux stencils relying on cell center potentials of "cells" lying outside of the domain, see examples in Figures 4.3 and 4.4. For a uniform square grid this means the cells and edges shown as shaded and bold in Figure 4.2.

In Appendix A, general formulas for the terms involved in calculating the local truncation errors  $v_k$  and  $w_j$  in Equations (4.26) and (4.41) have been developed. By using the approaches described in Sections 4.2 and 4.3 along with these formulas, we can calculate error bounds for the potential and fluxes associated with cells and edges yielding full internal stencil when the potential function in the representative Equation (2.20) is defined as

$$u(x, y) = \sin(x) \sin(y), \quad (4.42)$$

and

$$u(x, y) = \cos(x) \cos(y). \quad (4.43)$$

Sections 4.4.1 to 4.4.3 along with Appendix B and Section 4.5 contains a lot of technical calculations. Readers only interested in the result of the analysis conducted in Sections 4.4 and 4.5 are referred to the summary in Section 4.6.

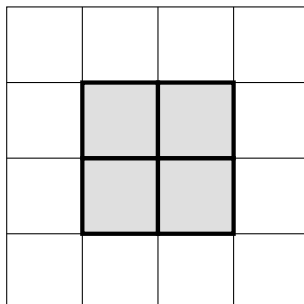


FIGURE 4.2: Cells (shaded) and edges (bold) having full internal stencils for the potential and the flux respectively in a uniform square grid.

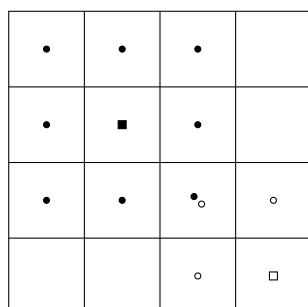


FIGURE 4.3: Example of full internal stencil (filled nodes) and boundary stencil (open nodes). Square nodes represent the cell the stencil belongs to.

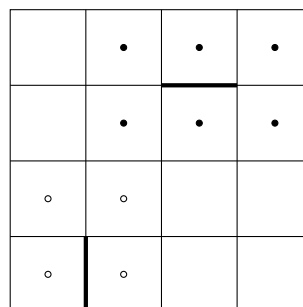


FIGURE 4.4: Example of full internal stencil (filled nodes) and boundary stencil (open nodes), belonging to the bold edges.

#### 4.4.1 Error Bound of the Potential

We start of by looking at the expression of  $v_k$  in Equation (4.26). In Equation (A.16) from Appendix A.1, the following formula has been derived for cell  $k$ ,  $k \in \mathcal{C}$ , where  $\mathcal{C}$  is the set containing the indexes of the cells yielding full internal stencil potential schemes, see Figure 4.2,

$$\sum_{l \in \mathcal{K}_k} m_l u_l^{(e)} = \sum_{\kappa=1}^{\infty} \sum_{\iota=0}^{\kappa} \binom{\kappa}{\iota} \frac{(\Delta x)^\kappa}{\kappa!} \frac{\partial^\kappa u}{\partial x^{\kappa-\iota} \partial y^\iota} \Big|_{(x_c, y_c)} T_p(\kappa - \iota, \iota). \quad (4.44)$$

Coordinate  $(x_c, y_c)$  refers to the top right corner of cell  $k$ , and function  $T_p(n, m)$  is defined as

$$T_p(n, m) = \begin{cases} c \left( \frac{3^n + 3^m - 1 - 3^{n+m}}{2} \right) + a(-3^n + 1) + b(-3^m + 1) \\ + \gamma \left( \frac{-3^n - 3^m - 1 - 3^{n+m}}{2} + 3^n + 3^m \right), & n \text{ and } m \text{ even numbers,} \\ c \left( \frac{-3^n + 3^m - 1 + 3^{n+m}}{2} \right) + a(3^n - 3) + b(3^m - 1) \\ + \gamma \left( \frac{3^n - 3^m - 1 + 3^{n+m}}{2} - 3^n - 3^m + 2 \right), & n \text{ odd and } m \text{ even,} \\ c \left( \frac{3^n - 3^m - 1 + 3^{n+m}}{2} \right) + a(3^n - 1) + b(3^m - 3) \\ + \gamma \left( \frac{-3^n + 3^m - 1 + 3^{n+m}}{2} - 3^n - 3^m + 2 \right), & n \text{ even and } m \text{ odd,} \\ c \left( \frac{-3^n - 3^m - 1 - 3^{n+m}}{2} \right) + a(-3^n + 3) + b(-3^m + 3) \\ + \gamma \left( \frac{3^n + 3^m - 1 - 3^{n+m}}{2} + 3^n + 3^m - 4 \right), & n \text{ and } m \text{ odd numbers.} \end{cases} \quad (4.45)$$

Here variables  $a$ ,  $b$ ,  $c$  and  $\gamma$  are the variables introduced in Section 3.5.

Lets us first consider the potential function (4.42). Notice that this function is infinitely smooth. By looking at how the different derivatives of this function evolves, we get the following formula

$$\frac{\partial^{n+m} u}{\partial x^n \partial y^m} = \begin{cases} (-1)^{t_1+t_2} \sin(x) \sin(y), & n = 2t_1 \text{ and } m = 2t_2, \\ (-1)^{t_1+t_2} \cos(x) \cos(y), & n = 2t_1 + 1 \text{ and } m = 2t_2 + 1, \\ (-1)^{t_1+t_2} \cos(x) \sin(y), & n = 2t_1 + 1 \text{ and } m = 2t_2, \\ (-1)^{t_1+t_2} \sin(x) \cos(y), & n = 2t_1 \text{ and } m = 2t_2 + 1 \end{cases}, \quad t_1, t_2 \in \mathbb{N}_0. \quad (4.46)$$

Using the formula in Equation (4.46) in Equation (4.44) we obtain

$$\begin{aligned}
\sum_{l=\mathcal{K}_k} m_l u_l^{(e)} = & \sin(x_c) \sin(y_c) \left[ -\frac{(\Delta x)^2}{2!} T_p(2, 0) - \frac{(\Delta x)^2}{2!} T_p(0, 2) + \frac{(\Delta x)^4}{4!} T_p(4, 0) \right. \\
& \left. + \frac{6(\Delta x)^4}{4!} T_p(2, 2) + \frac{(\Delta x)^4}{4!} T_p(0, 4) - \dots \right] \\
& + \cos(x_c) \sin(y_c) \left[ \Delta x T_p(1, 0) - \frac{(\Delta x)^3}{3!} T_p(3, 0) - \frac{(\Delta x)^3}{3!} T_p(1, 2) + \dots \right] \\
& + \sin(x_c) \cos(y_c) \left[ \Delta x T_p(0, 1) - \frac{(\Delta x)^3}{3!} T_p(2, 1) - \frac{(\Delta x)^3}{3!} T_p(0, 3) + \dots \right] \\
& + \cos(x_c) \cos(y_c) \left[ \frac{(\Delta x)^2}{2!} T_p(1, 1) - \frac{(\Delta x)^4}{4!} T_p(3, 1) \right. \\
& \left. - \frac{(\Delta x)^4}{4!} T_p(1, 3) + \dots \right].
\end{aligned} \tag{4.47}$$

This equation can be written in the more compact form

$$\begin{aligned}
\sum_{l=\mathcal{K}_k} m_l u_l^{(e)} = & \sin(x_c) \sin(y_c) \left[ \sum_{\kappa=0}^{\infty} \frac{(-1)^{\kappa+1} (\Delta x)^{2\kappa+2}}{(2\kappa+2)!} \left( \sum_{\iota=0}^{\kappa+1} \binom{2\kappa+2}{2\iota} T_p(2\kappa+2-2\iota, 2\iota) \right) \right] \\
& + \cos(x_c) \sin(y_c) \left[ \sum_{\kappa=0}^{\infty} \frac{(-1)^{\kappa} (\Delta x)^{2\kappa+1}}{(2\kappa+1)!} \left( \sum_{\iota=0}^{\kappa} \binom{2\kappa+1}{2\iota+1} T_p(2\iota+1, 2\kappa-2\iota) \right) \right] \\
& + \sin(x_c) \cos(y_c) \left[ \sum_{\kappa=0}^{\infty} \frac{(-1)^{\kappa} (\Delta x)^{2\kappa+1}}{(2\kappa+1)!} \left( \sum_{\iota=0}^{\kappa} \binom{2\kappa+1}{2\iota+1} T_p(2\kappa-2\iota, 2\iota+1) \right) \right] \\
& + \cos(x_c) \cos(y_c) \left[ \sum_{\kappa=0}^{\infty} \frac{(-1)^{\kappa} (\Delta x)^{2\kappa+2}}{(2\kappa+2)!} \left( \sum_{\iota=0}^{\kappa} \binom{2\kappa+2}{2\iota+1} T_p(2\kappa+1-2\iota, 2\iota+1) \right) \right].
\end{aligned} \tag{4.48}$$

To calculate the integral of the source in Equation (4.26) we apply the formula for this expression given in Equation (A.22) from Appendix A.1. By considering cell 5 in Figure 4.1 and the potential function (4.42), this formula yields

$$\begin{aligned}
\int_{x_2}^{x_3} \int_{y_2}^{y_3} f(x, y) dy dx = & (k_1 + k_4) \int_{x_2}^{x_3} \int_{y_2}^{y_3} \sin(x) \sin(y) dy dx \\
& - 2k_2 \int_{x_2}^{x_3} \int_{y_2}^{y_3} \cos(x) \cos(y) dy dx \\
= & (k_1 + k_4) I_1 - 2k_2 I_2.
\end{aligned} \tag{4.49}$$

In this equation we have assumed that we are working with a general permeability, which is given by

$$\mathbf{K} = \begin{pmatrix} k_1 & k_2 \\ k_2 & k_4 \end{pmatrix}. \tag{4.50}$$

Looking closer at the first integral,  $I_1$ , shows that

$$I_1 = \int_{x_2}^{x_3} \int_{y_2}^{y_3} \sin(x) \sin(y) dy dx = \cos(x_3) \cos(y_3) - \cos(x_2) \cos(y_3) - \cos(x_3) \cos(y_2) + \cos(x_2) \cos(y_2). \quad (4.51)$$

To better be able to compare  $I_1$  with Equation (4.48) we wish to write the entire expression of  $I_1$  in same spatial coordinate as Equation (4.48). Writing Equation (4.51) as a Taylor expansion from the top right corner  $(x_3, y_3)$  of cell 5 yields

$$\begin{aligned} I_1 &= \cos(x_3) \cos(y_3) - \cos(x_3 - 2\Delta x) \cos(y_3) \\ &\quad - \cos(x_3) \cos(y_3 - 2\Delta y) + \cos(x_3 - 2\Delta x) \cos(y_3 - 2\Delta y) \\ &= \sin(x_3) \sin(y_3) [s_3(1, 1, 2) - s_3(3, 1, 4) - s_3(1, 3, 4) + \dots] \\ &\quad + \cos(x_3) \sin(y_3) [s_2(1) - s_3(0, 1, 1) - s_2(3) + s_3(2, 1, 3) \\ &\quad\quad\quad + s_3(0, 3, 1) + \dots] \\ &\quad + \sin(x_3) \cos(y_3) [s_1(1) - s_3(1, 0, 1) - s_1(3) + s_3(3, 0, 1) \\ &\quad\quad\quad + s_3(1, 2, 3) + \dots] \\ &\quad + \cos(x_3) \cos(y_3) [1 - 1 - 1 + 1 + s_1(2) + s_2(2) - s_3(2, 0, 1) \\ &\quad\quad\quad - s_3(0, 2, 1) - s_1(4) - s_2(4) + s_3(4, 0, 1) \\ &\quad\quad\quad + s_3(2, 2, 1) + s_3(0, 4, 1) + \dots]. \end{aligned} \quad (4.52)$$

The functions  $s_i$ ,  $i = 1, 2, 3$ , in this expression are given by

$$\begin{aligned} s_1(n) &= \frac{(-1)^n 2^n}{n!} (\Delta x)^n, \\ s_2(m) &= \frac{(-1)^m 2^m}{m!} (\Delta y)^m, \\ s_3(n, m, \omega) &= \frac{(-1)^{m+n} 2^{m+n}}{(m+n)!} \omega (\Delta x)^n (\Delta y)^m, \end{aligned} \quad (4.53)$$

where  $\omega$  in  $s_3$  refers to the binomial coefficient coming from the two dimensional Taylor expansion, see Appendix C.1.

$I_1$  can be written in the more compact form

$$\begin{aligned}
I_1 = & \sin(x_3) \sin(y_3) \left[ \sum_{\kappa=0}^{\infty} (-1)^{\kappa} \left( \sum_{\iota=0}^{\kappa} s_3(2\kappa + 1 - 2\iota, 2\iota + 1, \omega_1) \right) \right] \\
& + \cos(x_3) \sin(y_3) \left[ \sum_{\kappa=0}^{\infty} (-1)^{\kappa} (s_2(2\kappa + 1)) \right. \\
& \quad \left. + \sum_{\kappa=0}^{\infty} (-1)^{\kappa+1} \left( \sum_{\iota=0}^{\kappa} s_3(2\kappa - 2\iota, 2\iota + 1, \omega_2) \right) \right] \\
& + \sin(x_3) \cos(y_3) \left[ \sum_{\kappa=0}^{\infty} (-1)^{\kappa} (s_1(2\kappa + 1)) \right. \\
& \quad \left. + \sum_{\kappa=0}^{\infty} (-1)^{\kappa+1} \left( \sum_{\iota=0}^{\kappa} s_3(2\iota + 1, 2\kappa - 2\iota, \omega_3) \right) \right] \\
& + \cos(x_3) \cos(y_3) \left[ \sum_{\kappa=0}^{\infty} (-1)^{\kappa} (s_1(2\kappa + 2) + s_2(2\kappa + 2)) \right. \\
& \quad \left. + \sum_{\kappa=0}^{\infty} (-1)^{\kappa+1} \left( \sum_{\iota=0}^{\kappa+1} s_3(2\kappa + 2 - 2\iota, 2\iota, \omega_4) \right) \right].
\end{aligned} \tag{4.54}$$

The binomial coefficients  $\omega_i$ ,  $i = 1, 2, 3, 4$ , are given by

$$\begin{aligned}
\omega_1 &= \binom{2\kappa + 2}{2\iota + 1}, & \omega_2 &= \binom{2\kappa + 1}{2\iota + 1}, \\
\omega_3 &= \binom{2\kappa + 1}{2\iota}, & \omega_4 &= \binom{2\kappa + 2}{2\iota}.
\end{aligned} \tag{4.55}$$

Doing the same calculations as we just did for  $I_1$  for the second integral,  $I_2$ , yields

$$\begin{aligned}
I_2 = & \sin(x_3) \sin(y_3) \left[ \sum_{\kappa=0}^{\infty} (-1)^{\kappa} (s_1(2\kappa + 2) + s_2(2\kappa + 2)) \right. \\
& \quad \left. + \sum_{\kappa=0}^{\infty} (-1)^{\kappa+1} \left( \sum_{\iota=0}^{\kappa+1} s_3(2\kappa + 2 - 2\iota, 2\iota, \omega_4) \right) \right] \\
& + \cos(x_3) \sin(y_3) \left[ \sum_{\kappa=0}^{\infty} (-1)^{\kappa+1} (s_1(2\kappa + 1)) \right. \\
& \quad \left. + \sum_{\kappa=0}^{\infty} (-1)^{\kappa+1} \left( \sum_{\iota=0}^{\kappa} s_3(2\kappa - 2\iota, 2\iota + 1, \omega_3) \right) \right] \\
& + \sin(x_3) \cos(y_3) \left[ \sum_{\kappa=0}^{\infty} (-1)^{\kappa+1} (s_2(2\kappa + 1)) \right. \\
& \quad \left. + \sum_{\kappa=0}^{\infty} (-1)^{\kappa+1} \left( \sum_{\iota=0}^{\kappa} s_3(2\iota + 1, 2\kappa - 2\iota, \omega_2) \right) \right] \\
& + \cos(x_3) \cos(y_3) \left[ \sum_{\kappa=0}^{\infty} (-1)^{\kappa} \left( \sum_{\iota=0}^{\kappa} s_3(2\kappa + 1 - 2\iota, 2\iota + 1, \omega_1) \right) \right].
\end{aligned} \tag{4.56}$$

By inserting the expressions for integrals  $I_1$  and  $I_2$  in Equations (4.54) and (4.56) back into Equation (4.49) we obtain

$$\begin{aligned}
& \int_{x_2}^{x_3} \int_{y_2}^{y_3} f(x, y) \, dy dx = (k_1 + k_4)I_1 - 2k_2I_2 \\
& = \sin(x_3) \sin(y_3) \left[ (k_1 + k_4) \left( \sum_{\kappa=0}^{\infty} (-1)^\kappa \left( \sum_{\iota=0}^{\kappa} s_3(2\kappa + 1 - 2\iota, 2\iota + 1, \omega_1) \right) \right) \right. \\
& \quad - 2k_2 \left( \sum_{\kappa=0}^{\infty} (-1)^\kappa (s_1(2\kappa + 2) + s_2(2\kappa + 2)) \right. \\
& \quad \left. \left. + \sum_{\kappa=0}^{\infty} (-1)^{\kappa+1} \left( \sum_{\iota=0}^{\kappa+1} s_3(2\kappa + 2 - 2\iota, 2\iota, \omega_4) \right) \right) \right] \\
& + \cos(x_3) \sin(y_3) \left[ (k_1 + k_4) \left( \sum_{\kappa=0}^{\infty} (-1)^\kappa (s_2(2\kappa + 1)) \right. \right. \\
& \quad \left. \left. + \sum_{\kappa=0}^{\infty} (-1)^{\kappa+1} \left( \sum_{\iota=0}^{\kappa} s_3(2\kappa - 2\iota, 2\iota + 1, \omega_2) \right) \right) \right. \\
& \quad - 2k_2 \left( \sum_{\kappa=0}^{\infty} (-1)^{\kappa+1} (s_1(2\kappa + 1)) \right. \\
& \quad \left. \left. + \sum_{\kappa=0}^{\infty} (-1)^{\kappa+1} \left( \sum_{\iota=0}^{\kappa} s_3(2\kappa - 2\iota, 2\iota + 1, \omega_3) \right) \right) \right] \tag{4.57} \\
& + \sin(x_3) \cos(y_3) \left[ (k_1 + k_4) \left( \sum_{\kappa=0}^{\infty} (-1)^\kappa (s_1(2\kappa + 1)) \right. \right. \\
& \quad \left. \left. + \sum_{\kappa=0}^{\infty} (-1)^{\kappa+1} \left( \sum_{\iota=0}^{\kappa} s_3(2\iota + 1, 2\kappa - 2\iota, \omega_3) \right) \right) \right. \\
& \quad - 2k_2 \left( \sum_{\kappa=0}^{\infty} (-1)^{\kappa+1} (s_2(2\kappa + 1)) \right. \\
& \quad \left. \left. + \sum_{\kappa=0}^{\infty} (-1)^{\kappa+1} \left( \sum_{\iota=0}^{\kappa} s_3(2\iota + 1, 2\kappa - 2\iota, \omega_2) \right) \right) \right] \\
& + \cos(x_3) \cos(y_3) \left[ (k_1 + k_4) \left( \sum_{\kappa=0}^{\infty} (-1)^\kappa (s_1(2\kappa + 2) + s_2(2\kappa + 2)) \right. \right. \\
& \quad \left. \left. + \sum_{\kappa=0}^{\infty} (-1)^{\kappa+1} \left( \sum_{\iota=0}^{\kappa+1} s_3(2\kappa + 2 - 2\iota, 2\iota, \omega_4) \right) \right) \right. \\
& \quad \left. - 2k_2 \left( \sum_{\kappa=0}^{\infty} (-1)^\kappa \left( \sum_{\iota=0}^{\kappa} s_3(2\kappa + 1 - 2\iota, 2\iota + 1, \omega_1) \right) \right) \right].
\end{aligned}$$

Notice that this formula holds not only for cell 5, but for an *arbitrary* cell in a uniform square grid. This is due to the fact that we may exchange the top right corner of cell 5,  $(x_3, y_3)$ , with the top right corner,  $(x_c, y_c)$ , of an arbitrary cell.

In Equations (4.48) and (4.57) we then have explicit expressions for the terms involved

in calculating the local truncation errors  $v_k$ ,  $k \in \mathcal{C}$ , making up elements in vector  $\mathbf{v}$ , from Equation (4.14), for the potential function (4.42). These terms may be written as

$$\begin{aligned} \sum_{l \in \mathcal{K}_k} m_l u_l^{(e)} &= \sin(x_c) \sin(y_c) \varphi_1 + \cos(x_c) \sin(y_c) \varphi_2 \\ &+ \sin(x_c) \cos(y_c) \varphi_3 + \cos(x_c) \cos(y_c) \varphi_4, \end{aligned} \quad (4.58)$$

and

$$\begin{aligned} \int_{\Omega_k} f(x, y) d\tau &= \sin(x_c) \sin(y_c) \psi_1 + \cos(x_c) \sin(y_c) \psi_2 \\ &+ \sin(x_c) \cos(y_c) \psi_3 + \cos(x_c) \cos(y_c) \psi_4. \end{aligned} \quad (4.59)$$

Hence, we can calculate  $v_k$  by

$$\begin{aligned} v_k &= \sum_{l \in \mathcal{K}_k} m_l u_l^{(e)} - \int_{\Omega_k} f(x, y) dy dx \\ &= \sin(x_c) \sin(y_c) [\varphi_1 - \psi_1] + \cos(x_c) \sin(y_c) [\varphi_2 - \psi_2] \\ &\quad + \sin(x_c) \cos(y_c) [\varphi_3 - \psi_3] + \cos(x_c) \cos(y_c) [\varphi_4 - \psi_4] \\ &= \sin(x_c) \sin(y_c) D_1 + \cos(x_c) \sin(y_c) D_2 \\ &\quad + \sin(x_c) \cos(y_c) D_3 + \cos(x_c) \cos(y_c) D_4. \end{aligned} \quad (4.60)$$

When the trigonometric terms in Equation (4.60) vanishes is dependent on the spatial position and size of our uniform square grid. So to analyze the expression for  $v_k$  for an arbitrary grid, we need to look at how the coefficients  $D_i$ ,  $i = 1, 2, 3, 4$ , of the trigonometric terms behaves.

Coefficient  $\varphi_1$  of  $\sin(x_c) \sin(y_c)$  is given as

$$\begin{aligned} \varphi_1 &= \sum_{\kappa=0}^{\infty} \frac{(-1)^{\kappa+1} (\Delta x)^{2\kappa+2}}{(2\kappa+2)!} \left[ \sum_{\iota=0}^{\kappa+1} \binom{2\kappa+2}{2\iota} \left( c \left( \frac{3^{2\kappa+2-2\iota} + 3^{2\iota} - 1 - 3^{2\kappa+2}}{2} \right) \right. \right. \\ &\quad \left. \left. + a(-3^{2\kappa+2-2\iota} + 1) + b(-3^{2\iota} + 1) \right. \right. \\ &\quad \left. \left. + \gamma \left( \frac{-3^{2\kappa+2-2\iota} - 3^{2\iota} - 1 - 3^{2\kappa+2}}{2} + 3^{2\kappa+2-2\iota} + 3^{2\iota} \right) \right) \right]. \end{aligned} \quad (4.61)$$

Here we have used the fact that the inputs  $n$  and  $m$  of function  $T_p(n, m)$ , defined in Equation (4.45), are always even numbers for  $\varphi_1$ . It is possible to simplify Equation (4.61) by using Property C.1.2 and Theorem C.2.2 from Appendices C.1 and C.2. Property C.1.2 can be applied by

$$\sum_{\iota=0}^{\kappa+1} \binom{2\kappa+2}{2\iota} t = 2^{\kappa+1} t, \quad t \in \mathbb{R}, \quad (4.62)$$

and Theorem C.2.2 can be used similarly to the following example

$$\begin{aligned}
\sum_{\iota=0}^{\kappa+1} \binom{2\kappa+2}{2\iota} 3^{2\kappa+2-2\iota} &= \sum_{\iota=0}^{\kappa+1} \binom{2\kappa+2}{2\iota} 3^{2\kappa+2-2\iota} 1^{2\iota} \\
&= \frac{1}{2} ((1+3)^{2\kappa+2} + (-3+1)^{2\kappa+2}) \\
&= \frac{1}{2} (2^{4\kappa+4} + (-1)^{2\kappa+2} 2^{2\kappa+2}) \\
&= 2^{4\kappa+3} + 2^{2\kappa+1}.
\end{aligned} \tag{4.63}$$

In Equation (4.63) we have used the fact that factor  $(1 + (-1)^k)$  in Theorem C.2.2 becomes  $(1 + (-1)^{2\kappa+2-2\iota}) = 2$ . Using Property C.1.2 and Theorem C.2.2 similar to the way shown in Equations (4.62) and (4.63),  $\varphi_1$  can be written as

$$\begin{aligned}
\varphi_1 = \sum_{\kappa=0}^{\infty} \frac{(-1)^{\kappa+1} (\Delta x)^{2\kappa+2}}{(2\kappa+2)!} &\left[ - (a+b) 2^{4\kappa+3} + c(2^{4\kappa+3} + 2^{2\kappa+1} - (1+3^{2\kappa+2}) 2^{2\kappa}) \right. \\
&\left. + \gamma(-2^{4\kappa+3} - 2^{2\kappa+1} - (1+3^{2\kappa+2}) 2^{2\kappa} + 2^{4\kappa+4} + 2^{2\kappa+2}) \right].
\end{aligned} \tag{4.64}$$

The other coefficient of  $\sin(x_c) \sin(y_c)$ ,  $\psi_1$ , takes the form

$$\begin{aligned}
\psi_1 &= \sum_{\kappa=0}^{\infty} (-1)^{\kappa} \left[ (k_1 + k_4) \left( \sum_{\iota=0}^{\kappa} \frac{(-1)^{2\kappa+2} 2^{2\kappa+2}}{(2\kappa+2)!} \binom{2\kappa+2}{2\iota+1} (\Delta x)^{2\kappa+1-2\iota} (\Delta y)^{2\iota+1} \right) \right. \\
&\quad - 2k_2 \left( \frac{(-1)^{2\kappa+2} 2^{2\kappa+2}}{(2\kappa+2)!} (\Delta x)^{2\kappa+2} + \frac{(-1)^{2\kappa+2} 2^{2\kappa+2}}{(2\kappa+2)!} (\Delta y)^{2\kappa+2} \right. \\
&\quad \left. \left. - \sum_{\iota=0}^{\kappa+1} \frac{(-1)^{2\kappa+2} 2^{2\kappa+2}}{(2\kappa+2)!} \binom{2\kappa+2}{2\iota} (\Delta x)^{2\kappa+2-2\iota} (\Delta y)^{2\iota} \right) \right] \\
&= \sum_{\kappa=0}^{\infty} \frac{(-1)^{3\kappa+2} 2^{2\kappa+2} (\Delta x)^{2\kappa+2}}{(2\kappa+2)!} \left[ (k_1 + k_4) \sum_{\iota=0}^{\kappa} \binom{2\kappa+2}{2\iota+1} - 2k_2 \left( 2 - \sum_{\iota=0}^{\kappa+1} \binom{2\kappa+2}{2\iota} \right) \right],
\end{aligned} \tag{4.65}$$

as seen from Equations (4.53), (4.55) and (4.57). In the second equality in Equation (4.65) the common factors  $(-1)^{3\kappa+2}$ ,  $2^{2\kappa+2}$ ,  $((2\kappa+2)!)^{-1}$  and  $(\Delta x)^{2\kappa+2}$  have been moved outside the parenthesis, recall that  $\Delta x = \Delta y$ . This expression may also be simplified by using Property C.1.2 the way that is shown in Equation (4.62). Then  $\psi_1$  becomes

$$\psi_1 = \sum_{\kappa=0}^{\infty} \frac{(-1)^{3\kappa+2} 2^{2\kappa+2} (\Delta x)^{2\kappa+2}}{(2\kappa+2)!} [(k_1 + k_4) 2^{2\kappa+1} - 2k_2 (2 - 2^{2\kappa+1})]. \tag{4.66}$$

Using Equations (4.64) and (4.66) the difference between  $\varphi_1$  and  $\psi_1$  is simplified to the expression

$$\begin{aligned}
D_1 = \varphi_1 - \psi_1 = \sum_{\kappa=0}^{\infty} \frac{(-1)^{\kappa+1} (\Delta x)^{2\kappa+2}}{(2\kappa+2)!} & \left[ - (a+b)2^{4\kappa+3} + c(2^{4\kappa+3} + 2^{2\kappa+1} - (1+3^{2\kappa+2})2^{2\kappa}) \right. \\
& + \gamma(-2^{4\kappa+3} - 2^{2\kappa+1} - (1+3^{2\kappa+2})2^{2\kappa} + 2^{4\kappa+4} + 2^{2\kappa+2}) + (k_1+k_4)2^{4\kappa+3} \\
& \left. - k_2(2^{2\kappa+4} - 2^{4\kappa+4}) \right].
\end{aligned} \tag{4.67}$$

Here we have used that  $(-1)(-1)^{3\kappa+2} = (-1)^{\kappa+1}(-1)^{2\kappa+2} = (-1)^{\kappa+1}$ .

Similar simplifications can also be done to the remaining coefficients in Equation (4.60).

This results in the following formulas

$$\begin{aligned}
D_2 = \sum_{\kappa=0}^{\infty} \frac{(-1)^{\kappa} (\Delta x)^{2\kappa+1}}{(2\kappa+1)!} & \left[ (a+b)(2^{4\kappa+1} - 2^{2\kappa+1}) + c(-2^{2\kappa} - (1-3^{2\kappa+1})2^{2\kappa-1}) \right. \\
& + \gamma(2^{2\kappa} - (1-3^{2\kappa+1})2^{2\kappa-1} - 2^{4\kappa+2} + 2^{2\kappa+1}) - (k_1+k_4)(2^{4\kappa+1} - 2^{2\kappa+1}) \\
& \left. - k_2(2^{4\kappa+2} - 2^{2\kappa+2}) \right], \\
D_3 = \sum_{\kappa=0}^{\infty} \frac{(-1)^{\kappa} (\Delta x)^{2\kappa+1}}{(2\kappa+1)!} & \left[ (a+b)(2^{4\kappa+1} - 2^{2\kappa+1}) + c(-2^{2\kappa} - (1-3^{2\kappa+1})2^{2\kappa-1}) \right. \\
& + \gamma(2^{2\kappa} - (1-3^{2\kappa+1})2^{2\kappa-1} - 2^{4\kappa+2} + 2^{2\kappa+1}) - (k_1+k_4)(2^{4\kappa+1} - 2^{2\kappa+1}) \\
& \left. - k_2(2^{4\kappa+2} - 2^{2\kappa+2}) \right], \\
D_4 = \sum_{\kappa=0}^{\infty} \frac{(-1)^{\kappa} (\Delta x)^{2\kappa+2}}{(2\kappa+2)!} & \left[ (a+b)(2^{2\kappa+3} - 2^{4\kappa+3}) + c(2^{2\kappa+1} - 2^{4\kappa+3} - (1+3^{2\kappa+2})2^{2\kappa}) \right. \\
& + \gamma(-2^{2\kappa+1} + 2^{4\kappa+3} - (1+3^{2\kappa+2})2^{2\kappa} + 2^{4\kappa+4} - 2^{2\kappa+2} - 2^{2\kappa+3}) \\
& \left. - (k_1+k_4)(2^{2\kappa+3} - 2^{4\kappa+3}) + k_2 2^{4\kappa+4} \right].
\end{aligned} \tag{4.68}$$

Simple calculations show that the expressions inside the big parentheses in Equations (4.67) and (4.68) disappears when  $\kappa = 0$ , independently of variables  $a$ ,  $b$ ,  $c$  and  $\gamma$ . For  $D_2$  and  $D_3$  this even happens for  $\kappa = 1$ . Therefore we adjust the starting values of the sums to disregard the terms that vanishes. In addition, we recall that the variables  $a$ ,  $b$  and  $c$  coincide with the values of the permeability on a uniform square grid, see Equation (4.9).

Using these two observations in the formulas in Equations (4.67) and (4.68) yields

$$\begin{aligned}
D_1 &= \sum_{\kappa=1}^{\infty} \frac{(-1)^{\kappa+1} (\Delta x)^{2\kappa+2}}{(2\kappa+2)!} \left[ \gamma(-2^{4\kappa+3} - 2^{2\kappa+1} - (1+3^{2\kappa+2})2^{2\kappa} + 2^{4\kappa+4} + 2^{2\kappa+2}) \right. \\
&\quad \left. - c(2^{2\kappa+4} - 2^{4\kappa+4} - 2^{4\kappa+3} - 2^{2\kappa+1} + (1+3^{2\kappa+2})2^{2\kappa}) \right], \\
D_2 &= \sum_{\kappa=2}^{\infty} \frac{(-1)^{\kappa} (\Delta x)^{2\kappa+1}}{(2\kappa+1)!} \left[ \gamma(2^{2\kappa} - (1-3^{2\kappa+1})2^{2\kappa-1} - 2^{4\kappa+2} + 2^{2\kappa+1}) \right. \\
&\quad \left. - c(2^{4\kappa+2} - 2^{2\kappa+2} + 2^{2\kappa} + (1-3^{2\kappa+1})2^{2\kappa-1}) \right], \\
D_3 &= \sum_{\kappa=2}^{\infty} \frac{(-1)^{\kappa} (\Delta x)^{2\kappa+1}}{(2\kappa+1)!} \left[ \gamma(2^{2\kappa} - (1-3^{2\kappa+1})2^{2\kappa-1} - 2^{4\kappa+2} + 2^{2\kappa+1}) \right. \\
&\quad \left. - c(2^{4\kappa+2} - 2^{2\kappa+2} + 2^{2\kappa} + (1-3^{2\kappa+1})2^{2\kappa-1}) \right], \\
D_4 &= \sum_{\kappa=1}^{\infty} \frac{(-1)^{\kappa} (\Delta x)^{2\kappa+2}}{(2\kappa+2)!} \left[ \gamma(-2^{2\kappa+1} + 2^{4\kappa+3} - (1+3^{2\kappa+2})2^{2\kappa} + 2^{4\kappa+4} - 2^{2\kappa+2} \right. \\
&\quad \left. - 2^{2\kappa+3}) + c(2^{4\kappa+4} + 2^{2\kappa+1} - 2^{4\kappa+3} - (1+3^{2\kappa+2})2^{2\kappa}) \right].
\end{aligned} \tag{4.69}$$

These coefficients may now be used to analyze the local truncation errors  $v_k$ .

All the above calculations are done for the potential function (4.42). If we instead were to use the potential function (4.43), a similar formula as the one in Equation (4.60) is obtained for the local truncation error  $v_k$ . The only difference is that coefficients  $D_1$  and  $D_4$ , and coefficients  $D_2$  and  $D_3$ , have traded places in relation to Equation (4.60). In addition, the factors  $(-1)^{\kappa}$  in Equation (4.69) have become  $(-1)^{\kappa+1}$  and vice versa.

#### 4.4.2 Error Bound of the Fluxes

A similar calculation as the one presented in Section 4.4.1 can be done for the truncation error  $w_j$ ,  $j \in \mathcal{E}$ , for the fluxes from Equation (4.41) for potential function (4.42). Set  $\mathcal{E}$  is the collection of indexes of the bold edges shown in Figure 4.2 yielding full internal stencils for the fluxes. For the interested reader these calculations are given in Appendix B. In this section we only present the results of the calculations.

The expression for  $w_j$ ,  $j \in \mathcal{E}$ , can be given as

$$w_j = \begin{cases} q_{te,v} - q_{e,v}, & \text{edge } j \text{ is a horizontal edge,} \\ q_{te,h} - q_{e,h}, & \text{edge } j \text{ is a vertical edge.} \end{cases} \tag{4.70}$$



FIGURE 4.5: Rightmost point on a horizontal edge

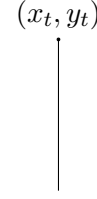


FIGURE 4.6: Top point on a vertical edge

Here subscripts  $v$  and  $h$  refers to vertical and horizontal fluxes respectively. The expressions in Equation (4.70) takes on the following forms

$$\begin{aligned} q_{te,v} - q_{e,v} &= \sin(x_r) \sin(y_r) D_{v_1} + \cos(x_r) \sin(y_r) D_{v_2} \\ &+ \sin(x_r) \cos(y_r) D_{v_3} + \cos(x_r) \cos(y_r) D_{v_4}, \end{aligned} \quad (4.71)$$

and

$$\begin{aligned} q_{te,h} - q_{e,h} &= \sin(x_t) \sin(y_t) D_{h_1} + \cos(x_t) \sin(y_t) D_{h_2} \\ &+ \sin(x_t) \cos(y_t) D_{h_3} + \cos(x_t) \cos(y_t) D_{h_4}. \end{aligned} \quad (4.72)$$

Coefficients  $D_{j_i}$ ,  $j = v, h$ ,  $i = 1, 2, 3, 4$ , are defined as

$$\begin{aligned} D_{v_1} &= \sum_{\kappa=1}^{\infty} \frac{(-1)^{\kappa+1} (\Delta x)^{2\kappa+2}}{(2\kappa+2)!} \left[ (2^{4\kappa+2} - 2^{2\kappa+2}) c \right], \\ D_{v_2} &= \sum_{\kappa=1}^{\infty} \frac{(-1)^{\kappa} (\Delta x)^{2\kappa+1}}{(2\kappa+1)!} \left[ (-2^{2\kappa} - 2^{4\kappa} + 2^{2\kappa+1}) c \right], \\ D_{v_3} &= \sum_{\kappa=1}^{\infty} \frac{(-1)^{\kappa} (\Delta x)^{2\kappa+1}}{(2\kappa+1)!} \left[ (2^{2\kappa+1} - 2^{4\kappa+1}) \beta \right], \\ D_{v_4} &= \sum_{\kappa=1}^{\infty} \frac{(-1)^{\kappa} (\Delta x)^{2\kappa+2}}{(2\kappa+2)!} \left[ (-2^{2\kappa+3} + 2^{4\kappa+3}) \beta \right], \end{aligned} \quad (4.73)$$

and

$$\begin{aligned} D_{h_1} &= \sum_{\kappa=1}^{\infty} \frac{(-1)^{\kappa+1} (\Delta x)^{2\kappa+2}}{(2\kappa+2)!} \left[ (2^{4\kappa+2} - 2^{2\kappa+2}) c \right], \\ D_{h_2} &= \sum_{\kappa=1}^{\infty} \frac{(-1)^{\kappa} (\Delta x)^{2\kappa+1}}{(2\kappa+1)!} \left[ (2^{2\kappa+1} - 2^{4\kappa+1}) \alpha \right], \\ D_{h_3} &= \sum_{\kappa=1}^{\infty} \frac{(-1)^{\kappa} (\Delta x)^{2\kappa+1}}{(2\kappa+1)!} \left[ (-2^{2\kappa} - 2^{4\kappa} + 2^{2\kappa+1}) c \right], \\ D_{h_4} &= \sum_{\kappa=1}^{\infty} \frac{(-1)^{\kappa} (\Delta x)^{2\kappa+2}}{(2\kappa+2)!} \left[ (-2^{2\kappa+3} + 2^{4\kappa+3}) \alpha \right]. \end{aligned} \quad (4.74)$$

Variables  $c$ ,  $\alpha$  and  $\beta$  are the variables introduced in Section 3.5, and coordinates  $(x_r, y_r)$  and  $(x_t, y_t)$  in Equations (4.71) and (4.72) refers to the rightmost and top point of a general horizontal and vertical edge respectively, see Figures 4.5 and 4.6.

Repeating all the calculations in Appendix B for the potential function (4.43) yields almost the same expression for the local truncation error as for (4.42). There are only two differences. The first one is that the factor  $(-1)^{\kappa+1}$  in  $D_{v_1}$  and  $D_{h_1}$  have been changed to  $(-1)^\kappa$ , and vice versa for the remaining coefficients in Equations (4.73) and (4.74). The second difference is that coefficients  $D_{j_1}$  and  $D_{j_4}$ , and coefficients  $D_{j_2}$  and  $D_{j_3}$ ,  $j = v, h$ , have traded places related to which trigonometric expression they are related to in Equations (4.71) and (4.72).

### 4.4.3 Analysis of the Error Bounds

In Sections 4.4.1 and 4.4.2 we have established general expressions for the local truncation errors  $v_k$  and  $w_j$  making up the elements in vectors  $\mathbf{v}$  and  $\mathbf{w}$ , from Equations (4.14) and (4.28), for cells and edges yielding full internal stencils for the potential functions (4.42) and (4.43). The errors are shown to be dependent on the variables  $a$ ,  $b$ ,  $c$  and  $\eta$ . This section is devoted to analyzing how  $v_k$  and  $w_j$  behaves for different values of these variables in order to establish bounds of  $\mathbf{v}$  and  $\mathbf{w}$  in the discrete  $\mathcal{L}^2$ -norm introduced in Sections 4.2 and 4.3.

The grid considered is still the uniform square grid shown in Figure 4.1. For this grid the variables  $a$ ,  $b$  and  $c$  are directly linked to the elements of the permeability matrix, see Equation (4.9). Therefore, the analysis is divided into the following two situations

- I)  $\mathbf{K}$  diagonal for  $\eta = 0$  and  $\eta \neq 0$ ,
- II)  $\mathbf{K}$  *not* diagonal for  $\eta = 0$  and  $\eta \neq 0$ .

### Potential

To obtain bounds on  $v_k$  for arbitrary uniform square grids, physical situations and  $\eta$ , we need to look at the coefficients  $D_i$ ,  $i = 1, 2, 3, 4$ , of the trigonometric expressions in Equation (4.60). Since these coefficients coincide for the potential function (4.42) and (4.43), except for the factor  $(-1)$  which has no effect on when the coefficients disappears, we only need to look at the coefficients for one of the functions. Equation (4.69) shows

that for the potential function Equation (4.42) these coefficients may be written as

$$\begin{aligned}
D_1 &= \sum_{\kappa=1}^{\infty} \frac{(-1)^{\kappa+1} (\Delta x)^{2\kappa+2}}{(2\kappa+2)!} \left[ \gamma (-2^{4\kappa+3} - 2^{2\kappa+1} - (1+3^{2\kappa+2})2^{2\kappa} + 2^{4\kappa+4} + 2^{2\kappa+2}) \right. \\
&\quad \left. - c(2^{2\kappa+4} - 2^{4\kappa+4} - 2^{4\kappa+3} - 2^{2\kappa+1} + (1+3^{2\kappa+2})2^{2\kappa}) \right], \\
D_2 &= \sum_{\kappa=2}^{\infty} \frac{(-1)^{\kappa} (\Delta x)^{2\kappa+1}}{(2\kappa+1)!} \left[ \gamma(2^{2\kappa} - (1-3^{2\kappa+1})2^{2\kappa-1} - 2^{4\kappa+2} + 2^{2\kappa+1}) \right. \\
&\quad \left. - c(2^{4\kappa+2} - 2^{2\kappa+2} + 2^{2\kappa} + (1-3^{2\kappa+1})2^{2\kappa-1}) \right], \\
D_3 &= \sum_{\kappa=2}^{\infty} \frac{(-1)^{\kappa} (\Delta x)^{2\kappa+1}}{(2\kappa+1)!} \left[ \gamma(2^{2\kappa} - (1-3^{2\kappa+1})2^{2\kappa-1} - 2^{4\kappa+2} + 2^{2\kappa+1}) \right. \\
&\quad \left. - c(2^{4\kappa+2} - 2^{2\kappa+2} + 2^{2\kappa} + (1-3^{2\kappa+1})2^{2\kappa-1}) \right], \\
D_4 &= \sum_{\kappa=1}^{\infty} \frac{(-1)^{\kappa} (\Delta x)^{2\kappa+2}}{(2\kappa+2)!} \left[ \gamma(-2^{2\kappa+1} + 2^{4\kappa+3} - (1+3^{2\kappa+2})2^{2\kappa} + 2^{4\kappa+4} - 2^{2\kappa+2} \right. \\
&\quad \left. - 2^{2\kappa+3}) + c(2^{4\kappa+4} + 2^{2\kappa+1} - 2^{4\kappa+3} - (1+3^{2\kappa+2})2^{2\kappa}) \right].
\end{aligned} \tag{4.75}$$

We start of by looking at situation I), when

$$\mathbf{K} = \begin{pmatrix} k_1 & 0 \\ 0 & k_4 \end{pmatrix} = \begin{pmatrix} a & c \\ c & b \end{pmatrix}. \tag{4.76}$$

For the case with  $\eta = 0$ ,  $\gamma$  disappears, and therefore also  $D_1$ - $D_4$ . Hence, for situation I),  $v_k$  vanishes for cells having a full internal stencil for the potential. Notice that this happens independently of the value of  $k_1$  and  $k_4$ . This means that the result holds for the case with isotropic permeability as well as the case with a general permeability with principal directions aligned with the grid directions.

By setting  $\eta \neq 0$ ,  $\gamma$  no longer disappears. For this case only the terms involving  $c$  disappears in the coefficients in Equation (4.75). Thus, we get a local truncation error which is not zero. Therefore, we turn to look for the nonzero coefficient associated with the smallest exponent on  $\Delta x$ . This term will dominate the elements  $v_k$ . The smallest exponent of  $\Delta x$  in this case is given in the  $\kappa = 1$  term in  $D_1$  and  $D_4$ , these terms yield  $(\Delta x)^4$ . Hence, in the case with diagonal permeability and  $\eta \neq 0$ , the local truncation errors  $v_k$  associated with cells having full internal stencils for the potentials are dominated by  $(\Delta x)^4$ .

Turning to situation II), the general permeability

$$\mathbf{K} = \begin{pmatrix} k_1 & k_2 \\ k_2 & k_4 \end{pmatrix} = \begin{pmatrix} a & c \\ c & b \end{pmatrix}, \quad (4.77)$$

is applied. For this situation none of the variables in (4.75) disappears. Also here the  $\kappa = 1$  term involving  $(\Delta x)^4$  dominates the local truncation errors  $v_k$  associated with cells yielding full internal stencils for the potential. This clearly holds for  $\eta = 0$ , but is there a way of choosing  $\eta$ ,  $\eta \neq 0$ , to obtain a larger exponent than 4 of  $\Delta x$  dominating  $v_k$  for a given  $c$ ?

Let us look at coefficient  $D_1$ . If we calculate the terms of this coefficient for  $\kappa = 1$  and  $\kappa = 2$  without specifying the value of  $\eta$ , we are able to find expressions  $\eta$  has to fulfill in order for the terms to disappear. The results were

$$\eta_1 = -\frac{c^2}{ab}, \quad (4.78)$$

$$\eta_2 = -\frac{12300c^2 + 5760\frac{2abc}{a+b}}{12300ab + 5760\frac{2abc}{a+b}}. \quad (4.79)$$

Writing  $\eta_i$ ,  $i = 1, 2$ , as a function of  $c$ , it is possible to model how to choose  $\eta$  depending on the size of the deviation between the principal directions of the permeability and the grid directions, the size of  $c$ , see Figure 2.3 in Section 2.2. Analysis of the two expression shows that they are equal for  $c = 0$  and  $c = \sqrt{ab}$ . For these values we get  $\eta_i(0) = 0$  and  $\eta_i(\sqrt{ab}) = -1$ ,  $i = 1, 2$ , respectively. Putting  $c = 0$ , and getting  $\eta = 0$ , is equivalent to situation I) with  $\eta = 0$  and has already been investigated. For  $c = \sqrt{ab}$  and  $\eta = -1$ , the MPFA discretization is degenerated. The continuity points all gather in the cell corners, and we lose the triangle shapes in each subcell, see Figure 3.8. This leads to the discretization no longer having enough unique degrees of freedom for determining the linear potential functions in each subcell of an interaction volume.

This shows that it is not possible to optimize the exponent of  $\Delta x$  dominating the local truncation errors  $v_k$ , corresponding to cells having full internal stencils, through the continuity point variable  $\eta$  for a given permeability with principal directions *not* aligned with the directions of the grid. Therefore, also for the case with  $\eta \neq 0$  in situation II) the local truncation errors  $v_k$  are dominated by  $(\Delta x)^4$ .

## Flux

As for the potential, the coefficients related to the local truncation error  $w_j$  coincides for the potential functions (4.42) and (4.43), except for the insignificant factor  $(-1)$ . Hence,

we need only to look at the coefficients for the potential function (4.42). The coefficients of the trigonometric functions in the expression for the local truncation errors  $w_j$ ,  $j \in \mathcal{E}$ , in Equations (4.71) and (4.72) are given by

$$\begin{aligned}
D_{v_1} &= \sum_{\kappa=1}^{\infty} \frac{(-1)^{\kappa+1} (\Delta x)^{2\kappa+2}}{(2\kappa+2)!} \left[ (2^{4\kappa+2} - 2^{2\kappa+2})c \right], \\
D_{v_2} &= \sum_{\kappa=1}^{\infty} \frac{(-1)^{\kappa} (\Delta x)^{2\kappa+1}}{(2\kappa+1)!} \left[ (-2^{2\kappa} - 2^{4\kappa} + 2^{2\kappa+1})c \right], \\
D_{v_3} &= \sum_{\kappa=1}^{\infty} \frac{(-1)^{\kappa} (\Delta x)^{2\kappa+1}}{(2\kappa+1)!} \left[ (2^{2\kappa+1} - 2^{4\kappa+1})\beta \right], \\
D_{v_4} &= \sum_{\kappa=1}^{\infty} \frac{(-1)^{\kappa} (\Delta x)^{2\kappa+2}}{(2\kappa+2)!} \left[ (-2^{2\kappa+3} + 2^{4\kappa+3})\beta \right],
\end{aligned} \tag{4.80}$$

and

$$\begin{aligned}
D_{h_1} &= \sum_{\kappa=1}^{\infty} \frac{(-1)^{\kappa+1} (\Delta x)^{2\kappa+2}}{(2\kappa+2)!} \left[ (2^{4\kappa+2} - 2^{2\kappa+2})c \right], \\
D_{h_2} &= \sum_{\kappa=1}^{\infty} \frac{(-1)^{\kappa} (\Delta x)^{2\kappa+1}}{(2\kappa+1)!} \left[ (2^{2\kappa+1} - 2^{4\kappa+1})\alpha \right], \\
D_{h_3} &= \sum_{\kappa=1}^{\infty} \frac{(-1)^{\kappa} (\Delta x)^{2\kappa+1}}{(2\kappa+1)!} \left[ (-2^{2\kappa} - 2^{4\kappa} + 2^{2\kappa+1})c \right], \\
D_{h_4} &= \sum_{\kappa=1}^{\infty} \frac{(-1)^{\kappa} (\Delta x)^{2\kappa+2}}{(2\kappa+2)!} \left[ (-2^{2\kappa+3} + 2^{4\kappa+3})\alpha \right].
\end{aligned} \tag{4.81}$$

It is easy to see that for the situation with  $\mathbf{K}$  diagonal and  $\eta = 0$ , all the coefficients disappears. When  $\eta \neq 0$ ,  $\alpha$  and  $\beta$  no longer vanishes. So for this case the  $\kappa = 1$  terms involving  $(\Delta x)^3$  dominates the local truncation errors  $w_j$  for both the vertical and horizontal fluxes.

The situation with  $\mathbf{K}$  not diagonal acts in a similar fashion. For this situation none of the variables  $c$ ,  $\alpha$  or  $\beta$  vanishes. Hence, also here the local truncation errors,  $w_j$ , are dominated by  $(\Delta x)^3$ . This holds for both  $\eta = 0$  and  $\eta \neq 0$ .

### Implications of These Results on the Error Approximation in the Discrete $\mathcal{L}^2$ -norms

The analysis above revealed the order of  $\Delta x$  dominating the expressions for the local truncation errors  $v_k$  and  $w_j$  for cells and edges yielding full internal stencils for the potentials and fluxes. This is equivalent to finding a bound on the vectors  $\mathbf{v}$  and  $\mathbf{w}$  in the maximum norm, assuming these vectors only contain elements related to the cells and edges having indexes in  $\mathcal{C}$  and  $\mathcal{E}$  respectively. For a diagonal permeability matrix

	$\eta = 0$	$\eta \neq 0$
$\nu_v$	$\rightarrow \infty$	4
$\nu_w$	$\rightarrow \infty$	2

TABLE 4.1: Results from situation I)

	$\eta = 0$	$\eta \neq 0$
$\nu_v$	4	4
$\nu_w$	2	2

TABLE 4.2: Results from situation II)

the results can be summarized by

$$\|\mathbf{v}\|_\infty = \begin{cases} 0, & \text{for } \eta = 0, \\ O((\Delta x)^4), & \text{for } \eta \neq 0, \end{cases} \quad \|\mathbf{w}\|_\infty = \begin{cases} 0, & \text{for } \eta = 0, \\ O((\Delta x)^3), & \text{for } \eta \neq 0, \end{cases} \quad (4.82)$$

and for a non-diagonal permeability matrix we obtained

$$\|\mathbf{v}\|_\infty = \begin{cases} O((\Delta x)^4), & \text{for } \eta = 0, \\ O((\Delta x)^4), & \text{for } \eta \neq 0, \end{cases} \quad \|\mathbf{w}\|_\infty = \begin{cases} O((\Delta x)^3), & \text{for } \eta = 0, \\ O((\Delta x)^3), & \text{for } \eta \neq 0. \end{cases} \quad (4.83)$$

To find the values  $\nu_v$  and  $\nu_w$  from Equations (4.20) and (4.35) we need bounds of  $\mathbf{v}$  and  $\mathbf{w}$  in the discrete  $\mathcal{L}^2$ -norms described in Equations (4.12) and (4.30), not the maximum norm. These bounds can be obtained by the following process.

Notice that

$$\max_k |v_k| = \|\mathbf{v}\|_\infty = M_1 = O((\Delta x)^{r_1}), \quad (4.84)$$

and

$$\max_j |w_j| = \|\mathbf{w}\|_\infty = M_2 = O((\Delta x)^{r_2}). \quad (4.85)$$

For  $\mathbf{v}$  we may thus write

$$\|\mathbf{v}\|_{\mathcal{L}^2} = \left( \frac{\sum_{k \in \mathcal{C}} A_k (v_k)^2}{\sum_{k \in \mathcal{C}} A_k} \right)^{\frac{1}{2}} \leq \left( (M_1)^2 \frac{\sum_{k \in \mathcal{C}} A_k}{\sum_{k \in \mathcal{C}} A_k} \right)^{\frac{1}{2}} = M_1 = O((\Delta x)^{r_1}). \quad (4.86)$$

In the case of  $\mathbf{w}$ , notice that on our uniform square grid all edges have the same length,  $|e_j|$ , and this length is of  $O(\Delta x)$ . Hence, we obtain

$$\|\mathbf{w}\|_{\mathcal{L}^2} = \left( \frac{\sum_{j \in \mathcal{E}} G_j \left( \frac{w_j}{|e_j|} \right)^2}{\sum_{j \in \mathcal{E}} G_j} \right)^{\frac{1}{2}} \leq \left( \left( \frac{M_2}{|e_j|} \right)^2 \frac{\sum_{j \in \mathcal{E}} G_j}{\sum_{j \in \mathcal{E}} G_j} \right)^{\frac{1}{2}} = \frac{M_2}{|e_j|} = O((\Delta x)^{r_2-1}). \quad (4.87)$$

Using the results (4.82) and (4.83) in Equations (4.86) and (4.87) the different values of  $\nu_v$  and  $\nu_w$  can be calculated, the results are summarized in Tables 4.1 and 4.2. Recall that these results hold for both the potential functions (4.42) and (4.43) when considering a general uniform square grid which is parallel to the frame of reference.

<b>K diagonal</b>	$\eta = 0$		$\eta \neq 0$	
	Potential	Flux	Potential	Flux
$u(x, y) = \sin(x) \sin(y)$	Exact	Exact	$O((\Delta x)^2)$	$O((\Delta x)^1)$
$u(x, y) = \cos(x) \cos(y)$	Exact	Exact	$O((\Delta x)^2)$	$O((\Delta x)^1)$

TABLE 4.3: Theoretical results for situation I)

<b>K not diagonal</b>	$\eta = 0$		$\eta \neq 0$	
	Potential	Flux	Potential	Flux
$u(x, y) = \sin(x) \sin(y)$	$O((\Delta x)^2)$	$O((\Delta x)^1)$	$O((\Delta x)^2)$	$O((\Delta x)^1)$
$u(x, y) = \cos(x) \cos(y)$	$O((\Delta x)^2)$	$O((\Delta x)^1)$	$O((\Delta x)^2)$	$O((\Delta x)^1)$

TABLE 4.4: Theoretical results for situation II)

Using these values of  $\nu_v$  and  $\nu_w$  in Equations (4.20) and (4.35), along with the values defined for  $\nu_A$  and  $\nu_T$  in Equations (4.24) and (4.40), we can calculate the error bounds of the potential and flux for the two potential functions (4.42) and (4.43) in the discrete  $\mathcal{L}^2$ -norm. The results are shown in Tables 4.3 and 4.4. Except for the exact case when  $\mathbf{K}$  is diagonal and  $\eta = 0$ , the convergence orders are consistent with earlier convergence proofs.

## 4.5 Error Analysis for Inner Cell Stencils on a Uniform Rectangular Grid in an Isotropic Medium

In this section we examine if the exactness phenomenon for the potential proved in Section 4.4 also hold for uniform rectangular grids in a isotropic medium when  $\eta = 0$ . This is a valid hypothesis due to a uniform square grid along with a diagonal, but not isotropic, permeability being equivalent to a uniform *rectangular* grid with isotropic permeability in the MPFA framework, see Equation (4.8) and the last paragraph in Section 4.1. The same is true for the situations described by having a uniform square grid with a non-diagonal permeability and a uniform *parallelogram* grid with an isotropic permeability. However, Section 4.4 showed that a non-diagonal permeability does *not* yield exactness, so it is unlikely that parallelogram cells then would.

To perform the analysis we leave the Taylor expansions presented in Section 4.4 and return to the basic framework developed in Section 3.5. This is done because it represents a fairly easier alternative when looking at one specific physical situation. Equation (3.47) along with variables (3.49) define the discretized left-hand side of the elliptic equation

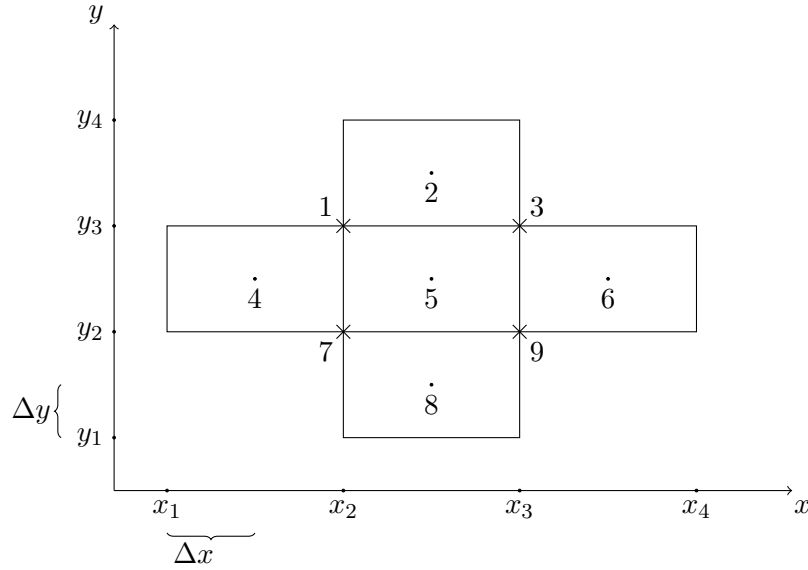


FIGURE 4.7: The spatial positions of the stencil coordinates for  $u$  (dots) and  $v$  (crosses) in a uniform rectangular grid.

(4.1) for a general inner cell. For cell 5, shown in Figure 4.7, this formula can be written as

$$\sum_{l \in \mathcal{K}_5} m_l u_l = a(2u_5 - u_4 - u_6) + b(2u_5 - u_2 - u_8). \quad (4.88)$$

Here we have used the fact that  $c$  and  $\gamma$  disappears for an isotropic permeability and  $\eta = 0$ . Potential values  $u_i$ ,  $i = 2, 4, 5, 6, 8$ , refers to the value of  $u(x, y) = \sin(x) \sin(y)$  in the cell centers of the grid in Figure 4.7. Equation (4.88) represents one line in the linear system

$$\mathbf{A} \mathbf{u}_e. \quad (4.89)$$

The right-hand side of Equation (4.1) for the same cell can be written as

$$\int_{\Omega_5} f \, d\tau = (k_1 + k_4)(v_3 - v_1 - v_9 + v_7) = 2(v_3 - v_1 - v_9 + v_7). \quad (4.90)$$

In this equation we have calculated the integral from Equation (A.22) in Appendix A.1 analytically using  $u(x, y) = \sin(x) \sin(y)$ , in addition to applying the fact that we have an isotropic permeability. The values  $v_i$ ,  $i = 1, 3, 7, 9$ , refers to the values of  $v(x, y) = \cos(x) \cos(y)$  in the coordinates marked by 1, 3, 7 and 9 in Figure 4.7. By looking at when Equation (4.88) equals Equation (4.90), we can find out when the MPFA method yields exact cell center potentials for uniform rectangular grids in an isotropic medium.

From Equation (4.8) in Section 4.1 we see that the general formulas for variables  $a$  and  $b$  can be written as

$$\begin{aligned} a &= \frac{k_1(\Delta y)^2}{\Delta x \Delta y}, \\ b &= \frac{k_4(\Delta x)^2}{\Delta x \Delta y}. \end{aligned} \quad (4.91)$$

For a general uniform rectangular grid we can write the following relation between  $\Delta x$  and  $\Delta y$

$$\Delta x = \xi \Delta y, \quad \xi \in (0, \infty), \quad (4.92)$$

where the case with  $\xi = 1$  is equivalent to having a uniform square grid. Using Equation (4.92) and the fact that the uniform rectangular grid is situated in an isotropic medium, variables  $a$  and  $b$  can be given by

$$\begin{aligned} a &= \frac{1}{\xi}, \\ b &= \xi. \end{aligned} \quad (4.93)$$

By applying Equations (4.92) and (4.93) when comparing Equations (4.88) and (4.90) it is possible to write Equations (4.88) and (4.90) as functions of the proportionality variable  $\xi$  from Equation (4.92)

$$\begin{aligned} L(\xi) &= \sum_{l \in \mathcal{K}_5} m_l u_l = a(2u_5 - u_4 - u_6) + b(2u_5 - u_2 - u_8) = a l_1(\xi) + b l_2(\xi), \\ , H(\xi) &= \int_{\Omega_5} f \, d\tau = 2(v_3 - v_1 - v_9 + v_7) = 2h(\xi). \end{aligned} \quad (4.94)$$

Calculating the difference between these two functions yield

$$E(\xi) = L(\xi) - H(\xi) = a l_1(\xi) + b l_2(\xi) - 2h(\xi). \quad (4.95)$$

Analyzing when  $E(\xi)$  disappears we obtain information about which relations between  $\Delta x$  and  $\Delta y$  the MPFA method yields exact cell center potentials for. Recall that formula (4.95) only holds for one cell at a time.

Calculating  $E(\xi)$  numerically for cell 5 in Figure 4.7 produced results of the form shown in Figures 4.8 and 4.9. The figures display an oscillating behavior around the  $\xi$ -axis revealing the existence of multiple values of  $\xi$  causing  $E(\xi)$  to disappear.

These results clearly indicates that the MPFA stencil for cell 5 in Figure 4.7 should be exact for  $u(x, y) = \sin(x) \sin(y)$  for certain proportionalities  $\xi$  between  $\Delta x$  and  $\Delta y$ . The key question is though, does the same values of  $\xi$  causing the stencil in cell 5 to yield exact potential cause the stencils in the remaining cells in the grid to yield exact potentials?

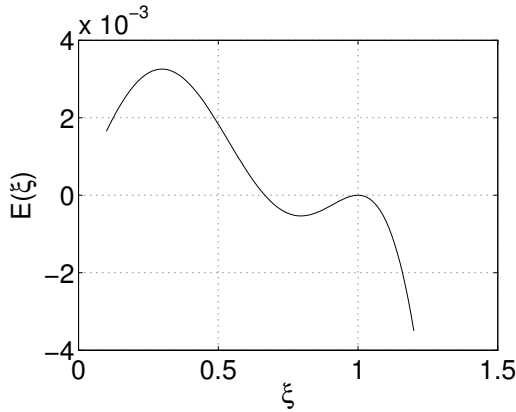


FIGURE 4.8: The oscillating effect of  $E(\xi)$  near  $\xi = 1$ .

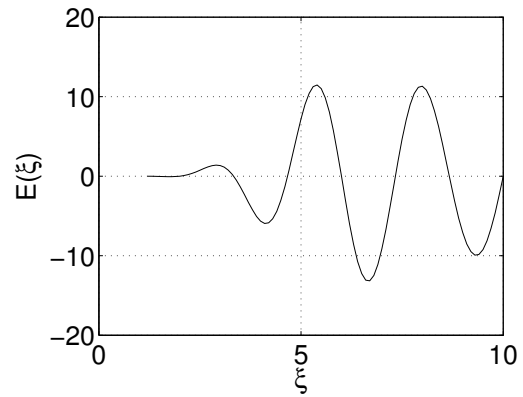


FIGURE 4.9: The oscillating effect of  $E(\xi)$  for larger values of  $\xi$ .

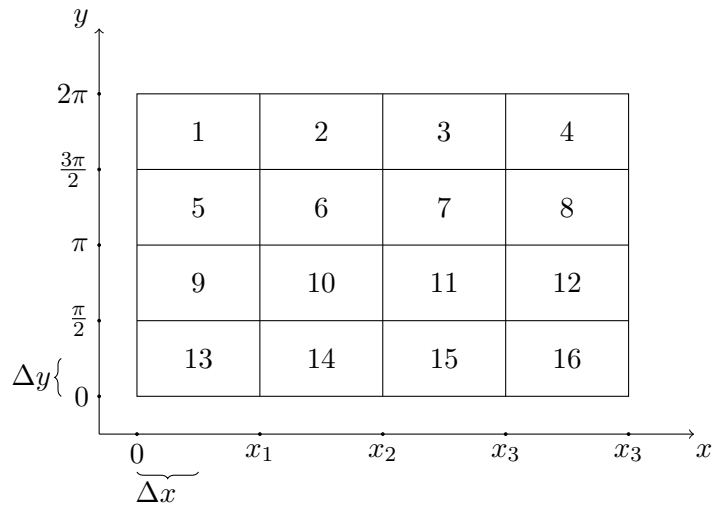


FIGURE 4.10: Sixteen cell uniform rectangular grid.

To test this we consider the grid shown in Figure 4.10. Calculating  $E(\xi)$  numerically for cells 1, 6, 7, 10, 11 for different values of  $\xi$  produced the results shown in Figure 4.11. All the cells in Figure 4.10 were tested but a selected few is presented in this figure to make it more readable. Taking a closer look at the results in Figure 4.11 shows that the only  $\xi$  causing  $E(\xi)$  to disappear for each of the cells is  $\xi = 1$  and  $\xi = 4, 8, 12, 16, \dots$ . The situation when  $\xi = 1$  is the case when we have square cells, and has already been investigated.

The example in the last paragraph for the grid in Figure 4.10 used  $\Delta y = \frac{\pi}{4}$ . By decreasing this value to  $\Delta y = \frac{\pi}{8}$ , the values of  $\xi$ , other than  $\xi = 1$ , causing  $E(\xi)$  to disappear then became  $\xi = 8, 16, 24, \dots$ , see Figure 4.12. A similar trend is found when further decreasing  $\Delta y$  by a factor of  $\frac{1}{2}$ , next yielding  $\xi = 16, 32, 48, \dots$  and then  $\xi = 32, 64, 96, \dots$

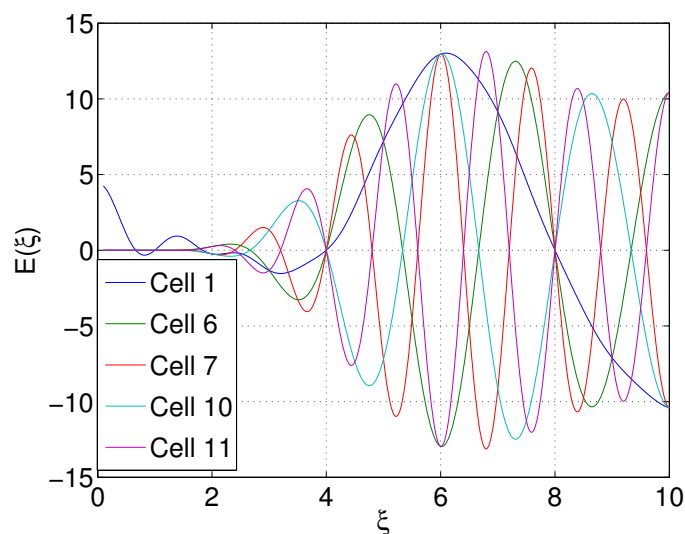


FIGURE 4.11: The oscillating effect of  $E(\xi)$  for cells 1, 6, 7, 10, 11 from Figure 4.10.

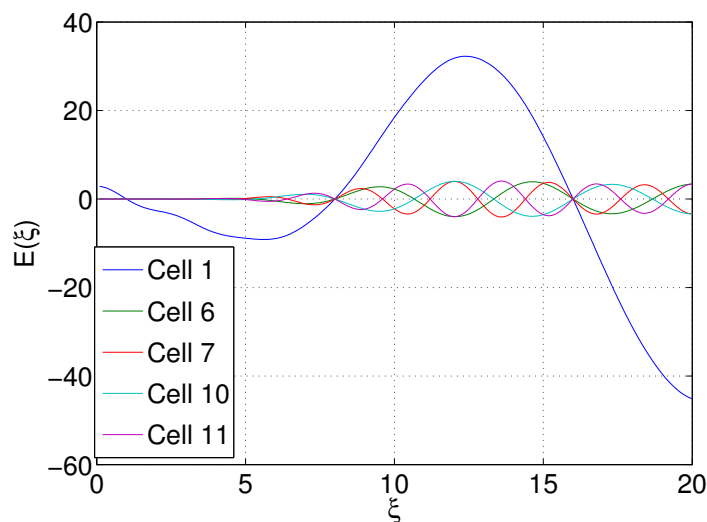


FIGURE 4.12: The oscillating effect of  $E(\xi)$  for cells 1, 6, 7, 10, 11 from a similar grid as Figure 4.10 using  $\Delta y = \frac{\pi}{8}$ .

The same kind of recurrence is seen for  $u(x, y) = \cos(x) \cos(y)$ , but now for  $\xi = 2, 6, 10, \dots$  and similar values of  $\xi$  for different  $\Delta y$ .

These results show that it is *not* generally possible to obtain exact potential values for the MPFA method when rewriting a problem on a uniform square grid with a diagonal permeability matrix as a problem on a uniform rectangular grid in an isotropic medium for our trigonometric potential functions. This suggests that the exactness phenomenon occurs due to a cancellation effect for the trigonometric potential functions when applying a uniform square grid. The cancellation effect does however hold for uniform rectangular grids having certain special ratios between the side lengths of the cells.

A similar analysis as the one presented in this section has *not* been conducted for the fluxes. However, it is likely to believe that also the fluxes, *at most*, only yield exactness for certain values of  $\xi$  for uniform rectangular grids. This assumption is based on the numerical results obtained in Chapter 5.

## 4.6 Summary of the Theoretical Results

In Section 4.4 we obtained theoretical error bounds of the potential and flux for cells and edges yielding full internal stencils, see beginning Section 4.4 and Figures 4.2 to 4.4, of the MPFA method for potential functions (4.42) and (4.43). The error bounds hold for general permeabilities and different positions of the continuity points of the method, and was calculated in the discrete  $\mathcal{L}^2$ -norms given in Equations (4.12) and (4.30). The results, listed in Tables 4.3 and 4.4, show the method to be exact for both the potential and the flux for diagonal permeability matrices when  $\eta = 0$ . The situation involving a diagonal permeability matrix and  $\eta \neq 0$ , in addition to the situations with a non-diagonal permeability matrix with both  $\eta = 0$  and  $\eta \neq 0$ , yielded the expected bound for both the potential and the flux based on earlier convergence proofs.

Looking to see if the exactness phenomenon for the potential could be extended to a uniform rectangular grid in an isotropic medium showed that this is possible only for a limited number of ratios between the side lengths in the rectangular cells. Therefore, a uniform rectangular grid in an isotropic medium will generally *not* yield exact potential for the MPFA method with  $\eta = 0$ . This result was obtained in Section 4.5.



## Chapter 5

# Numerical Results

In Chapter 4 we derived theoretical error estimates for the MPFA method for cells and edges yielding full internal stencils for the potential functions (4.42) and (4.43) on a uniform square grid in a homogeneous medium. In this chapter the results are tested numerically. This is done in the first part of this chapter. Here we have implemented the method using *periodic boundary conditions*, yielding a grid without a boundary. In Section 5.3 we apply Neumann and Dirichlet boundary conditions in order to develop a numerical overview of the exactness phenomenon. A priori conditions imposed on the Neumann and Dirichlet boundary conditions in order to retain the possibility of the MPFA method yielding exact potential and fluxes in Section 5.3 is briefly discussed in Section 5.2. The last part of this chapter is devoted to investigating application of the exactness phenomenon to general potential functions which has been approximated by Fourier series.

In all implementations a Gaussian quadrature of sufficiently high order is applied to calculate the integral of the source term in the representative equation (2.20). This is done in order to not corrupt the convergence results of the MPFA method with errors coming from the calculation of the integral. The computer used to obtain the results presented in this chapter had a working precision of order  $10^{-16}$ . Boundary conditions were handled by using smaller interaction volumes close to the boundary, not by having ghost cells with zero permeability outside the grid.

### 5.1 Numerical Results with Periodic Boundary Conditions

By using periodic boundary conditions it is possible to mimic the conditions of having full internal stencils, explained in Section 4.4, for the potential and fluxes on each cell

1	2	1	2	1	2
3	4	3	4	3	4
1	2	1	2	1	2
3	4	3	4	3	4
1	2	1	2	1	2
3	4	3	4	3	4

FIGURE 5.1: A uniform square grid with periodic boundary conditions (thick layer) can be regarded as a subgrid in an infinitely large grid built by placing the grid as "tiles" next to each other.

and edge in a grid. This is done by letting the influx on the left boundary equal the outflux of the right boundary, and the influx of the bottom boundary equal the outflux of the top boundary. Then the grid reappears as tiles around the original grid, as shown in Figure 5.1. The cells of the original grid is thus only internal cells in a larger grid, and we obtain full internal stencils for both the potential and the flux for all cells and edges.

Consider the situations from Section 4.4.3

- I)  $\mathbf{K}$  diagonal for  $\eta = 0$  and  $\eta \neq 0$ ,
- II)  $\mathbf{K}$  *not* diagonal for  $\eta = 0$  and  $\eta \neq 0$ .

We choose the permeabilities of situations I) and II) to be respectively

$$\mathbf{K} = \begin{pmatrix} 0.5 & 0 \\ 0 & 2 \end{pmatrix}, \quad (5.1)$$

and

$$\mathbf{K} = \begin{pmatrix} 0.5 & 0.1 \\ 0.1 & 2 \end{pmatrix}. \quad (5.2)$$

For the case with  $\eta \neq 0$  we set  $\eta = \frac{1}{3}$ .

Having implemented the MPFA method with periodic boundary conditions, we ran the situations I) and II) on the domain  $[0, 2\pi] \times [0, 2\pi]$ . A uniform square grid as the one shown in Figure 4.1 in Section 4.1 was applied, starting out with four cells. Then we made six refinements of the grid, each time dividing each of the cells into four new cells. The results obtained are shown in Tables 5.1 and 5.2.

<b>K diagonal</b>	$\eta = 0$		$\eta = \frac{1}{3}$	
	Potential	Flux	Potential	Flux
$u(x, y) = \sin(x) \sin(y)$	Exact	Exact	$O((\Delta x)^2)$	Exact
$u(x, y) = \cos(x) \cos(y)$	Exact	Exact	$O((\Delta x)^2)$	Exact

TABLE 5.1: Numerical results for situation I)

<b>K not diagonal</b>	$\eta = 0$		$\eta = \frac{1}{3}$	
	Potential	Flux	Potential	Flux
$u(x, y) = \sin(x) \sin(y)$	$O((\Delta x)^2)$	$O((\Delta x)^2)$	$O((\Delta x)^2)$	$O((\Delta x)^2)$
$u(x, y) = \cos(x) \cos(y)$	$O((\Delta x)^2)$	$O((\Delta x)^2)$	$O((\Delta x)^2)$	$O((\Delta x)^2)$

TABLE 5.2: Numerical results for situation II)

Recall the results of the theoretical error analysis of situations I) and II) for full internal stencils shown in Tables 4.3 and 4.4 in Section 4.4.3. Comparing these results with the ones in Tables 5.1 and 5.2 shows a perfect match for all the potentials. For the fluxes our theoretical results are verified for a diagonal permeability and  $\eta = 0$ . In addition, we see the expected second order convergence numerically, as in previous articles. However, situation I) with  $\eta = \frac{1}{3}$  yields exact flux, which is not foreseen in any way.

Why we get exact fluxes for situation I) with  $\eta = \frac{1}{3}$ , which differs significantly from the second order convergence found in the theoretical results, is not clear. To establish an overview of the situation we would first like to check if there is something special with the domain  $[0, 2\pi] \times [0, 2\pi]$  causing the phenomenon. In order to preserve a well-posed problem with periodic boundary conditions for trigonometric potential functions (4.42) and (4.43), we need to require the domains to have length  $2n\pi$ ,  $n = 1, 2, 3, \dots$ , in each grid direction. Testing for the domains

$$\left[ \frac{\pi}{2}, \frac{5\pi}{2} \right] \times \left[ \frac{\pi}{2}, \frac{5\pi}{2} \right], \quad [2\pi, 8\pi] \times [2\pi, 8\pi], \quad \left[ \frac{\pi}{2}, \frac{9\pi}{2} \right] \times \left[ \frac{\pi}{2}, \frac{9\pi}{2} \right],$$

having length  $2\pi$ ,  $6\pi$  and  $4\pi$  respectively in each grid direction, yielded the same result as for the domain  $[0, 2\pi] \times [0, 2\pi]$ . Thus, the result seems to hold for general uniform square grids preserving well-posedness for the problem.

The phenomenon of obtaining exact fluxes when having a diagonal  $\mathbf{K}$  and  $\eta = \frac{1}{3}$ , as expected, disappears when considering rectangular cells. For this case we get second order convergence for both the potential and flux. However, by setting  $\eta = \frac{1}{2}$  the convergence order of the fluxes for a uniform rectangular grid increases to fourth order,

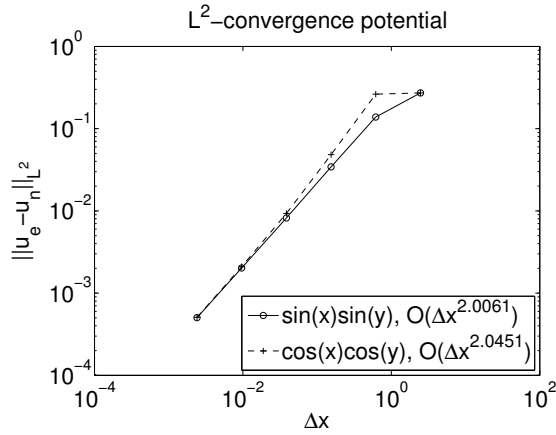


FIGURE 5.2: Convergence plot of the potential for a diagonal permeability and  $\eta = \frac{1}{2}$  on uniform rectangular grids.

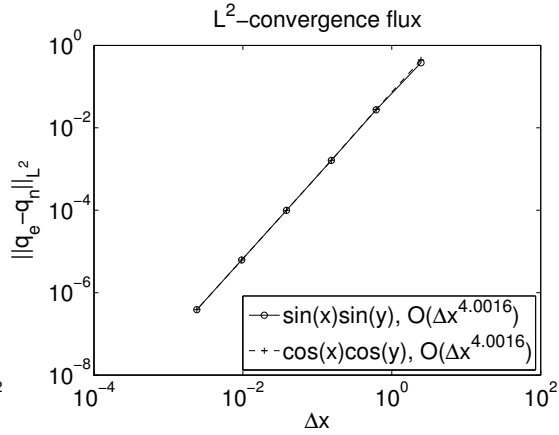


FIGURE 5.3: Convergence plot of the flux for a diagonal permeability and  $\eta = \frac{1}{2}$  on uniform rectangular grids.

<b>K diagonal</b> , $\eta \neq 0$	Uniform square grid	Uniform rectangular grid	
	All $\eta \neq 0$	$\eta = \frac{1}{2}$	Other $\eta \neq 0$
$u(x, y) = \sin(x) \sin(y)$	Exact	$O((\Delta x)^4)$	$O((\Delta x)^2)$
$u(x, y) = \cos(x) \cos(y)$	Exact	$O((\Delta x)^4)$	$O((\Delta x)^2)$

TABLE 5.3: Numerical results for the fluxes in situation I) with  $\eta \neq 0$  for different grid types and  $\eta$ .

see Figures 5.2 and 5.3. For small deviations in  $\eta$  from  $\frac{1}{2}$  we also see close to fourth order convergence for the early refinements of the grid, before dropping to second order for finer refinements. All other values of  $\eta \neq 0$  shows the same behavior as for  $\eta = \frac{1}{3}$ . This indicates that the value  $\eta = \frac{1}{2}$  might be special. The numerical results for situation I) with different grid types and  $\eta$  are organized in Table 5.3.

Among the results in Table 5.3 only the second order convergence is as expected. For the exact and superconvergent (fourth order convergent) cases, the error analysis gives no indication as to why this happens. By looking closer at the formula (4.70) for specific grids and  $\eta$ , no signs of deviation from the results obtained in Table 4.3 in Section 4.4.3 are found. However, the error estimate in Equation (4.35) from Section 4.3 only gives an upper bound on the error. It is therefore unproblematic that the numerical convergence rates are larger than this approximation. Hence we conclude that the results seen in Table 5.3 can not be explained by our error analysis, but there is nothing in our calculations contradicting the result.

In light of the recent discoveries of the importance of  $\eta = \frac{1}{2}$  when  $\mathbf{K}$  is diagonal, we want to see if this value of  $\eta$  plays a similar role when  $\mathbf{K}$  is not diagonal. Testing if  $\eta = \frac{1}{2}$  yield any changes in convergence orders in Table 5.2 for situation II) shows no

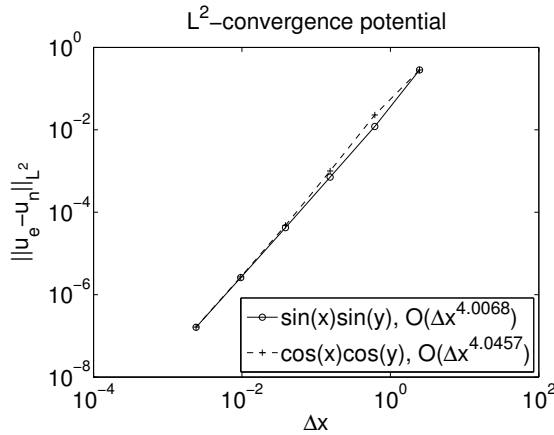


FIGURE 5.4: Convergence plot of the potential for isotropic permeability and  $\eta = 0$  on uniform rectangular grids.

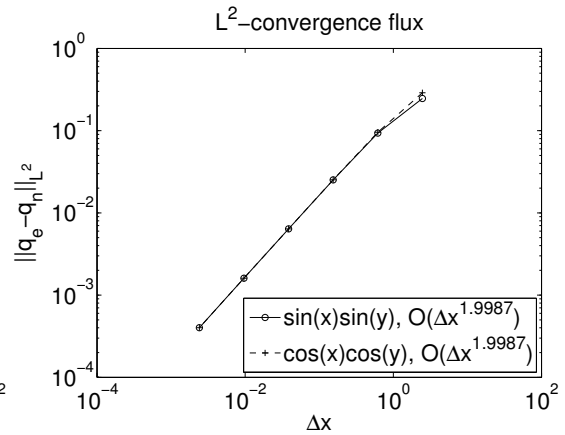


FIGURE 5.5: Convergence plot of the flux for isotropic permeability and  $\eta = 0$  on uniform rectangular grids.

changes. Other values of  $\eta$  and other non-diagonal permeabilities than the one given in Equation (5.2) also seem to have no effect on the result. No changes are observed for the situation with  $\mathbf{K}$  not diagonal and  $\eta = 0$  either when varying the domain and the permeability.

Next we test what happens with the convergence rate when having a uniform *rectangular* grid in a medium related to a diagonal permeability when  $\eta = 0$ . Numerical test for the domains

$$[0, 4\pi] \times [0, 2\pi],$$

$$[0, 2\pi] \times \left[ \frac{\pi}{2}, \frac{13\pi}{2} \right],$$

shows the regular second order convergence for both the potential and the flux. However, if we let the permeability be isotropic, the potential yields superconvergence along the order of  $(\Delta x)^4$  while the flux remains at second order convergence, see Figures 5.4 and 5.5. There are no result from Chapter 4 explaining why this occurs. We also see exact potential for certain values of  $\xi$ ,  $\Delta x = \xi \Delta y$ , depending on the size of  $\Delta y$  in isotropic mediums, as predicted in Section 4.5. However, making more refinements of the grid (decreasing  $\Delta y$ ) requires larger and larger values of  $\xi$ , making the cells more and more stretched, to sustain the exactness of the potential. This stretching of the cells in return seems to distort the convergence of the flux. Hence, we do not consider the exactness phenomenon for certain values of  $\xi$  for uniform rectangular grids as we move on to consider Neumann and Dirichlet boundary conditions to develop a numerical overview of when the MPFA method yields exact both potential and flux.

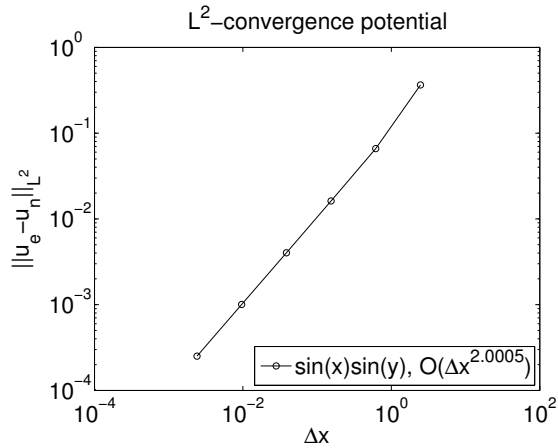


FIGURE 5.6: Convergence plot of the potential for diagonal permeability and  $\eta = \frac{1}{2}$  on uniform rectangular grids in domains yielding zero Dirichlet Boundary Conditions.

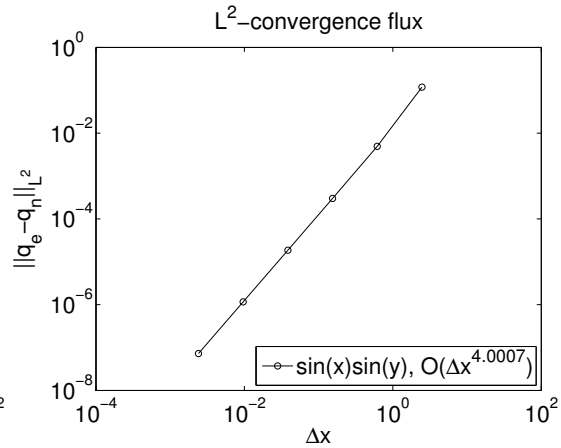


FIGURE 5.7: Convergence plot of the flux for diagonal permeability and  $\eta = \frac{1}{2}$  on uniform rectangular grids in domains yielding zero Dirichlet Boundary Conditions.

## 5.2 A Short Comment on Boundary Conditions

For the MPFA method to retain the possibility of obtaining exact potential and fluxes for problems involving boundary conditions we need these conditions to be exact. Using Neumann boundary conditions this means that the boundary fluxes have to be calculated exactly, and for Dirichlet conditions only zero boundary conditions are acceptable. This is due to the fact that Dirichlet conditions enter the method as potential values in the continuity points on the boundary edges. These values need to capture information about the exact flux across the entire edge. This is only possible when having zero boundary conditions, because nonzero conditions would create an error when approximating the fluxes across the boundary edges of the domain from only the one potential value on each edge.

## 5.3 Numerical Overview of the Exactness Phenomenon

Having obtained numerical results for the MPFA method when using periodic boundary conditions, we now consider the case with Neumann and Dirichlet boundary conditions. This is done in order to establish a complete numerical overview of the exactness phenomenon.

When applying Neumann boundary conditions we obtain exact potential and fluxes on arbitrary uniform square grids when  $\mathbf{K}$  is diagonal and  $\eta = 0$ . For rectangular domains the exactness phenomenon disappears. These results hold for both trigonometric potential functions (4.42) and (4.43).

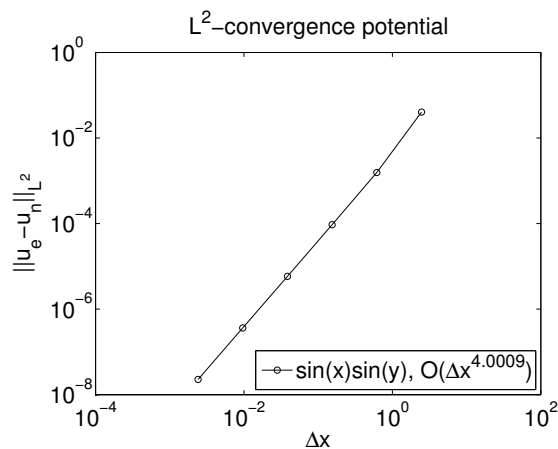


FIGURE 5.8: Convergence plot of the potential for isotropic permeability and  $\eta = 0$  on uniform rectangular grids in domains yielding zero Dirichlet Boundary Conditions.

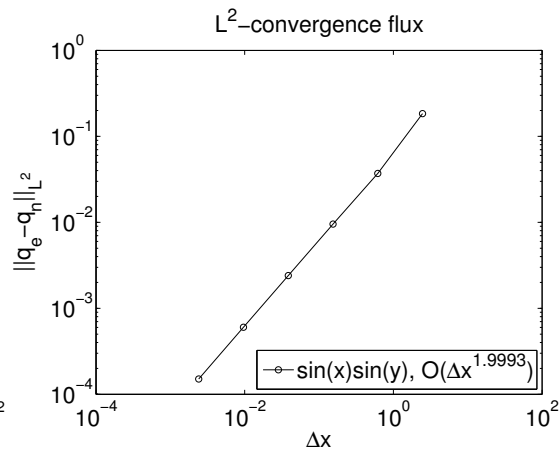


FIGURE 5.9: Convergence plot of the flux for isotropic permeability and  $\eta = 0$  on uniform rectangular grids in domains yielding zero Dirichlet Boundary Conditions.

Using Dirichlet boundary condition, the exactness is obtained on uniform square grids yielding zero boundary conditions for a diagonal  $\mathbf{K}$  and  $\eta = 0$ . Setting  $\eta \neq 0$  we observe the same flux exactness and superconvergence (fourth order convergence) for the flux as for the periodic boundary conditions when having a square and rectangular domain respectively with zero boundary conditions, see for example Figures 5.6 and 5.7. Also the same fourth order convergence for the potential is seen on uniform rectangular grids yielding zero boundary conditions for isotropic permeability when  $\eta = 0$ , see Figures 5.8 and 5.9. The Dirichlet case was also tested for both (4.42) and (4.43).

By combining these results with the results obtained in Section 5.1, we can create the following numerical overview of the grids causing the exactness phenomenon for different types of boundary conditions when having diagonal permeability matrix and  $\eta = 0$ :

- **Periodic boundary conditions:** Uniform square grid preserving well-posedness of the problem.
- **Neumann boundary conditions:** Uniform square grid.
- **Dirichlet boundary conditions:** Uniform square grid yielding zero boundary conditions.

These results support the explanation of the exactness phenomenon occurring due to a cancellation effect in the MPFA method for the trigonometric potential function on a uniform square grid for diagonal  $\mathbf{K}$  and  $\eta = 0$ .

Numerical test of the MPFA method applied to potential functions  $u(x) = \sin(x)$  and  $u(x) = \cos(x)$  in one and two dimensions gave no results above second order convergence for potential and flux.

## 5.4 Investigation of Application of the Exactness Phenomenon to Fourier Series

During a visit to the annual NUPUS conference in Freudenstadt, Germany, this thesis was discussed with PhD-student David Seus and Professor Christian Rohde from the University of Stuttgart. They proposed that the results obtained in Chapter 4 and Sections 5.1 and 5.3 might suggest that it is possible to obtain exact potential and flux for the MPFA method when using general potential functions approximated by Fourier series. This section is devoted to investigating this proposal.

Potential function  $u(x, y) \in \mathcal{L}^2([0, 2\pi] \times [0, 2\pi])$  can be written as the Fourier series [33]

$$u(x, y) = \sum_{m, n \in \mathbb{Z}} \alpha_{n, m} e^{inx} e^{imy}. \quad (5.3)$$

Rewritten in trigonometric form using Euler's formula, Equation (5.3) becomes

$$u(x, y) = \sum_{m, n \in \mathbb{N}_0} \left[ A_{n, m} \cos(mx) \cos(ny) + B_{n, m} \sin(mx) \cos(ny) + C_{n, m} \cos(mx) \sin(ny) + D_{n, m} \sin(mx) \sin(ny) \right]. \quad (5.4)$$

The formulas describing the complex coefficients  $\alpha_{n, m}$ ,  $A_{n, m}$ ,  $B_{n, m}$ ,  $C_{n, m}$  and  $D_{n, m}$  are omitted, as these formulas have no significance for the conclusions drawn in this section. The only condition implied on the coefficients is that we need them to tend to zeros as the number of terms in the Fourier series goes to infinity. If this property is not fulfilled, the truncation error of leaving out the tail of the series when implementing the function on a finite computer will corrupt the exactness of the MPFA method.

Since the elliptic operator  $\nabla \cdot (\mathbf{K}\nabla \cdot)$  is a linear operator, due to the linearity of the divergence and gradient operator and linearity of matrix calculations, the following results holds for function  $u(x, y)$  from Equation (5.3)

$$-\nabla \cdot (\mathbf{K}\nabla u(x, y)) = f(x, y) \quad \Leftrightarrow \quad -\sum_{m, n \in \mathbb{Z}} \alpha_{n, m} \nabla \cdot (\mathbf{K}\nabla (e^{inx} e^{imy})) = f(x, y). \quad (5.5)$$

Assume that potential function  $u(x, y)$  can be exactly approximated by a finite Fourier series. Looking at Equation (5.4) we see that not all of the trigonometric functions contained in this expression is part of our results from Chapter 4 and Sections 5.1 and 5.3. Therefore, we test the convergence of the following functions numerically

$$u(x, y) = \cos(x) \sin(y), \quad (5.6)$$

$$u(x, y) = \sin(x) \cos(y), \quad (5.7)$$

$$u(x, y) = \sin(nx) \sin(my), \quad n, m \in \mathbb{N}_0. \quad (5.8)$$

After extensive numerical testing the same results as for the potential functions (4.42) and (4.43) were obtained for functions (5.6) and (5.7). For function of the type (5.8), the results were more discouraging. When  $n = m$  the MPFA method was exact for potential and flux on uniform square grids with  $\mathbf{K}$  diagonal and  $\eta = 0$ , rectangular cells yielded second order convergence. This result was to be expected, and coincide perfectly with the results obtained in Sections 5.1 and 5.3. However, when  $n \neq m$  the result changes. For this situation we obtain second order convergence on uniform square grids, and exact potential and flux on domains where either the length of the cells in the x-direction has been scaled with the ratio  $\frac{m}{n}$  or the length in the y-direction has been scaled by  $\frac{n}{m}$ . The same results were obtained for all three types of boundary conditions, taking into account well-posedness for the periodic case and zero boundary conditions for the Dirichlet case.

These results clearly show that the only time the MPFA method may yield exact potential and flux for potential functions approximated by Fourier series is when all terms with  $n \neq m$  from Equation (5.4) disappears. The number of functions satisfying this condition for its Fourier approximation is significantly low. Therefore, we conclude from this section that it is *not* possible to use a Fourier approximation of general potential functions in order to obtain exact potential and flux using the MPFA method. Even though this investigation proved to be futile, the numerical results for functions of the type (5.8) with  $n \neq m$  gives new insight into the explanation of the exactness phenomenon. Based on the numerical results obtained in this section it seems that the exactness phenomenon occurs due to a cancellation effect when the trigonometric functions has *an equal number of oscillations in both spatial directions in the domain*. This clearly shows that the exactness phenomenon of the MPFA method for the trigonometric potential functions  $u(x, y) = \sin(x) \sin(y)$  and  $u(x, y) = \cos(x) \cos(y)$  is a two dimensional phenomenon.



## Chapter 6

# Conclusion

In this thesis we have established theoretical error estimates for the MPFA  $O(\eta)$ -method (MPFA) applied to the elliptic equation (2.20) with periodic boundary conditions on uniform square grids in a homogeneous medium for the potential functions

$$u(x, y) = \sin(x) \sin(y), \quad u(x, y) = \cos(x) \cos(y). \quad (1.1)$$

These estimates were based on the theoretical framework presented by Nordbotten et al. in [21], which is explained in Section 3.5. An extension of these result to uniform *rectangular* grids were discussed, and shown to hold for certain special ratios between the side lengths in the rectangular cells. In Chapter 5 the theoretical result were tested numerically, and differences between theoretical and numerical convergence rates were discussed.

Both the theoretical error estimates and the numerical tests clearly show that the potential functions (1.1) yield potential and fluxes exact to working precision on uniform square grids preserving well-posedness of the problem for the situation described above when the permeability,  $\mathbf{K}$ , is diagonal and  $\eta = 0$ . This convergence is proved to hold for *any* anisotropy within a diagonal permeability. Along with the uniform flow case, these are the only examples of functions proved to be exact for the MPFA method. However, exactness is also seen numerically for the MPFA method for 3. degree polynomials in [34], which might also be an instance worth taking a closer look at.

We have also numerically seen exact fluxes for the case when the permeability is diagonal and  $\eta \neq 0$  on uniform square grids preserving well-posedness of the problem. Super-convergence (fourth order convergence) on uniform rectangular grids is observed for the fluxes for a diagonal permeability and  $\eta = \frac{1}{2}$ , and for the potential for an isotropic permeability and  $\eta = 0$ . These result have though not been established theoretically

by the error analysis. The same odd results are also obtained numerically using zero Dirichlet conditions.

Exactness of the potential and the fluxes is also seen numerically for Neumann boundary conditions on arbitrary uniform square grids and for Dirichlet boundary conditions on uniform square grids yielding zero boundary conditions. These results, along with the results from the case with periodic boundary conditions, shows that there is a cancellation effect causing the exactness phenomenon when the trigonometric potential functions (1.1) are applied to uniform square grids in a homogeneous medium related to a diagonal permeability matrix for  $\eta = 0$ .

In Section 5.4 we also briefly investigated the possibility of the MPFA method yielding exact potential and flux for general potential functions approximated by Fourier series. Large limitations on the number of potential functions yielding Fourier approximations which were able of producing exact potential and flux using the MPFA method were found. Hence, due to the lack of application to more general functions, further investigations were dropped. Even though the investigation proved futile, it produced results expanding our knowledge of the exactness phenomenon. This resulted in the explanation of the exactness phenomenon occurring due to a cancellation effect when the trigonometric potential functions has an equal number of oscillations in both spatial directions in the domain. This clearly indicates that the exactness phenomenon is a two dimensional phenomenon.

## Appendix A

# General Truncation Error Formulas for Inner Cell and Edge Stencils on Uniform Square Grids

In this appendix we derive general expression for the terms used to calculate the local truncation errors  $v_k$  and  $w_j$  related to cells and edges yielding *full internal stencils*, explained in the introduction to Section 4.4 and shown in Figure 4.2. These errors make up the elements of vectors  $\mathbf{v}$  and  $\mathbf{w}$  from Equations (4.14) and (4.28), and are given by Equations (4.26) and (4.41). As a framework for our calculations we use the situation explained in Section 4.1.

### A.1 General Formula for the Potential

We start of by looking at the expression

$$\sum_{l \in \mathcal{K}_k} m_l u_l^{(e)}, \quad (\text{A.1})$$

from Equation (4.26) in Section 4.2. By letting Equation (A.1) represent the mass conservation for cell 5 in Figure 4.1, the expression can be written as

$$\sum_{l \in \mathcal{K}_5} m_l u_l^{(e)} = m_1(u_1^{(e)} + u_9^{(e)}) + m_3(u_3^{(e)} + u_7^{(e)}) + m_4(u_4^{(e)} + u_6^{(e)}) + m_2(u_2^{(e)} + u_8^{(e)}) + m_5 u_5^{(e)}, \quad (\text{A.2})$$

see [21]. The weights  $m_l$ ,  $l = 1, 2, 3, 4, 5$ , are given in Equation (3.49) in Section 3.5. To easier be able to compare the terms in Equation (4.26) we want to write them in terms

of the value of the potential at a single point in the grid. This point is chosen to be the top right corner of cell 5. We can then write Equation (A.2) as a Taylor expansion from this coordinate

$$\begin{aligned}
 \sum_{l \in \mathcal{K}_5} m_l u_l^{(e)} &= m_1(u(x_3 - 3\Delta x, y_3 + \Delta y) + u(x_3 + \Delta x, y_3 - 3\Delta y)) \\
 &\quad + m_3(u(x_3 + \Delta x, y_3 + \Delta y) + u(x_3 - 3\Delta x, y_3 - 3\Delta y)) \\
 &\quad + m_4(u(x_3 - 3\Delta x, y_3 - \Delta y) + u(x_3 + \Delta x, y_3 - \Delta y)) \\
 &\quad + m_2(u(x_3 - \Delta x, y_3 + \Delta y) + u(x_3 - \Delta x, y_3 - 3\Delta y)) \\
 &\quad + m_5 u(x_3 - \Delta x, y_3 - \Delta y).
 \end{aligned} \tag{A.3}$$

From Equation (C.2) in Appendix C.1 we know that a general two dimensional Taylor expansion takes the form

$$\begin{aligned}
 f(x' + \Delta x, y' + \Delta y) &= f(x, y) + \left[ \Delta x \frac{\partial f}{\partial x} \Big|_{(x', y')} + \Delta y \frac{\partial f}{\partial y} \Big|_{(x', y')} \right] \\
 &\quad + \frac{1}{2!} \left[ (\Delta x)^2 \frac{\partial^2 f}{\partial x^2} \Big|_{(x', y')} + 2\Delta x \Delta y \frac{\partial^2 f}{\partial x \partial y} \Big|_{(x', y')} \right. \\
 &\quad \left. + (\Delta y)^2 \frac{\partial^2 f}{\partial y^2} \Big|_{(x', y')} \right] + \frac{1}{3!} \left[ (\Delta x)^3 \frac{\partial^3 f}{\partial x^3} \Big|_{(x', y')} \right. \\
 &\quad \left. + 3(\Delta x)^2 \Delta y \frac{\partial^3 f}{\partial x^2 \partial y} \Big|_{(x', y')} + 3\Delta x (\Delta y)^2 \frac{\partial^3 f}{\partial x \partial y^2} \Big|_{(x', y')} \right. \\
 &\quad \left. + (\Delta y)^3 \frac{\partial^3 f}{\partial y^3} \Big|_{(x', y')} \right] + \dots
 \end{aligned} \tag{A.4}$$

Here we have assumed that  $u(x, y)$  exists and is continuous in a neighborhood of  $(x', y')$ , such that the following equality holds

$$\frac{\partial^2 u}{\partial x \partial y}(x, y) = \frac{\partial^2 u}{\partial y \partial x}(x, y). \tag{A.5}$$

Assume that  $u(x, y)$  is infinitely smooth. Applying the general Taylor formula, Equation (A.4), to Equation (A.3) and rearranging the terms then yields

$$\begin{aligned}
 \sum_{l \in \mathcal{K}_5} m_l u_l^{(e)} &= u(x_3, y_3) \left[ \sum_{l'=1}^5 m_{l'} g_{l'}(0, 0, 1) \right] + \frac{\partial u}{\partial x} \Big|_{(x_3, y_3)} \left[ \sum_{l'=1}^5 m_{l'} g_{l'}(1, 0, 1) \right] \\
 &\quad + \frac{\partial u}{\partial y} \Big|_{(x_3, y_3)} \left[ \sum_{l'=1}^5 m_{l'} g_{l'}(0, 1, 1) \right] + \frac{\partial^2 u}{\partial x^2} \Big|_{(x_3, y_3)} \left[ \sum_{l'=1}^5 m_{l'} g_{l'}(2, 0, 1) \right] \\
 &\quad + \frac{\partial^2 u}{\partial x \partial y} \Big|_{(x_3, y_3)} \left[ \sum_{l'=1}^5 m_{l'} g_{l'}(1, 1, 2) \right] + \frac{\partial^2 u}{\partial y^2} \Big|_{(x_3, y_3)} \left[ \sum_{l'=1}^5 m_{l'} g_{l'}(0, 2, 1) \right] \\
 &\quad + \dots
 \end{aligned} \tag{A.6}$$

Functions  $g_{l'}$ ,  $l' = 1, 2, \dots, 5$ , are given by

$$\begin{aligned}
 g_1(n, m, \omega) &= \begin{cases} 2, & n = m = 0, \\ \frac{1}{(n+m)!} [(-1)^n 3^n \omega (\Delta x)^n (\Delta y)^m + (-1)^m 3^m \omega (\Delta x)^n (\Delta y)^m], & \text{otherwise,} \end{cases} \\
 g_2(n, m, \omega) &= \begin{cases} 2, & n = m = 0, \\ \frac{1}{(n+m)!} [(-1)^n \omega (\Delta x)^n (\Delta y)^m + (-1)^{n+m} 3^m \omega (\Delta x)^n (\Delta y)^m], & \text{otherwise,} \end{cases} \\
 g_3(n, m, \omega) &= \begin{cases} 2, & n = m = 0, \\ \frac{1}{(n+m)!} [\omega (\Delta x)^n (\Delta y)^m + (-1)^{n+m} 3^{n+m} \omega (\Delta x)^n (\Delta y)^m], & \text{otherwise,} \end{cases} \\
 g_4(n, m, \omega) &= \begin{cases} 2, & n = m = 0, \\ \frac{1}{(n+m)!} [(-1)^{n+m} 3^n \omega (\Delta x)^n (\Delta y)^m + (-1)^m \omega (\Delta x)^n (\Delta y)^m], & \text{otherwise,} \end{cases} \\
 g_5(n, m, \omega) &= \begin{cases} 1, & n = m = 0, \\ \frac{1}{(n+m)!} (-1)^{n+m} \omega (\Delta x)^n (\Delta y)^m, & \text{otherwise.} \end{cases}
 \end{aligned} \tag{A.7}$$

Here  $\omega$  are the binomial coefficients coming from the Taylor expansion, as explained in Appendix C.1. If  $u(x, y)$  were to be finite times differentiable, series (A.6) becomes a finite series.

It is easy to see from Equation (A.7) that when  $n + m \geq 1$  we may write

$$\sum_{l'=1}^5 m_{l'} g_{l'}(n, m, \omega) = \frac{\omega}{(n+m)!} (\Delta x)^n (\Delta y)^m T_p(n, m). \tag{A.8}$$

The formulas of  $g_{l'}$ ,  $l' = 1, 2, \dots, 5$ , in Equation (A.7) shows that  $T_p(n, m)$  will vary depending on  $n$  and  $m$  being even or odd numbers. By using this fact and applying the formulas for the weights  $m_{l'}$ ,  $l' = 1, 2, \dots, 5$ , from Equation (3.49) in Section 3.5,  $T_p(n, m)$  in Equation (A.8) can be represented in the following ways:

i) If  $n$  and  $m$  are even numbers

$$\begin{aligned}
 T_p(n, m) &= m_1(3^n + 3^m) + m_3(1 + 3^{n+m}) + m_4(3^n + 1) + m_2(1 + 3^m) + m_5 \\
 &= c \left( \frac{3^n + 3^m - 1 - 3^{n+m}}{2} \right) + a(-3^n + 1) + b(-3^m + 1) \\
 &+ \gamma \left( \frac{-3^n - 3^m - 1 - 3^{n+m}}{2} + 3^n + 3^m \right),
 \end{aligned} \tag{A.9}$$

ii) If  $n$  is odd and  $m$  is even

$$T_p(n, m) = c \left( \frac{-3^n + 3^m - 1 + 3^{n+m}}{2} \right) + a(3^n - 3) + b(3^m - 1) \\ + \gamma \left( \frac{3^n - 3^m - 1 + 3^{n+m}}{2} - 3^n - 3^m + 2 \right), \quad (\text{A.10})$$

iii) If  $n$  is even and  $m$  is odd

$$T_p(n, m) = c \left( \frac{3^n - 3^m - 1 + 3^{n+m}}{2} \right) + a(3^n - 1) + b(3^m - 3) \\ + \gamma \left( \frac{-3^n + 3^m - 1 + 3^{n+m}}{2} - 3^n - 3^m + 2 \right), \quad (\text{A.11})$$

iv) If  $n$  and  $m$  are odd numbers

$$T_p(n, m) = c \left( \frac{-3^n - 3^m - 1 - 3^{n+m}}{2} \right) + a(-3^n + 3) + b(-3^m + 3) \\ + \gamma \left( \frac{3^n + 3^m - 1 - 3^{n+m}}{2} + 3^n + 3^m - 4 \right). \quad (\text{A.12})$$

Writing Equation (A.6) using the result obtained in Equation (A.8) and Equations (A.9) to (A.12) we obtain the expression

$$\sum_{l \in \mathcal{K}_5} m_l u_l^{(e)} = u(x_3, y_3)(2m_1 + 2m_3 + 2m_4 + 2m_2 + m_5) + \Delta x \frac{\partial u}{\partial x} \Big|_{(x_3, y_3)} T_p(1, 0) \\ + \Delta y \frac{\partial u}{\partial y} \Big|_{(x_3, y_3)} T_p(0, 1) + \frac{(\Delta x)^2}{2!} \frac{\partial^2 u}{\partial x^2} \Big|_{(x_3, y_3)} T_p(2, 0) \\ + 2 \frac{\Delta x \Delta y}{2!} \frac{\partial^2 u}{\partial x \partial y} \Big|_{(x_3, y_3)} T_p(1, 1) + \frac{(\Delta y)^2}{2!} \frac{\partial^2 u}{\partial y^2} \Big|_{(x_3, y_3)} T_p(0, 2) + \dots \quad (\text{A.13})$$

Looking closer at the coefficients related to the value  $u(x_3, y_3)$  in Equation (A.13) shows that this term disappears

$$2m_1 + 2m_3 + 2m_4 + 2m_2 + m_5 = 2 \left( \frac{c}{2} - \frac{\gamma}{2} \right) + 2 \left( -\frac{c}{2} - \frac{\gamma}{2} \right) + 2(-a + \gamma) \\ + 2(-b + \gamma) + (2a + 2b - 2\gamma) \\ = c - \gamma - c - \gamma - 2a + 2\gamma - 2b + 2\gamma + 2a \\ + 2b - 2\gamma \\ = 0. \quad (\text{A.14})$$

Hence, we end up with the following formula for the left-hand side of the mass conservation equation for cell 5

$$\begin{aligned}
 \sum_{l \in \mathcal{K}_5} m_l u_l^{(e)} &= \Delta x \frac{\partial u}{\partial x} \Big|_{(x_3, y_3)} T_p(1, 0) + \Delta y \frac{\partial u}{\partial y} \Big|_{(x_3, y_3)} T_p(0, 1) \\
 &+ \frac{(\Delta x)^2}{2!} \frac{\partial^2 u}{\partial x^2} \Big|_{(x_3, y_3)} T_p(2, 0) + 2 \frac{\Delta x \Delta y}{2!} \frac{\partial^2 u}{\partial x \partial y} \Big|_{(x_3, y_3)} T_p(1, 1) \\
 &+ \frac{(\Delta y)^2}{2!} \frac{\partial^2 u}{\partial y^2} \Big|_{(x_3, y_3)} T_p(0, 2) + \dots
 \end{aligned} \tag{A.15}$$

Equation (A.15) is specific to cell 5 in Figure 4.1, as seen by the specified coordinate  $(x_3, y_3)$  giving the top right corner of this cell. This coordinate can be exchanged by the coordinate of the top right corner  $(x_c, y_c)$  of an *arbitrary* cell. Thus, we have obtained a general formula for cells yielding full internal stencils for the potential. Also applying the fact that for a uniform square grid  $\Delta x = \Delta y$ , we obtain

$$\sum_{l \in \mathcal{K}_k} m_l u_l^{(e)} = \sum_{\kappa=1}^{\infty} \sum_{\iota=0}^{\kappa} \binom{\kappa}{\iota} \frac{(\Delta x)^{\kappa}}{\kappa!} \frac{\partial^{\kappa} u}{\partial x^{\kappa-\iota} \partial y^{\iota}} \Big|_{(x_c, y_c)} T_p(\kappa - \iota, \iota). \tag{A.16}$$

Similarly, it is possible to give a rather general expression for

$$\int_{\Omega_k} f(x, y) d\tau, \tag{A.17}$$

where  $\Omega_k$  refers to an arbitrary cell. Recall that we are considering the elliptic equation

$$-\nabla \cdot (\mathbf{K} \nabla u(x, y)) = f(x, y). \tag{A.18}$$

Using a general permeability

$$\mathbf{K} = \begin{pmatrix} k_1 & k_2 \\ k_2 & k_4 \end{pmatrix}, \tag{A.19}$$

the source term may be written as

$$\begin{aligned}
 f(x, y) &= -\nabla \cdot \left( \mathbf{K} \begin{pmatrix} \frac{\partial u}{\partial x}(x, y) & \frac{\partial u}{\partial y}(x, y) \end{pmatrix}^T \right) \\
 &= -\nabla \cdot \left( \begin{pmatrix} k_1 \frac{\partial u}{\partial x}(x, y) + k_2 \frac{\partial u}{\partial y}(x, y) & k_2 \frac{\partial u}{\partial x}(x, y) + k_4 \frac{\partial u}{\partial y}(x, y) \end{pmatrix}^T \right) \\
 &= -\left( k_1 \frac{\partial^2 u}{\partial x^2}(x, y) + k_2 \frac{\partial^2 u}{\partial x \partial y}(x, y) + k_2 \frac{\partial^2 u}{\partial y \partial x}(x, y) + k_4 \frac{\partial^2 u}{\partial y^2}(x, y) \right) \\
 &= -\left( k_1 \frac{\partial^2 u}{\partial x^2}(x, y) + 2k_2 \frac{\partial^2 u}{\partial x \partial y}(x, y) + k_4 \frac{\partial^2 u}{\partial y^2}(x, y) \right).
 \end{aligned} \tag{A.20}$$

Also here we have assumed that  $u(x, y)$  exists and is continuous in a neighborhood of  $(x, y)$ , such that

$$\frac{\partial^2 u}{\partial x \partial y}(x, y) = \frac{\partial^2 u}{\partial y \partial x}(x, y). \quad (\text{A.21})$$

The expression for Equation (A.17) is then simply the integral over the cell of Equation (A.20)

$$\int_{\Omega_k} f(x, y) d\tau = - \int_{\Omega_k} \left( k_1 \frac{\partial^2 u}{\partial x^2}(x, y) + 2k_2 \frac{\partial^2 u}{\partial x \partial y}(x, y) + k_4 \frac{\partial^2 u}{\partial y^2}(x, y) \right) d\tau. \quad (\text{A.22})$$

## A.2 General Formulas for the Flux

Consider the vertical and horizontal fluxes between cells 5 and 2, and cells 5 and 6 in Figure 4.1. These fluxes can be expressed like in Equations (3.42) and (3.43) from Section 3.5 respectively, with weights given in Equation (3.44) in the same section. As in Appendix A.1, we want to develop an expression for the flux terms in Equation (4.41) in Section 4.3 using the potential value at only a single point in space. For the vertical flux this point is chosen to be the rightmost point on the edge, and for the horizontal flux the top point on the edge, see Figures 4.5 and 4.6. This will significantly ease the analysis of elements  $w_j$  from Equation (4.41) done in Appendix B.

We start off by looking at the formula for the vertical flux between cells 5 and 2 in Equation (3.42). Observe that if this formula is applied to the grid shown in Figure 4.1, the equation may be written as a Taylor expansion from the rightmost point on the edge  $(x_3, y_3)$

$$\begin{aligned} q_{te,v} = & t_{1,5}(u(x_3 - \Delta x, y_3 - \Delta y) - u(x_3 - \Delta x, y_3 + \Delta y)) \\ & + t_{1,6}(u(x_3 + \Delta x, y_3 - \Delta y) - u(x_3 - 3\Delta x, y_3 + \Delta y)) \\ & + t_{1,3}(u(x_3 + \Delta x, y_3 + \Delta y) - u(x_3 - 3\Delta x, y_3 - \Delta y)). \end{aligned} \quad (\text{A.23})$$

Here subscript  $v$  represents fluxes in the vertical direction.

By assuming that  $u(x, y)$  is infinitely smooth, Equation (A.23) may be rewritten as

$$\begin{aligned}
 q_{te,v} = & u(x_3, y_3)(t_{1,5}g_{v,1}(0, 0, 1) + t_{1,6}g_{v,2}(0, 0, 1) + t_{1,3}g_{v,3}(0, 0, 1)) \\
 & + \frac{\partial u}{\partial x} \Big|_{(x_3, y_3)} (t_{1,5}g_{v,1}(1, 0, 1) + t_{1,6}g_{v,2}(1, 0, 1) + t_{1,3}g_{v,3}(1, 0, 1)) \\
 & + \frac{\partial u}{\partial y} \Big|_{(x_3, y_3)} (t_{1,5}g_{v,1}(0, 1, 1) + t_{1,6}g_{v,2}(0, 1, 1) + t_{1,3}g_{v,3}(0, 1, 1)) \\
 & + \frac{\partial^2 u}{\partial x^2} \Big|_{(x_3, y_3)} (t_{1,5}g_{v,1}(2, 0, 1) + t_{1,6}g_{v,2}(2, 0, 1) + t_{1,3}g_{v,3}(2, 0, 1)) \\
 & + \frac{\partial^2 u}{\partial x \partial y} \Big|_{(x_3, y_3)} (t_{1,5}g_{v,1}(1, 1, 2) + t_{1,6}g_{v,2}(1, 1, 2) + t_{1,3}g_{v,3}(1, 1, 2)) \\
 & + \frac{\partial^2 u}{\partial y^2} \Big|_{(x_3, y_3)} (t_{1,5}g_{v,1}(0, 2, 1) + t_{1,6}g_{v,2}(0, 2, 1) + t_{1,3}g_{v,3}(0, 2, 1)) \\
 & + \dots
 \end{aligned} \tag{A.24}$$

Functions  $g_{v,i}$ ,  $i = 1, 2, 3$ , are given by

$$\begin{aligned}
 g_{v,1}(n, m, \omega_v) &= \frac{(-1)^{n+m}}{(n+m)!} \omega_v (\Delta x)^n (\Delta y)^m - \frac{(-1)^n}{(n+m)!} \omega_v (\Delta x)^n (\Delta y)^m, \\
 g_{v,2}(n, m, \omega_v) &= \frac{(-1)^m}{(n+m)!} \omega_v (\Delta x)^n (\Delta y)^m - \frac{(-1)^n 3^n}{(n+m)!} \omega_v (\Delta x)^n (\Delta y)^m, \\
 g_{v,3}(n, m, \omega_v) &= \frac{1}{(n+m)!} \omega_v (\Delta x)^n (\Delta y)^m - \frac{(-1)^{n+m} 3^n}{(n+m)!} \omega_v (\Delta x)^n (\Delta y)^m.
 \end{aligned} \tag{A.25}$$

Coefficient  $\omega_v$  again refers to the binomial coefficients obtained when Taylor expanding in two dimensions, explained in Appendix C.1. If  $u(x, y)$  is finite times differentiable, Equation (A.24) turns into a finite series.

Notice that the situation when  $n = m = 0$  and  $\omega_v = \binom{0}{0} = 1$  yields

$$\begin{aligned}
 g_{v,1}(0, 0, 1) &= 0, \\
 g_{v,2}(0, 0, 1) &= 0, \\
 g_{v,3}(0, 0, 1) &= 0.
 \end{aligned} \tag{A.26}$$

Hence, the term involving  $u(x_3, y_3)$  in Equation (A.24) disappears.

Consider a general term in Equation (A.24) involving the potential differentiated  $n$  times with respect to  $x$  and  $m$  times with respect to  $y$ . Using the weights from Equation (3.44)

in Section 3.5, this term can be written as

$$\begin{aligned}
 & \frac{\partial^{n+m}u}{\partial x^n \partial y^m} \Big|_{(x_3, y_3)} \left[ t_{1,5}g_{v,1}(n, m, \omega_v) + t_{1,6}g_{v,2}(n, m, \omega_v) + t_{1,3}g_{v,3}(n, m, \omega_v) \right] \\
 &= \frac{\partial^{n+m}u}{\partial x^n \partial y^m} \Big|_{(x_3, y_3)} \frac{\omega_v(\Delta x)^n(\Delta y)^m}{(n+m)!} \left[ (b-\beta)((-1)^{n+m} - (-1)^n) \right. \\
 & \quad \left. + \left( -\frac{c}{4} + \frac{\beta}{2} \right) ((-1)^m - (-1)^n 3^n) + \left( -\frac{c}{4} - \frac{\beta}{2} \right) (1 - (-1)^{n+m} 3^n) \right] \\
 &= \frac{\partial^{n+m}u}{\partial x^n \partial y^m} \Big|_{(x_3, y_3)} \frac{\omega_v(\Delta x)^n(\Delta y)^m}{(n+m)!} \left[ b((-1)^{n+m} - (-1)^n) \right. \\
 & \quad + \beta \left( (-1)^{n+m+1} - (-1)^{n+1} + \frac{(-1)^m - (-1)^n 3^n - 1 - (-1)^{n+m+1} 3^n}{2} \right) \\
 & \quad \left. + c \left( \frac{(-1)^{m+1} - (-1)^{n+1} 3^n - 1 - (-1)^{n+m+1} 3^n}{4} \right) \right] \\
 &= \frac{\partial^{n+m}u}{\partial x^n \partial y^m} \Big|_{(x_3, y_3)} \frac{\omega_v(\Delta x)^n(\Delta y)^m}{(n+m)!} T_v(n, m). \tag{A.27}
 \end{aligned}$$

The function  $T_v(n, m)$  introduced in the last equality in Equation (A.27) changes drastically depending on  $n$  and  $m$  being even or odd numbers. Using this advantage and writing  $T_v(n, m)$  as a multi-valued function yields the following formula

$$T_v(n, m) = \begin{cases} c(-\frac{1}{2} + \frac{3^n}{2}), & n \text{ and } m \text{ even numbers,} \\ c(-\frac{1}{2} - \frac{3^n}{2}), & n \text{ odd and } m \text{ even,} \\ -2b + \beta(1 - 3^n), & n \text{ even and } m \text{ odd,} \\ 2b + \beta(-3 + 3^n), & n \text{ and } m \text{ odd numbers.} \end{cases} \tag{A.28}$$

By inserting the results from Equations (A.27) and (A.28) into Equation (A.24) we obtain

$$\begin{aligned}
 q_{te,v} &= \frac{\partial u}{\partial x} \Big|_{(x_3, y_3)} \Delta x T_v(1, 0) + \frac{\partial u}{\partial y} \Big|_{(x_3, y_3)} \Delta y T_v(0, 1) \\
 & \quad + \frac{\partial^2 u}{\partial x^2} \Big|_{(x_3, y_3)} \frac{(\Delta x)^2}{2!} T_v(2, 0) + \frac{\partial^2 u}{\partial x \partial y} \Big|_{(x_3, y_3)} \frac{2\Delta x \Delta y}{2!} T_v(1, 1) \\
 & \quad + \frac{\partial^2 u}{\partial y^2} \Big|_{(x_3, y_3)} \frac{(\Delta y)^2}{2!} T_v(0, 2) + \dots \tag{A.29}
 \end{aligned}$$

The same procedure can be applied to the horizontal flux,  $q_{te,h}$ , between cells 5 and 6. This results in the following expression for the term involving the potential differentiated  $n$  times with respect to  $x$  and  $m$  times with respect to  $y$

$$\frac{\partial^{n+m}u}{\partial x^n \partial y^m} \Big|_{(x_3, y_3)} \left[ t_{2,5}g_{h,1}(n, m, \omega_h) + t_{2,3}g_{h,2}(n, m, \omega_h) + t_{2,2}g_{h,3}(n, m, \omega_h) \right]. \tag{A.30}$$

Here  $\omega_h$  are again binomial coefficients from the Taylor expansion, see Appendix C.1. Recall that the we now Taylor expand to the top point of the edge, which in this case happens to be the same point as the rightmost point on the edge between cells 5 and 2. Functions  $g_{h,i}$ ,  $i = 1, 2, 3$ , are given by

$$\begin{aligned} g_{h,1}(n, m, \omega_h) &= \frac{(-1)^{n+m}}{(n+m)!} \omega_h(\Delta x)^n (\Delta y)^m - \frac{(-1)^m}{(n+m)!} \omega_h(\Delta x)^n (\Delta y)^m, \\ g_{h,2}(n, m, \omega_h) &= \frac{1}{(n+m)!} \omega_h(\Delta x)^n (\Delta y)^m - \frac{(-1)^{n+m} 3^m}{(n+m)!} \omega_h(\Delta x)^n (\Delta y)^m, \\ g_{h,3}(n, m, \omega_h) &= \frac{(-1)^n}{(n+m)!} \omega_h(\Delta x)^n (\Delta y)^m - \frac{(-1)^m 3^m}{(n+m)!} \omega_h(\Delta x)^n (\Delta y)^m. \end{aligned} \quad (\text{A.31})$$

As for the  $q_{te,v}$  case, it is easy to see that  $g_{h,i}$ ,  $i = 1, 2, 3$ , disappears whenever  $n = m = 0$  and  $\omega_h = \binom{0}{0} = 1$ . Hence, the term involving  $u(x_3, y_3)$  vanishes from the general expression of the horizontal fluxes.

Writing out the expression in Equation (A.30) using the functions in Equation (A.31) and weights  $t_{2,i}$ ,  $i = 5, 3, 2$ , from Equation (3.44) in Section 3.5 yield

$$\begin{aligned} & \left. \frac{\partial^{n+m} u}{\partial x^n \partial y^m} \right|_{(x_3, y_3)} \left[ t_{2,5} g_{h,1}(n, m, \omega_h) + t_{2,3} g_{h,2}(n, m, \omega_h) + t_{2,2} g_{h,3}(n, m, \omega_h) \right] \\ &= \left. \frac{\partial^{n+m} u}{\partial x^n \partial y^m} \right|_{(x_3, y_3)} \frac{\omega_h(\Delta x)^n (\Delta y)^m}{(n+m)!} \left[ (a - \alpha) ((-1)^{n+m} - (-1)^m) \right. \\ & \quad \left. + \alpha \left( (-1)^{n+m+1} - (-1)^{m+1} + \frac{-1 - (-1)^{n+m+1} 3^m + (-1)^n - (-1)^m 3^m}{2} \right) \right] \\ & \quad \left. + c \left( \frac{-1 - (-1)^{n+m+1} 3^m + (-1)^{n+1} - (-1)^{m+1} 3^m}{4} \right) \right] \\ &= \left. \frac{\partial^{n+m} u}{\partial x^n \partial y^m} \right|_{(x_3, y_3)} \frac{\omega_h(\Delta x)^n (\Delta y)^m}{(n+m)!} T_h(n, m). \end{aligned} \quad (\text{A.32})$$

By once again considering how the function  $T_h(n, m)$  evolves when  $n$  and  $m$  varies between being odd and even numbers, the following multi-valued function is obtained

$$T_h(n, m) = \begin{cases} c(-\frac{1}{2} + \frac{3^m}{2}), & n \text{ and } m \text{ even numbers,} \\ -2a + \alpha(1 - 3^m), & n \text{ odd and } m \text{ even,} \\ c(-\frac{1}{2} - \frac{3^m}{2}), & n \text{ even and } m \text{ odd,} \\ 2a + \alpha(-3 + 3^m), & n \text{ and } m \text{ odd numbers.} \end{cases} \quad (\text{A.33})$$

By using Equations (A.32) and (A.33), a general expression for the horizontal flux between cells 5 and 6 may be written as

$$\begin{aligned}
 q_{te,h} &= \frac{\partial u}{\partial x} \Big|_{(x_3,y_3)} \Delta x T_h(1,0) + \frac{\partial u}{\partial y} \Big|_{(x_3,y_3)} \Delta y T_h(0,1) \\
 &+ \frac{\partial^2 u}{\partial x^2} \Big|_{(x_3,y_3)} \frac{(\Delta x)^2}{2!} T_h(2,0) + \frac{\partial^2 u}{\partial x \partial y} \Big|_{(x_3,y_3)} \frac{2\Delta x \Delta y}{2!} T_h(1,1) \\
 &+ \frac{\partial^2 u}{\partial y^2} \Big|_{(x_3,y_3)} \frac{(\Delta y)^2}{2!} T_h(0,2) + \dots
 \end{aligned} \tag{A.34}$$

In Equations (A.29) and (A.34) the rightmost and top point,  $(x_3, y_3)$ , of the edges we are considering are only used in the evaluation of the derivatives of our potential function. Thus, it is easy to make these formulas general. This is done by exchanging  $(x_3, y_3)$  with the rightmost point  $(x_r, y_r)$  and top point  $(x_t, y_t)$  of an arbitrary horizontal and vertical edge yielding full internal stencils for the fluxes respectively, see Figures 4.5 and 4.6. In addition, recall that for a uniform square grid we have  $\Delta x = \Delta y$ . Hence, we can write the formulas from Equations (A.29) and (A.34) as

$$\begin{aligned}
 q_{te,v} &= \sum_{\kappa=1}^{\infty} \sum_{\iota=0}^{\kappa} \binom{\kappa}{\iota} \frac{(\Delta x)^{\kappa}}{\kappa!} \frac{\partial^{\kappa} u}{\partial x^{\kappa-\iota} \partial y^{\iota}} \Big|_{(x_r,y_r)} T_v(\kappa-\iota, \iota), \\
 q_{te,h} &= \sum_{\kappa=1}^{\infty} \sum_{\iota=0}^{\kappa} \binom{\kappa}{\iota} \frac{(\Delta x)^{\kappa}}{\kappa!} \frac{\partial^{\kappa} u}{\partial x^{\kappa-\iota} \partial y^{\iota}} \Big|_{(x_t,y_t)} T_h(\kappa-\iota, \iota).
 \end{aligned} \tag{A.35}$$

The *exact* fluxes  $q_{e,v}$  and  $q_{e,h}$  between cells 5 and 2 and cells 5 and 6 respectively are represented by

$$q_{e,v} = \int_{x_2}^{x_3} \mathbf{n}_1^T \mathbf{K} \nabla u \Big|_{y=y_3} dx = - \int_{x_2}^{x_3} \left( k_2 \frac{\partial u}{\partial x}(x, y_3) + k_4 \frac{\partial u}{\partial y}(x, y_3) \right) dx, \tag{A.36}$$

$$q_{e,h} = - \int_{y_2}^{y_3} \mathbf{n}_2^T \mathbf{K} \nabla u \Big|_{x=x_3} dy = - \int_{y_2}^{y_3} \left( k_1 \frac{\partial u}{\partial x}(x_3, y) + k_2 \frac{\partial u}{\partial y}(x_3, y) \right) dy. \tag{A.37}$$

Here variables  $k_i$ ,  $i = 1, 2, 4$ , refers to the elements of the general permeability

$$\mathbf{K} = \begin{pmatrix} k_1 & k_2 \\ k_2 & k_4 \end{pmatrix}, \tag{A.38}$$

and vectors  $\mathbf{n}_1$  and  $\mathbf{n}_2$  are the normal vectors defined in Equation (4.6).

## Appendix B

# Detailed Calculation of the Truncation Errors in Section 4.4.2

In this appendix we wish to develop a similar expression as Equation (4.60) for the local truncation errors of the fluxes over edges yielding full internal stencils, see introduction Section 4.4 and Figure 4.2. This is done by looking at the elements  $w_j$ ,  $j \in \mathcal{E}$ , of vector  $\mathbf{w}$ , from Equation (4.41), where  $\mathcal{E}$  is the collection of bold edges shown in Figure 4.2. Notice, when considering a uniform square grid which is parallel to the axes of the coordinate system, it is only possible to have fluxes in the vertical or the horizontal direction. This is organized by the subscripts  $v$  and  $h$  for the vertical and horizontal direction respectively throughout this appendix.

Equation (A.35) from Appendix A.2 gives general expressions for the fluxes  $q_{te,j}$  from Equation (4.41) corresponding to edges yielding full internal stencils. These are

$$q_{te,v} = \sum_{\kappa=1}^{\infty} \sum_{\iota=0}^{\kappa} \binom{\kappa}{\iota} \frac{(\Delta x)^{\kappa}}{\kappa!} \frac{\partial^{\kappa} u}{\partial x^{\kappa-\iota} \partial y^{\iota}} \Big|_{(x_r, y_r)} T_v(\kappa - \iota, \iota), \quad (\text{B.1})$$

and

$$q_{te,h} = \sum_{\kappa=1}^{\infty} \sum_{\iota=0}^{\kappa} \binom{\kappa}{\iota} \frac{(\Delta x)^{\kappa}}{\kappa!} \frac{\partial^{\kappa} u}{\partial x^{\kappa-\iota} \partial y^{\iota}} \Big|_{(x_t, y_t)} T_h(\kappa - \iota, \iota). \quad (\text{B.2})$$

Here  $(x_r, y_r)$  and  $(x_t, y_t)$  refers to the rightmost and top point of a general horizontal and vertical edge respectively, see Figures B.1 and B.2. Notice that vertical fluxes travels across horizontal edges and vice versa. The functions  $T_v(n, m)$  and  $T_h(n, m)$  in

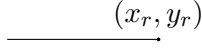


FIGURE B.1: Rightmost point on a horizontal edge

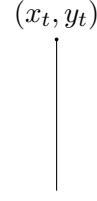


FIGURE B.2: Top point on a vertical edge

Equations (B.1) and (B.2) are given by

$$T_v(n, m) = \begin{cases} c(-\frac{1}{2} + \frac{3^n}{2}), & n \text{ and } m \text{ even numbers,} \\ c(-\frac{1}{2} - \frac{3^n}{2}), & n \text{ odd and } m \text{ even,} \\ -2b + \beta(1 - 3^n), & n \text{ even and } m \text{ odd,} \\ 2b + \beta(-3 + 3^n), & n \text{ and } m \text{ odd numbers,} \end{cases} \quad (\text{B.3})$$

and

$$T_h(n, m) = \begin{cases} c(-\frac{1}{2} + \frac{3^m}{2}), & n \text{ and } m \text{ even numbers,} \\ -2a + \alpha(1 - 3^m), & n \text{ odd and } m \text{ even,} \\ c(-\frac{1}{2} - \frac{3^m}{2}), & n \text{ even and } m \text{ odd,} \\ 2a + \alpha(-3 + 3^m), & n \text{ and } m \text{ odd numbers.} \end{cases} \quad (\text{B.4})$$

Variables  $a$ ,  $b$ ,  $c$ ,  $\alpha$  and  $\beta$  refers to the variables introduced in Section 3.5.

Applying potential function (4.42) to the formulas in Equations (B.1) and (B.2), and remembering how the derivatives of this functions develops, Equation (4.46), yields

$$\begin{aligned} q_{te,v} = & \sin(x_r) \sin(y_r) \left[ \sum_{\kappa=0}^{\infty} \frac{(-1)^{\kappa+1} (\Delta x)^{2\kappa+2}}{(2\kappa+2)!} \left( \sum_{\iota=0}^{\kappa+1} \binom{2\kappa+2}{2\iota} T_v(2\kappa+2-2\iota, 2\iota) \right) \right] \\ & + \cos(x_r) \sin(y_r) \left[ \sum_{\kappa=0}^{\infty} \frac{(-1)^{\kappa} (\Delta x)^{2\kappa+1}}{(2\kappa+1)!} \left( \sum_{\iota=0}^{\kappa} \binom{2\kappa+1}{2\iota+1} T_v(2\iota+1, 2\kappa-2\iota) \right) \right] \\ & + \sin(x_r) \cos(y_r) \left[ \sum_{\kappa=0}^{\infty} \frac{(-1)^{\kappa} (\Delta x)^{2\kappa+1}}{(2\kappa+1)!} \left( \sum_{\iota=0}^{\kappa} \binom{2\kappa+1}{2\iota+1} T_v(2\kappa-2\iota, 2\iota+1) \right) \right] \\ & + \cos(x_r) \cos(y_r) \left[ \sum_{\kappa=0}^{\infty} \frac{(-1)^{\kappa} (\Delta x)^{2\kappa+2}}{(2\kappa+2)!} \left( \sum_{\iota=0}^{\kappa} \binom{2\kappa+2}{2\iota+1} T_v(2\kappa+1-2\iota, 2\iota+1) \right) \right], \end{aligned} \quad (\text{B.5})$$

and

$$\begin{aligned}
q_{te,h} = & \sin(x_t) \sin(y_t) \left[ \sum_{\kappa=0}^{\infty} \frac{(-1)^{\kappa+1} (\Delta x)^{2\kappa+2}}{(2\kappa+2)!} \left( \sum_{\iota=0}^{\kappa+1} \binom{2\kappa+2}{2\iota} T_h(2\kappa+2-2\iota, 2\iota) \right) \right] \\
& + \cos(x_t) \sin(y_t) \left[ \sum_{\kappa=0}^{\infty} \frac{(-1)^{\kappa} (\Delta x)^{2\kappa+1}}{(2\kappa+1)!} \left( \sum_{\iota=0}^{\kappa} \binom{2\kappa+1}{2\iota+1} T_h(2\iota+1, 2\kappa-2\iota) \right) \right] \\
& + \sin(x_t) \cos(y_t) \left[ \sum_{\kappa=0}^{\infty} \frac{(-1)^{\kappa} (\Delta x)^{2\kappa+1}}{(2\kappa+1)!} \left( \sum_{\iota=0}^{\kappa} \binom{2\kappa+1}{2\iota+1} T_h(2\kappa-2\iota, 2\iota+1) \right) \right] \\
& + \cos(x_t) \cos(y_t) \left[ \sum_{\kappa=0}^{\infty} \frac{(-1)^{\kappa} (\Delta x)^{2\kappa+2}}{(2\kappa+2)!} \left( \sum_{\iota=0}^{\kappa} \binom{2\kappa+2}{2\iota+1} T_h(2\kappa+1-2\iota, 2\iota+1) \right) \right].
\end{aligned} \tag{B.6}$$

These formulas have been derived in a similar way as Equation (4.48) in Section 4.4.1. As for the potential in Section 4.4.1, Equations (B.5) and (B.6) may now be written as

$$\begin{aligned}
q_{te,v} = & \sin(x_r) \sin(y_r) \varphi_{v_1} + \cos(x_r) \sin(y_r) \varphi_{v_2} \\
& + \sin(x_r) \cos(y_r) \varphi_{v_3} + \cos(x_r) \cos(y_r) \varphi_{v_4},
\end{aligned} \tag{B.7}$$

and

$$\begin{aligned}
q_{te,h} = & \sin(x_t) \sin(y_t) \varphi_{h_1} + \cos(x_t) \sin(y_t) \varphi_{h_2} \\
& + \sin(x_t) \cos(y_t) \varphi_{h_3} + \cos(x_t) \cos(y_t) \varphi_{h_4}.
\end{aligned} \tag{B.8}$$

Turning to calculate the exact fluxes  $q_{e,j}$  from Equation (4.41), Equations (A.36) and (A.37) in Appendix A.2 gives formulas for the exact fluxes across the top and right edge of cell 5 in Figure 4.1. These are

$$q_{e,v} = \int_{x_2}^{x_3} \mathbf{n}_1^T \mathbf{K} \nabla u \Big|_{y=y_3} dx = - \int_{x_2}^{x_3} \left( k_2 \frac{\partial u}{\partial x}(x, y_3) + k_4 \frac{\partial u}{\partial y}(x, y_3) \right) dx, \tag{B.9}$$

and

$$q_{e,h} = - \int_{y_2}^{y_3} \mathbf{n}_2^T \mathbf{K} \nabla u \Big|_{x=x_3} dy = - \int_{y_2}^{y_3} \left( k_1 \frac{\partial u}{\partial x}(x_3, y) + k_2 \frac{\partial u}{\partial y}(x_3, y) \right) dy. \tag{B.10}$$

The variables  $k_i$ ,  $i = 1, 2, 4$ , in Equations (B.9) and (B.10) refers to the elements of the general permeability

$$\mathbf{K} = \begin{pmatrix} k_1 & k_2 \\ k_2 & k_4 \end{pmatrix}, \tag{B.11}$$

and vectors  $\mathbf{n}_1$  and  $\mathbf{n}_2$  are the normal vectors defined in Equation (4.6).

Next, we apply potential function (4.42) in Equations (B.9) and (B.10). In the vertical case this leads to

$$\begin{aligned}
q_{e,v} &= - \int_{x_2}^{x_3} \left( k_2 \frac{\partial u}{\partial x} + k_4 \frac{\partial u}{\partial y} \right) \Big|_{y=y_3} dx \\
&= -k_2 \sin(y_3) \int_{x_2}^{x_3} \cos(x) dx - k_4 \cos(y_3) \int_{x_2}^{x_3} \sin(x) dx \\
&= -k_2 \sin(y_3) (\sin(x_3) - \sin(x_2)) + k_4 \cos(y_3) (\cos(x_3) - \cos(x_2)) \\
&= -k_2 \sin(x_3) \sin(y_3) + k_4 \cos(x_3) \cos(y_3) + k_2 \sin(x_2) \sin(y_3) - k_4 \cos(x_2) \cos(y_3).
\end{aligned} \tag{B.12}$$

Writing  $\sin(x_2)$  and  $\cos(x_2)$  as one dimensional Taylor expansions around  $x_3$  for the two last terms in this equation yields an equation only dependent on a single point, the rightmost point of the edge, see Figure B.1,

$$\begin{aligned}
q_{e,v} &= -k_2 \sin(x_3) \sin(y_3) + k_4 \cos(x_3) \cos(y_3) + k_2 \sin(x_3 - 2\Delta x) \sin(y_3) - k_4 \cos(x_3 - 2\Delta x) \cos(y_3) \\
&= -\cancel{k_2 \sin(x_3) \sin(y_3)} + \cancel{k_4 \cos(x_3) \cos(y_3)} \\
&+ k_2 \sin(y_3) \left[ \cancel{\sin(x_3)} + (-1)2\Delta x \cos(x_3) - \frac{(-1)^2 2^2 (\Delta x)^2}{2!} \sin(x_3) - \frac{(-1)^3 2^3 (\Delta x)^3}{3!} \cos(x_3) + \dots \right] \\
&- k_4 \cos(y_3) \left[ \cancel{\cos(x_3)} - (-1)2\Delta x \sin(x_3) - \frac{(-1)^2 2^2 (\Delta x)^2}{2!} \cos(x_3) + \frac{(-1)^3 2^3 (\Delta x)^3}{3!} \cos(x_3) + \dots \right] \\
&= k_2 \sin(x_3) \sin(y_3) \left[ -\frac{(-1)^2 2^2 (\Delta x)^2}{2!} + \frac{(-1)^4 2^4 (\Delta x)^4}{4!} - \frac{(-1)^6 2^6 (\Delta x)^6}{6!} + \dots \right] \\
&+ k_2 \cos(x_3) \sin(y_3) \left[ (-1)2\Delta x - \frac{(-1)^3 2^3 (\Delta x)^3}{3!} + \frac{(-1)^5 2^5 (\Delta x)^5}{5!} - \dots \right] \\
&+ k_4 \sin(x_3) \cos(y_3) \left[ (-1)2\Delta x - \frac{(-1)^3 2^3 (\Delta x)^3}{3!} + \frac{(-1)^5 2^5 (\Delta x)^5}{5!} - \dots \right] \\
&+ k_4 \cos(x_3) \cos(y_3) \left[ \frac{(-1)^2 2^2 (\Delta x)^2}{2!} - \frac{(-1)^4 2^4 (\Delta x)^4}{4!} + \frac{(-1)^6 2^6 (\Delta x)^6}{6!} - \dots \right].
\end{aligned} \tag{B.13}$$

By observing the patterns that arise in Equation (B.13), we can write it in the compact form

$$\begin{aligned}
q_{e,v} &= k_2 \sin(x_3) \sin(y_3) \left[ \sum_{\kappa=0}^{\infty} (-1)^{\kappa+1} \frac{(-1)^{2\kappa+2} 2^{2\kappa+2} (\Delta x)^{2\kappa+2}}{(2\kappa+2)!} \right] \\
&+ k_2 \cos(x_3) \sin(y_3) \left[ \sum_{\kappa=0}^{\infty} (-1)^{\kappa} \frac{(-1)^{2\kappa+1} 2^{2\kappa+1} (\Delta x)^{2\kappa+1}}{(2\kappa+1)!} \right] \\
&+ k_4 \sin(x_3) \cos(y_3) \left[ \sum_{\kappa=0}^{\infty} (-1)^{\kappa} \frac{(-1)^{2\kappa+1} 2^{2\kappa+1} (\Delta x)^{2\kappa+1}}{(2\kappa+1)!} \right] \\
&+ k_4 \cos(x_3) \cos(y_3) \left[ \sum_{\kappa=0}^{\infty} (-1)^{\kappa} \frac{(-1)^{2\kappa+2} 2^{2\kappa+2} (\Delta x)^{2\kappa+2}}{(2\kappa+2)!} \right].
\end{aligned} \tag{B.14}$$

Doing the same calculations for  $q_{e,h}$  in Equation (B.10) yields the following result

$$\begin{aligned}
q_{e,h} &= \int_{y_2}^{y_3} \left( k_1 \frac{\partial u}{\partial x} + k_2 \frac{\partial u}{\partial y} \right) \Big|_{x=x_3} dy \\
&= k_2 \sin(x_3) \sin(y_3) \left[ \sum_{\kappa=0}^{\infty} (-1)^{\kappa+1} \frac{(-1)^{2\kappa+2} 2^{2\kappa+2} (\Delta y)^{2\kappa+2}}{(2\kappa+2)!} \right] \\
&+ k_2 \cos(x_3) \sin(y_3) \left[ \sum_{\kappa=0}^{\infty} (-1)^{\kappa} \frac{(-1)^{2\kappa+1} 2^{2\kappa+1} (\Delta y)^{2\kappa+1}}{(2\kappa+1)!} \right] \\
&+ k_1 \sin(x_3) \cos(y_3) \left[ \sum_{\kappa=0}^{\infty} (-1)^{\kappa} \frac{(-1)^{2\kappa+1} 2^{2\kappa+1} (\Delta y)^{2\kappa+1}}{(2\kappa+1)!} \right] \\
&+ k_1 \cos(x_3) \cos(y_3) \left[ \sum_{\kappa=0}^{\infty} (-1)^{\kappa} \frac{(-1)^{2\kappa+2} 2^{2\kappa+2} (\Delta y)^{2\kappa+2}}{(2\kappa+2)!} \right].
\end{aligned} \tag{B.15}$$

Observe that expressions (B.14) and (B.15) only involve the rightmost and top point of the top and right edges of cell 5 in the trigonometric functions. Thus, exchanging these with the rightmost point,  $(x_r, y_r)$ , and top point,  $(x_t, y_t)$ , of an *arbitrary* horizontal and vertical edge respectively, see Figures B.1 and B.2, we obtain general expressions for the exact vertical and horizontal fluxes.

Using these general coordinates, Equations (B.14) and (B.15) may be written as

$$\begin{aligned}
q_{e,v} &= k_2 \sin(x_r) \sin(y_r) \psi_{v_1} + k_2 \cos(x_r) \sin(y_r) \psi_{v_2} \\
&+ k_4 \sin(x_r) \cos(y_r) \psi_{v_3} + k_4 \cos(x_r) \cos(y_r) \psi_{v_4},
\end{aligned} \tag{B.16}$$

and

$$\begin{aligned}
q_{e,h} &= k_2 \sin(x_t) \sin(y_t) \psi_{h_1} + k_2 \cos(x_t) \sin(y_t) \psi_{h_2} \\
&+ k_1 \sin(x_t) \cos(y_t) \psi_{h_3} + k_1 \cos(x_t) \cos(y_t) \psi_{h_4}.
\end{aligned} \tag{B.17}$$

This form resembles the short form of the fluxes  $q_{te,i}$ ,  $i = v, h$ , in Equations (B.7) and (B.8). Therefore, the local truncation errors  $w_j$ ,  $j \in \mathcal{E}$ , defined by Equation (4.41), can be expressed in the following way

$$w_j = \begin{cases} q_{te,v} - q_{e,v}, & \text{edge } j \text{ is a horizontal edge,} \\ q_{te,h} - q_{e,h}, & \text{edge } j \text{ is a vertical edge.} \end{cases} \tag{B.18}$$

These differences are then given by

$$\begin{aligned}
q_{te,v} - q_{e,v} &= \sin(x_r) \sin(y_r) (\varphi_{v_1} - \psi_{v_1}) + \cos(x_r) \sin(y_r) (\varphi_{v_2} - \psi_{v_2}) \\
&+ \sin(x_r) \cos(y_r) (\varphi_{v_3} - \psi_{v_3}) + \cos(x_r) \cos(y_r) (\varphi_{v_4} - \psi_{v_4}) \\
&= \sin(x_r) \sin(y_r) D_{v_1} + \cos(x_r) \sin(y_r) D_{v_2} \\
&+ \sin(x_r) \cos(y_r) D_{v_3} + \cos(x_r) \cos(y_r) D_{v_4},
\end{aligned} \tag{B.19}$$

and

$$\begin{aligned}
q_{te,h} - q_{e,h} &= \sin(x_t) \sin(y_t)(\varphi_{h_1} - \psi_{h_1}) + \cos(x_t) \sin(y_t)(\varphi_{h_2} - \psi_{h_2}) \\
&\quad + \sin(x_t) \cos(y_t)(\varphi_{h_3} - \psi_{h_3}) + \cos(x_t) \cos(y_t)(\varphi_{h_4} - \psi_{h_4}) \\
&= \sin(x_t) \sin(y_t)D_{h_1} + \cos(x_t) \sin(y_t)D_{h_2} \\
&\quad + \sin(x_t) \cos(y_t)D_{h_3} + \cos(x_t) \cos(y_t)D_{h_4}.
\end{aligned} \tag{B.20}$$

As for the potential, the situations when the trigonometric functions vanishes is dependent on the spatial position and size of our grid. Therefore, we need to look at the coefficients  $D_{j_i}$ ,  $j = v, h$ ,  $i = 1, 2, 3, 4$ , to analyze when the local truncation error  $w_j$  disappears for general situations. Looking closer at coefficient  $D_{v_1}$  we see that

$$\begin{aligned}
D_{v_1} &= \sum_{\kappa=0}^{\infty} \frac{(-1)^{\kappa+1}(\Delta x)^{2\kappa+2}}{(2\kappa+2)!} \left( \sum_{\iota=0}^{\kappa+1} \binom{2\kappa+2}{2\iota} T_v(2\kappa+2-2\iota, 2\iota) \right) \\
&\quad - \sum_{\kappa=0}^{\infty} (-1)^{\kappa+1} \frac{(-1)^{2\kappa+2} 2^{2\kappa+2} (\Delta x)^{2\kappa+2}}{(2\kappa+2)!} k_2 \\
&= \sum_{\kappa=0}^{\infty} \frac{(-1)^{\kappa+1}(\Delta x)^{2\kappa+2}}{(2\kappa+2)!} \left( \sum_{\iota=0}^{\kappa+1} \binom{2\kappa+2}{2\iota} T_v(2\kappa+2-2\iota, 2\iota) - 2^{2\kappa+2} k_2 \right)
\end{aligned} \tag{B.21}$$

The inner parenthesis related to different powers of  $\Delta x$  in this expression is the key to understanding the coefficient  $D_{v_1}$ . By using the definition of  $T_v(n, m)$ , Property C.1.2 and Theorem C.2.2 from Appendices C.1 and C.2, examples of usage shown in Equations (4.62) and (4.63) in Section 4.4.1, the big parenthesis in Equation (B.21) can be written as

$$\begin{aligned}
&\sum_{\iota=0}^{\kappa+1} \binom{2\kappa+2}{2\iota} T_v(2\kappa+2-2\iota, 2\iota) - 2^{2\kappa+2} k_2 \\
&= \sum_{\iota=0}^{\kappa+1} \binom{2\kappa+2}{2\iota} \left( \left( -\frac{1}{2} + \frac{3^{2\kappa+2-2\iota}}{2} \right) c \right) - 2^{2\kappa+2} k_2 \\
&= (-2^{2\kappa} + 2^{4\kappa+2} + 2^{2\kappa}) c - 2^{2\kappa+2} k_2 \\
&= 2^{4\kappa+2} c - 2^{2\kappa+2} k_2.
\end{aligned} \tag{B.22}$$

Here  $T_v(n, m)$ , from Equation (B.3), becomes the case with both  $n$  and  $m$  being even numbers. This is due to the fact that  $2\kappa+2-2\iota$  and  $2\iota$  are even for any  $\kappa$  and  $\iota$ .

Using the same procedure to simplify all the coefficients  $D_{v_i}$ ,  $i = 1, 2, 3, 4$ , in Equation (B.19) yields

$$\begin{aligned}
D_{v_1} &= \sum_{\kappa=0}^{\infty} \frac{(-1)^{\kappa+1} (\Delta x)^{2\kappa+2}}{(2\kappa+2)!} \left[ 2^{4\kappa+2} c - 2^{2\kappa+2} k_2 \right], \\
D_{v_2} &= \sum_{\kappa=0}^{\infty} \frac{(-1)^{\kappa} (\Delta x)^{2\kappa+1}}{(2\kappa+1)!} \left[ (-2^{2\kappa} - 2^{4\kappa}) c + 2^{2\kappa+1} k_2 \right], \\
D_{v_3} &= \sum_{\kappa=0}^{\infty} \frac{(-1)^{\kappa} (\Delta x)^{2\kappa+1}}{(2\kappa+1)!} \left[ -2^{2\kappa+1} b + \beta(2^{2\kappa+1} - 2^{4\kappa+1}) + 2^{2\kappa+1} k_4 \right], \\
D_{v_4} &= \sum_{\kappa=0}^{\infty} \frac{(-1)^{\kappa} (\Delta x)^{2\kappa+2}}{(2\kappa+2)!} \left[ 2^{2\kappa+2} b + \beta(-2^{2\kappa+3} + 2^{4\kappa+3}) - 2^{2\kappa+2} k_4 \right].
\end{aligned} \tag{B.23}$$

Doing the same for the  $D_{h_i}$ ,  $i = 1, 2, 3, 4$ , in Equation (B.20) gives the following result, recall that  $\Delta x = \Delta y$ ,

$$\begin{aligned}
D_{h_1} &= \sum_{\kappa=0}^{\infty} \frac{(-1)^{\kappa+1} (\Delta x)^{2\kappa+2}}{(2\kappa+2)!} \left[ 2^{4\kappa+2} c - 2^{2\kappa+2} k_2 \right], \\
D_{h_2} &= \sum_{\kappa=0}^{\infty} \frac{(-1)^{\kappa} (\Delta x)^{2\kappa+1}}{(2\kappa+1)!} \left[ -2^{2\kappa+1} a + \alpha(2^{2\kappa+1} - 2^{4\kappa+1}) + 2^{2\kappa+1} k_1 \right], \\
D_{h_3} &= \sum_{\kappa=0}^{\infty} \frac{(-1)^{\kappa} (\Delta x)^{2\kappa+1}}{(2\kappa+1)!} \left[ c(-2^{2\kappa} - 2^{4\kappa}) + 2^{2\kappa+1} k_2 \right], \\
D_{h_4} &= \sum_{\kappa=0}^{\infty} \frac{(-1)^{\kappa} (\Delta x)^{2\kappa+2}}{(2\kappa+2)!} \left[ 2^{2\kappa+2} a + \alpha(-2^{2\kappa+3} + 2^{4\kappa+3}) - 2^{2\kappa+2} k_1 \right].
\end{aligned} \tag{B.24}$$

It is possible to further simplify the expressions in (B.23) and (B.24). We know that on uniform square grids, variables  $a$ ,  $b$  and  $c$  corresponds directly to the equivalently placed element in the permeability matrix, Equation (4.9). In addition, it is easy to see that the parentheses disappears for the term  $\kappa = 0$  for all the coefficients. Hence, we finally obtain the formulas

$$\begin{aligned}
D_{v_1} &= \sum_{\kappa=1}^{\infty} \frac{(-1)^{\kappa+1} (\Delta x)^{2\kappa+2}}{(2\kappa+2)!} \left[ (2^{4\kappa+2} - 2^{2\kappa+2}) c \right], \\
D_{v_2} &= \sum_{\kappa=1}^{\infty} \frac{(-1)^{\kappa} (\Delta x)^{2\kappa+1}}{(2\kappa+1)!} \left[ (-2^{2\kappa} - 2^{4\kappa} + 2^{2\kappa+1}) c \right], \\
D_{v_3} &= \sum_{\kappa=1}^{\infty} \frac{(-1)^{\kappa} (\Delta x)^{2\kappa+1}}{(2\kappa+1)!} \left[ (2^{2\kappa+1} - 2^{4\kappa+1}) \beta \right], \\
D_{v_4} &= \sum_{\kappa=1}^{\infty} \frac{(-1)^{\kappa} (\Delta x)^{2\kappa+2}}{(2\kappa+2)!} \left[ (-2^{2\kappa+3} + 2^{4\kappa+3}) \beta \right],
\end{aligned} \tag{B.25}$$

and

$$\begin{aligned}
D_{h_1} &= \sum_{\kappa=1}^{\infty} \frac{(-1)^{\kappa+1} (\Delta x)^{2\kappa+2}}{(2\kappa+2)!} \left[ (2^{4\kappa+2} - 2^{2\kappa+2})c \right], \\
D_{h_2} &= \sum_{\kappa=1}^{\infty} \frac{(-1)^{\kappa} (\Delta x)^{2\kappa+1}}{(2\kappa+1)!} \left[ (2^{2\kappa+1} - 2^{4\kappa+1})\alpha \right], \\
D_{h_3} &= \sum_{\kappa=1}^{\infty} \frac{(-1)^{\kappa} (\Delta x)^{2\kappa+1}}{(2\kappa+1)!} \left[ (-2^{2\kappa} - 2^{4\kappa} + 2^{2\kappa+1})c \right], \\
D_{h_4} &= \sum_{\kappa=1}^{\infty} \frac{(-1)^{\kappa} (\Delta x)^{2\kappa+2}}{(2\kappa+2)!} \left[ (-2^{2\kappa+3} + 2^{4\kappa+3})\alpha \right].
\end{aligned} \tag{B.26}$$

By analyzing these expressions we may now analyze how the local truncation error  $w_j$ ,  $j \in \mathcal{E}$ , behaves. This analysis is done in Section 4.4.3.

## Appendix C

# Two Dimensional Taylor Expansion and Properties

This appendix gives a brief recap of the conditions and properties associated with the two dimensional Taylor expansion. In Appendix C.2 we also look closer at the binomial theorem, and develop an alternative binomial theorem which will prove useful in the calculations done in Section 4.4.1 and Appendix B. Most of the concepts introduced in this appendix are well know from calculus.

### C.1 Two Dimensional Taylor Expansion and Pascal's Triangle

The formula for an n-dimensional Taylor expansion is given by

$$f(x_1 + \Delta x_1, \dots, x_n + \Delta x_n) = \sum_{j=0}^{\infty} \left[ \frac{1}{j!} \left( \sum_{k=1}^n \Delta x_k \frac{\partial}{\partial x'_k} \right)^j f(x'_1, \dots, x'_n) \right] \Bigg|_{x'_1=x_1, \dots, x'_n=x_n}. \quad (\text{C.1})$$



This can be seen from

$$\begin{aligned}
 2^0 &= 1 = 1, \\
 2^1 &= 2 = 1 + 1, \\
 2^2 &= 4 = 1 + 2 + 1, \\
 2^3 &= 8 = 1 + 3 + 3 + 1, \\
 2^4 &= 16 = 1 + 4 + 6 + 4 + 1, \\
 2^5 &= 32 = 1 + 5 + 10 + 10 + 5 + 1.
 \end{aligned}
 \tag{C.3}$$

The other property we would like to take advantage of is the following

**Property C.1.2.** *From row one, the sum of every second term in a row in Pascal's triangle sums up to exactly half of the sum of the entire row.*

This is true independent of which term we start at, and it is easy to see from

$$\begin{aligned}
 2^{1-1} &= 1 = 1 = 1, \\
 2^{2-1} &= 2 = 1 + 1 = 2, \\
 2^{3-1} &= 4 = 1 + 3 = 3 + 1, \\
 2^{4-1} &= 8 = 1 + 6 + 1 = 4 + 4, \\
 2^{5-1} &= 16 = 1 + 10 + 5 = 5 + 10 + 1, \\
 2^{6-1} &= 32 = 1 + 15 + 15 + 1 = 6 + 20 + 6.
 \end{aligned}
 \tag{C.4}$$

## C.2 The Binomial Theorem and Applications

The binomial theorem from Calculus is stated as

**Theorem C.2.1.** *(The Binomial Theorem)*

$$(x + y)^n = \sum_{k=0}^n \binom{n}{k} x^{n-k} y^k.$$

Now look at the expression

$$(x + y)^n \pm (-x + y)^n. \tag{C.5}$$

Applying the binomial theorem, Theorem C.2.1, to this expression yields

$$\begin{aligned}
 (x + y)^n \pm (-x + y)^n &= \sum_{k=0}^n \binom{n}{k} x^{n-k} y^k \pm \sum_{k=0}^n \binom{n}{k} (-1)^{n-k} x^{n-k} y^k \\
 &= \sum_{k=0}^n \binom{n}{k} x^{n-k} y^k (1 \pm (-1)^{n-k}).
 \end{aligned}
 \tag{C.6}$$

The same is true if the minus sign is moved to the  $y$ . We formulate this result in the following theorem

**Theorem C.2.2.**

$$(x + y)^n \pm (-x + y)^n = \sum_{k=0}^n \binom{n}{k} x^{n-k} y^k (1 \pm (-1)^{n-k}),$$
$$(x + y)^n \pm (x - y)^n = \sum_{k=0}^n \binom{n}{k} x^{n-k} y^k (1 \pm (-1)^k).$$

This theorem will prove helpful in the calculations done in Section 4.4.1 and Appendix B.

# Bibliography

- [1] J. M. Nordbotten and M. A. Celia. *Geological Storage of CO<sub>2</sub>: Modeling Approaches for Large-Scale Simulation*. Wiley, 2012. ISBN 978-0-470-88946-6.
- [2] A. Tambue, I. Berre, J. M. Nordbotten, and T. H. Sandve. Exponential euler time integrator for simulation of geothermal processes in heterogeneous porous media. In *Proceedings, thirty-seventh workshop on geothermal reservoir engineering, Stanford University, Stanford, California*, 2012.
- [3] F. A. Radu, M. Bause, P. Knabner, G. W. Lee, and W. C. Friess. Modeling of drug release from collagen matrices. *Journal of pharmaceutical sciences*, 91(4):964–972, 2002.
- [4] I. Aavatsmark. Bevarelsesmetoder for elliptiske differensialligninger, 2007. URL <http://folk.uib.no/fciia/elliptisk.pdf>. Department of Mathematics, University of Bergen.
- [5] I. Aavatsmark, T. Barkve, Ø. Bøe, and T. Mannseth. Discretization on non-orthogonal, curvilinear grids for multi-phase flow. In *4th European Conference on the Mathematics of Oil Recovery*, 1994.
- [6] M. G. Edwards and C. F. Rogers. A flux continuous scheme for the full tensor pressure equation. In *4th European Conference on the Mathematics of Oil Recovery*, 1994.
- [7] J. M. Nordbotten and G. T. Eigestad. Discretization on quadrilateral grids with improved monotonicity properties. *Journal of computational physics*, 203(2):744–760, 2005.
- [8] I. Aavatsmark and G. T. Eigestad. Numerical convergence of the mpfa o-method and u-method for general quadrilateral grids. *International journal for numerical methods in fluids*, 51(9-10):939–961, 2006.
- [9] I. Aavatsmark, G. T. Eigestad, B. T. Mallison, and J. M. Nordbotten. A compact multipoint flux approximation method with improved robustness. *Numerical Methods for Partial Differential Equations*, 24(5):1329–1360, 2008.

- 
- [10] R. A. Klausen and R. Winther. Convergence of multipoint flux approximations on quadrilateral grids. *Numerical methods for partial differential equations*, 22(6):1438–1454, 2006.
- [11] R. A. Klausen and R. Winther. Robust convergence of multi point flux approximation on rough grids. *Numerische Mathematik*, 104(3):317–337, 2006.
- [12] M. F. Wheeler and I. Yotov. A multipoint flux mixed finite element method. *SIAM Journal on Numerical Analysis*, 44(5):2082–2106, 2006.
- [13] R. A. Klausen and A. F. Stephansen. Mimetic mpfa. In *Proc. 11th European conference on the mathematics of oil recovery*, pages 8–11, 2008.
- [14] R. A. Klausen and A. F. Stephansen. Convergence of the mpfa o-method on general grids. *Preprint series. Pure mathematics*, 2010.
- [15] R. A. Klausen and A. F. Stephansen. Convergence of multi-point flux approximations on general grids and media. *International Journal of Numerical Analysis & Modeling*, 9(3), 2012.
- [16] L. Agelas and R. Masson. Convergence of the finite volume mpfa o scheme for heterogeneous anisotropic diffusion problems on general meshes. *Comptes Rendus Mathematique*, 346(17):1007–1012, 2008.
- [17] G. T. Eigestad and R. A. Klausen. On the convergence of the multi-point flux approximation o-method: Numerical experiments for discontinuous permeability. *Numerical methods for partial differential equations*, 21(6):1079–1098, 2005.
- [18] I. Aavatsmark, G. T. Eigestad, and R. A. Klausen. Numerical convergence of the mpfa o-method for general quadrilateral grids in two and three dimensions. In *Compatible spatial discretizations*, pages 1–21. Springer, 2006.
- [19] I. Aavatsmark, G. T. Eigestad, R. A. Klausen, M. F. Wheeler, and I. Yotov. Convergence of a symmetric mpfa method on quadrilateral grids. *Computational geosciences*, 11(4):333–345, 2007.
- [20] M. Pal, M. G. Edwards, and A. R. Lamb. Convergence study of a family of flux-continuous, finite-volume schemes for the general tensor pressure equation. *International journal for numerical methods in fluids*, 51(9-10):1177–1203, 2006.
- [21] J. M. Nordbotten, I. Aavatsmark, and G. T. Eigestad. Monotonicity of control volume methods. *Numerische Mathematik*, 106(2):255–288, 2007.
- [22] S. S. Mundal. *Conservative Numerical Methods for Elliptic Problems with Applications to Simulation of Near-well Flow*. PhD thesis, University of Bergen, Norway, 2009.

- 
- [23] A. F. Radu. Lecture notes on flow in porous medium. Personally communicated, 2012.
- [24] I. Aavatsmark. An introduction to multipoint flux approximations for quadrilateral grids. *Computational Geosciences*, 6(3-4):405–432, 2002.
- [25] F. Brezzi, K. Lipnikov, and M. Shashkov. Convergence of the mimetic finite difference method for diffusion problems on polyhedral meshes. *SIAM Journal on Numerical Analysis*, 43(5):1872–1896, 2005.
- [26] C. Guichard L. Agelas and R. Masson. Convergence of the finite volume mpfa o scheme for heterogeneous anisotropic diffusion problems on general meshes. *IJVF*, 7(2), 2010.
- [27] S. S. Mundal, E. Keilegavlen, and I. Aavatsmark. Simulation of anisotropic heterogeneous near-well flow using mpfa methods on flexible grids. *Computational Geosciences*, 14(4):509–525, 2010.
- [28] R. J. LeVeque. Finite difference methods for differential equations. *Draft version for use in AMath*, 585(6), 1998.
- [29] G. H. Golub and C. F. Van Loan. *Matrix computations*, volume 3. JHU Press, 1996. ISBN 0-8018-5413-X.
- [30] W. Cheney. *Analysis for applied mathematics*, volume 208. Springer, 2001. ISBN 0-387-95279-9.
- [31] D. C. Lay. *Linear algebra and its applications*, volume 3. Addison Wesley, 2006. ISBN 0-321-28713-4.
- [32] A. Laptev. Dirichlet and neumann eigenvalue problems on domains in euclidean spaces. *journal of functional analysis*, 151(2):531–545, 1997.
- [33] C. Fefferman. On the convergence of multiple fourier series. *Bulletin of the American Mathematical Society*, 77(5):744–745, 1971.
- [34] I. Aavatsmark, G. T. Eigestad, B. Heimsund, B. Mallison, J. M. Nordbotten, and E. et al. Øian. A new finite-volume approach to efficient discretization on challenging grids. *SPE Journal*, 15(03):658–669, 2010.
- [35] V. E. Hoggatt. A new angle on pascal’s triangle. In *The Fibonacci Quarterly*. Citeseer, 1968.